MORPHOLOGY DEPENDENCE OF VIBRATIONAL SPECTRA OF POLYOXYMETHYLENE AND POLY(ETHYLENE OXIDE) CRYSTALS

A Doctoral Thesis

by

Masaki Shimomura

Submitted to the Faculty

of Science, Osaka University

November, 1993

Morphology Dependence of Vibrational Spectra of Polyoxymethylene and Poly(ethylene oxide) Crystals

A Doctoral Thesis

by

Masaki Shimomura

Submitted to the Faculty
of Science, Osaka University

November, 1993

Approvals

November, 1993

This thesis is approved as to
style and content by

小林雅通

Member–in–chief

Yoshimasa Kyogoku

Member

寺本明夫

Member

岡代孝二

Member

Acknowledgments

This research work was carried out at the Research Institute for Polymers and Textiles, Agency of Industrial Science and Technology, Ministry of International Trade and Industry and Faculty of Science, Osaka University. The author would like to express his gratitude to Professor Masamichi Kobayashi of Osaka University and Drs. Masatoshi Iguchi, Yoshikazu Tanabe and Katsuhiko Ueno of the National Institute of Material Science (formerly the Research Institute for Polymers and Textiles) for their continuing guidance, encouragement and support throughout the course of this work. Grateful acknowledgment is also made to Dr. Hiroko Kyotani of the National Institute of Material Science, Dr. Kohji Tashiro of Osaka University and Dr. Hirofumi Morishita of Nagasaki University for their fruitful discussions. The author is grateful to Ms. Yuka Watanabe of ICI Japan for her collaboration. The author would also like to thank his colleagues at the Research Institute for Polymers and Textiles and members of Professor Kobayashi's Laboratory for their friendship.

Finally the author would like to thank his wife, Mieko, and his family for their encouragement in preparing this thesis.

Masaki Shimomura

November, 1993

Contents

Chapter 1

General Introduction

Polyoxymethylene (POM) is one of the polymers having the simplest chemical structure, $\{CH_2O\}_n$, *i.e.*, a methylene unit and an oxygen atom appear alternatively along the backbone. POM has been a well known polymer since the dawn of the polymer science (1920's) and has been used in wide variety of industrial products. In 1956, Du Pont acquired a patent on the polymerization of formaldehyde and the polymer was called "Delrin". Several years later, Celanese began to produce "Celcon", a copolymer of trioxane and ethylene oxide. Since those days, POM, the polyacetal resin, became one of the most important polymeric materials. At present, it still plays an important role in various industrial usages.

In the field of science, POM also has been one of the most important polymers for a long time. The first scientific literature about POM is published in 1859, reporting a white resin produced through polymerization of paraformaldehyde.[1] In 1920's, Staudinger and his group established the concept of "macromolecules" and made many studies for that purpose on POM.[2] POM might be as important as polyethylene in the polymer science, because of its simple chemical structure and of its complement nature to polyethylene, *e.g.*, polar and non-polar, helical conformation and planar zig-zag conformation, and so on. Nevertheless, the number of papers published on POM is not so many compared with that on polyethylene, partly because POM lacks in well defined low molecular weight analogues such as *n*-alkanes that played important roles in the research of polyethylene. Though POM has a long history in the polymer science, it still has some problems to be solved

in many fields, including the vibrational spectroscopy.

POM is known as a typical crystalline polymer and its crystal structures have been almost established by X-ray diffraction and other techniques.[3-6] Two crystal modifications of POM are known so far. One is the stable trigonal form (*t*-POM) consisting of molecular chains with 9/5 helical conformation. Exact spatial arrangement of the chains in crystallites remained unsettled yet. For instance, it is not known whether the chains in one crystallite turn in the same direction or right-turn and left-turn helices are mixed statistically with equal probability, and the relative heights of the chains along the *c*-axis are not determined yet. The other crystal modification is metastable orthorhombic form (*o*-POM) with molecular chains of 2/1 helical conformation.[7,8] *O*-POM was first obtained by Mortillario *et al.* through polymerization of formaldehyde in aqueous solution.[7] Recently, *o*-POM crystal was found in a cationic polymerization system of trioxane and the molecular chains are found to be fully extended.[8-10] The pressure-induced solid-state phase transition from *t*-POM to *o*-POM is the third method to realize the metastable phase.[11,12] In this case, original morphologies of crystals are maintained during the phase transition, *i.e.*, folded-chain crystals, which are recrystallized from dilute solution, are transformed to folded-chain crystals of *o*-POM and extended-chain crystals of *t*-POM change to extended-chain crystals of *o*-POM.

Vibrational spectroscopy is a very powerful method for the investigation of molecular-level structures of various types (molecular conformation, crystal structure, surface structure, intra- and intermolecular forces, etc.) in connection with physical properties of materials. It is quite natural that infra-red and Raman spectra of *t*-POM samples have been studied by many authors. Success in preparation of metastable *o*-POM

samples presented new interesting subjects in the field of polymer spectroscopy.[9-12,29-31] For the trigonal crystal, an assignment of the infra-red and Raman bands has been established in reference to the normal mode analysis of an infinitely extended 9/5 helical chain.[13] The experimental data used in the normal mode calculation, however, are those obtained for highly crystalline and highly oriented films of POM. It has been believed that basic studies of the vibrational spectra of POM crystals as well as the analysis of crystal structure had been established, through the excellent previous works.

It has been notified that infra-red spectra of POM exhibited substantial changes in the 1200–900 cm^{-1} region depending on the state and/or the route of processing of the samples subjected to the measurement. However, these changes have not been recognized as due to an essentially important spectroscopic phenomenon related to the morphologies of polymer crystals. Variation of infra-red spectrum in the 1200–900 cm^{-1} region of *t*-POM, was first reported by Zamboni and Zerbi in 1964.[14] The bands in this region were also studied in more detail by Oleinik and Enikolopyan on a series of oligomeric homologues.[15] They considered that the bands at 903 and 1238 cm^{-1} were "regularity bands" associated with longer *gauche* helix, whereas "additional" bands at 985 and 1130 cm^{-1} were affiliated to planar zig-zag chains in non-crystalline part of samples. Terlemezyan *et al.* studied the structure of *t*-POM samples obtained by cationic polymerization of trioxane in various solvents, and classified the spectra taken on these samples into two types.[16-18] They concluded that the differences in the spectra were connected with conformational defects contained in polymer chains constructing the crystalline part, on the basis of their experimental results concerning the effect of temperature and applied mechanical forces on the content of *gauche* conformation in POM samples. Thereafter, Fawcett proposed another

interpretation.[19] He considered that the spectral changes were due to difference in the chain packing, *i.e.*, some molecules slid by 1/2 pitch of a helix along the *c*-axis accompanied with some changes in intermolecular interactions which induced the infra-red spectral changes depending on the amount of slid chains. In order to examine experimentally this idea, Terlemezyan *et al.* measured the infra-red spectra of copolymer of trioxane and dioxolane.[20] Because of $-O\left(CH_2\right)_2O-$ units in the copolymer, an oxygen atom and the methylene unit do not always align alternatively along the chain. Therefore, in the crystalline phase, chains in some parts are well-aligned and chains in other parts slid each other by 1/2 pitch of helix. If Fawcett's interpretation is true, the copolymer should give rise to an infra-red spectrum different from that of *t*-POM. However, the infra-red spectra of folded-chain crystals of homopolymer and copolymer were identical. In spite of these previous works, the characteristics and molecular mechanism of the spectroscopic phenomenon is not clarified yet. The studies made so far were only qualitative, partly due to the lack of idealized standard samples with which quantitative intensity analysis could be made.

In 1973, needle-like crystals of POM were obtained by a heterogeneous cationic polymerization of trioxane.[21] One piece of the crystals was found to be a single crystal of *t*-POM, which has an honor to be the first polymer whisker.[22-25] *Figure 1-1* shows an optical micrograph of the needle-like crystals of *t*-POM (as polymerized). One single crystal appears several tens to 100 μm in length and about 10 μm in thickness and the cross section has hexagon-shape, reflecting its trigonal crystal system. Through X-ray diffraction and various other measurements, molecular chains in the needle-like crystals are thought to be fully extended and the crystals show extremely high perfection as a crystal of polymers.[23-25] Iguchi and his

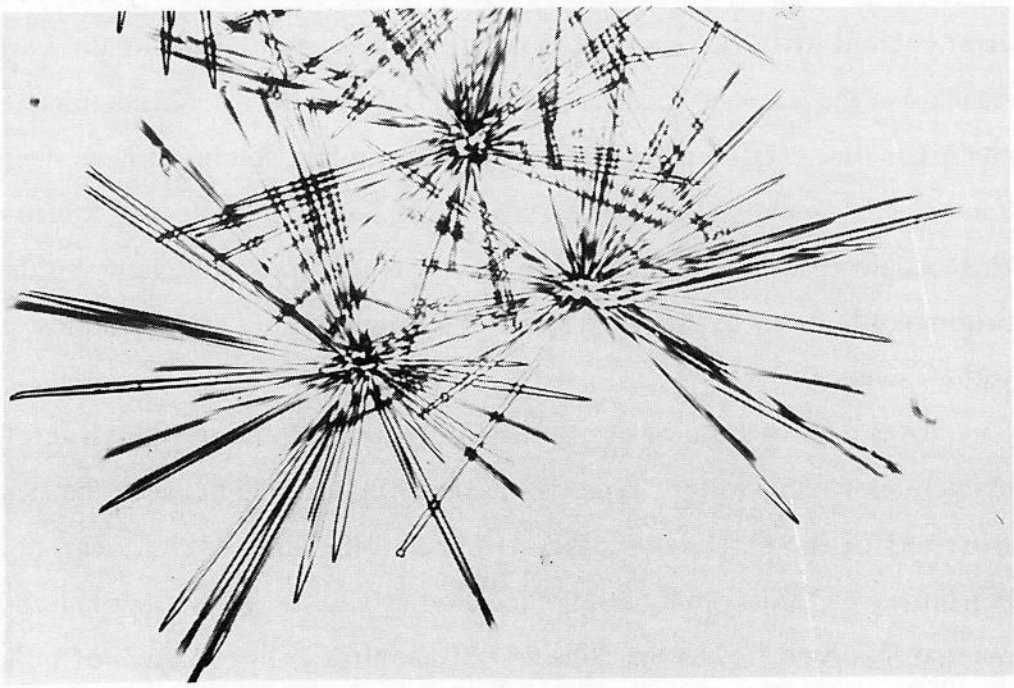

Figure 1–1 Optical micrograph of the needle–like crystals (whisker) of polyoxymethylene.

coworkers established the polymerization procedure and the needle-like crystals became available for being supplied to various studies.[26)]

The needle-like crystals have attracted technological interests, because of their high Young's modulus.[26-28)] However, extremely high crystalline perfection of the needle-like crystals is another interesting character. Since the needle-like crystals of POM are constructed by ideally ordered arrangement of fully extended molecules, they can be used as the best standard of the extended-chain crystal of *t*-POM. On the other hand, folded-chain lamellar crystals of *t*-POM grown from dilute solutions, have been known as well-defined single crystals. Using both extended- and folded-chain single crystals, it is expected to make a breakthrough for clarifying the origin and features of the large spectral changes among POM samples of various sources.

In the solid state of crystalline polymers, there are constructed crystallites having various types of morphology situated between the two extremes of the extended-chain crystal and the folded-chain crystal, depending on the crystallization condition as well as on the thermal and mechanical histories of the sample. Since physical properties of bulk crystalline polymers are strongly influenced by the crystal morphology, the control and the characterization of the morphology have become more and more important in the studies of high-performance polymers, such as high-strength and high-modulus fibres, electric conducting polymers and so on. Nevertheless, the infra-red spectroscopy has not played important roles in the studies of crystal morphology of polymers, because it has generally been believed that the vibrational spectroscopy in the mid infra-red region is not informative for studying higher-order polymer structure, like crystal morphology. Contrary to this general notion, the present author tried to

explain the above-mentioned spectral changes in terms of morphology-dependence of infra-red spectra, hoping to clarify the origin of the changes and to develop new field in infra-red spectroscopy for the research of higher-order structures including morphology.

The next problem of this work is to know whether the spectral changes are limited to *t*-POM as discovered for the first time, or observed commonly in polymer crystals. To solve this problem, crystalline polymer samples, which have both extended- and folded-chain crystal morphologies, have to be examined. As mentioned above, the extended- and folded-chain crystals of *o*-POM became available by the pressure-induced solid-state phase transition from *t*-POM crystals. Thus, *o*-POM is considered as the second polymer to be examined. Poly(ethylene oxide) (PEO) is a crystalline polymer of molecular chains in 7/2 helical conformation[32,33] and contains oxygen atoms in the main chain as well as POM. PEO is another polymer to be measured. It has been known that the folded-chain crystals of PEO can be grown from dilute solution. Well-drawn and highly crystalline films of PEO can be used as extended-chain crystals. By measuring vibrational spectra of these crystalline polymer samples, the generality of the spectral change among polymer crystals will be clarified.

Following chapters of this thesis deal with the above-mentioned problems concerning the anomalously large change in the vibrational spectra of polymer crystals. A theoretical explanation of the phenomena will also be proposed.

In Chapter 2, infra-red spectra of various *t*-POM samples, different in origin and/or in history of processing, will be surveyed. In order to investigate the spectral changes quantitatively, the absorption profile of each

sample is separated into several components using a curve resolver and their intensities are analyzed quantitatively. The bands are classified into two types, one is sample–sensitive and the other is sample–insensitive.

In Chapter 3, the infra–red and Raman spectra of two typical *t*–POM single crystals, the needle–like extended–chain crystals (ECC) prepared by a cationic polymerization of trioxane, and the folded–chain crystals (FCC) grown from dilute bromobenzene solution, will be presented. In order to clarify the characteristics of sample–sensitive infra–red bands mentioned in Chapter 2, the X–ray diffraction and infra–red and Raman spectra of these two samples of extremely high crystallinity and different from each other in crystal morphology are investigated. The symmetry species of unassigned bands of the FCC sample were determined to be A_2 by the polarization measurement, using random and plane–oriented specimens. It is shown that the spectral change is caused by the shift of the A_2 bands having the transition dipole parallel to the chain axis induced by the difference in crystal morphology. Infra–red spectral difference between the ECC and FCC of deuterated POM is also shown in comparison with normal POM crystals. Adequacy of previously proposed interpretations and possible molecular mechanisms of the spectroscopic phenomenon will be discussed.

Chapter 4 presents vibrational spectra of a series of linear oligomers of POM having acetoxy terminal groups. X–ray diffraction patterns of the oligomers are also investigated. Since the oligomers form trigonal crystals of the lamella type consisting of short extended molecular chains without folding parts, the role of the chain foldings and/or the lamellar structure in the morphology–dependent bandshift is expected to be clarified from the spectral variation with chain length of the oligomers. Effects of mechanical deformation induced by shear stress and subsequent melt crystallization on the

infra-red spectra are investigated for both oligomers and FCC of high molecular weight POM.

In Chapter 5, the preparation and identification of orthorhombic POM (*o*-POM) will be presented. In order to know whether the morphology-dependent spectral change is characteristic of *t*-POM alone or common phenomenon observable more or less in polymer crystals, the morphology-dependent infra-red bandshift of *o*-POM is examined. Since the morphology of the starting crystal is maintained through the pressure-induced solid-state phase transition, the ECC and FCC of *o*-POM can be generated from ECC and FCC of *t*-POM, respectively, although the amounts of the orthorhombic phase generated are limited to 10 - 20 % at most. Using the spectral subtraction technique, the infra-red spectra of both ECC and FCC of pure *o*-POM are obtained, and parallel bands (B_1) and perpendicular bands (B_2 and B_3) of both crystals of *o*-POM are compared.

In Chapter 6, infra-red and Raman spectra of poly(ethylene oxide) (PEO) are presented for the same purpose as in Chapter 5. As an idealized ECC of PEO is not available by now, a highly-drawn film sample is used instead. The FCC of PEO can be grown from dilute solution. A Fourier transform infra-red spectrometer and the subtraction technique make it possible to separate the parallel (A_2) and perpendicular (E_1) bands and to detect rather small bandshifts. Characteristics of the spectral changes of PEO are discussed and compared with those of POM crystals. The effects of mechanical deformation and heat treatment on the infra-red spectra of PEO are also presented in comparison with the results of FCC of *t*-POM and the oligomers.

Chapter 7 deals with a "dynamic ferroelectric" theory explaining the morphology-dependent bandshift of the parallel bands. Since it was pointed

out that the dipolar interactions are important to the bandshift, large interactions among transition dipole moments are assumed for a crystal of sufficiently large stem-length. These interactions yield "dynamic ferroelectric" state, where the large interactions results in the large nonlinear vibration and the shift of the parallel bands.

In Chapter 8, summary and conclusion of the present study will be presented.

References

1 A. M. Butlerov, *Ann.*, **111**, 242 (1859)

2 H. Staudinger, "Die Hochmolekularen Organischen Verbindungen", Berlin Springer (1932)

3 H. Tadokoro, S. Yasumoto, S. Murahashi and I. Nitta, *J. Polym. Sci.*, **44**, 266 (1960)

4 T. Uchida and H. Tadokoro, *J. Polym. Sci. (A-2)*, **5**, 63 (1967)

5 G. Carazzolo, *J. Polym. Sci. (A)*, **1**, 1573 (1963)

6 H. Tadokoro, "Structure of Crystalline Polymers", John Wiley & Sons (1979)

7 L. Mortillario, G. Galliazzo and S. Bessi, *Chem. Ind. (Milan)*, **46**, 139 (1964), *ibid* **46**, 144 (1964)

8 M. Iguchi, *Polymer*, **24**, 915 (1983)

9 M. Kobayashi, Y. Itoh, H. Tadokoro, M. Shimomura and M. Iguchi, *Polym. Commun.*, **24**, 38 (1983)

10 M. Kobayashi, H. Morishita, T. Ishioka, M. Iguchi and M. Shimomura, *J. Mol. Struc.*, **146**, 155 (1986)

11 M. Kobayashi, H. Morishita and M. Shimomura, *Rep. Prog. Polym. Phys. Jpn.*, **31**, 473 (1988)

12 H. Morishita, M. Kobayashi, M. Shimomura, M. Iguchi and H. Kuwahara, *Sci. Bull. Fac. Educ., Nagasaki Univ.* **41**, 1 (1989)

13 H. Tadokoro, M. Kobayashi, Y. Kawaguchi, A. Kobayashi and S. Murahashi, *J. Chem. Phys.*, **38**, 703 (1063)

14 V. Zamboni and G. Zerbi, *J. Polym. Sci. (C)*, **7**, 153 (1964)

15 E. F. Oleinik and N. S. Enikolopyan, *J. Polym. Sci. (C)*, **16**, 3677 (1968)

16 L. Terlemezyan, M. Mihailov, P. Schmidt and B. Schneider, *Makromol. Chem.*, **179**, 807 (1978)

17 L. Terlemezyan, M. Mihailov, P. Schmidt and B. Schneider, *Makromol. Chem.*, **179**, 2315 (1978)

18 L. Terlemezyan and M. Mihailov, *Eur. Polym. J.*, **17**, 1115 (1981)

19 A. H. Fawcett, *Polym. Commun.*, **23**, 1865 (1982)

20 L. Terlemezyan and M. Mihailov, *Polym. Commun.*, **25**, 80 (1984)

21 M. Iguchi, *Br. Polym. J.*, **5**, 195 (1973)

22 M. Iguchi and I. Murase, *J. Crystal Growth*, **24/25**, 596 (1974)

23 M. Iguchi, I. Murase and K. Watanabe, *Br. Polym. J.*, **6**, 61 (1974)

24 M. Iguchi, *Makromol. Chem.*, **177**, 549 (1976)

25 T. Mashimoto, T. Sakai and M. Iguchi, *J. Phys. (D)*, **12**, 1567 (1979)

26 T. Suehiro, M. Iguchi, A. Yamauchi, Y. Nishi, M. Uryu and N. Fujiwara, *Bull. Res. Inst. Polym. Textiles*, **162**, 19 (1990)

27) M. Shimomura, Y. Maeda and Y. Tanabe, *J. Mater. Sci.*, **24**, 2245 (1989)

28 M. Iguchi, T. Suehiro, Y. Watanabe, Y. Nishi and M. Uryu, *J. Mater. Sci.*, **17**, 1632 (1982)

29 H. Morishita, M. Kobayashi, M. Shimomura and M. Iguchi, *Sci. Bull. Fac. Educ., Nagasaki Univ.* **39**, 47 (1988)

30 M. Kobayashi, H. Morishita, M. Shimomura and M. Iguchi, *Macromolecules*, **20**, 2453 (1987)

31 M. Kobayashi, H. Morishita and M. Shimomura, *Macromolecules*, **22**, 3726 (1989)

32 Y. Takahashi and H. Tadokoro, *Macromolecules*, **6**, 672 (1973)

33 Y. Takahashi, I. Sumita and H. Tadokoro, *J. Polym. Sci., Polym. Phys. Ed.*, **11**, 363 (1973)

Chapter 2

Infra-red Spectra of Various Polyoxymethylene Specimens

2.1 Introduction

"Crystallinity bands" or "regularity bands", appearing on infra-red spectra, are characteristic of individual polymers and they are distinguished in polymers having relatively simple backbone structures. For this reason, the application of infra-red spectroscopy for the measurement of crystallinity lacks the generality of X-ray and density methods which are based on the assumption of the crystalline-amorphous binary-phase model. Nevertheless, the analysis of infra-red spectra is useful for investigating the regularity or the local disordering of molecular conformation in crystals or crystallites.

From this point of view, a vast number of studies on various polymers have been published in the last three decades. Among them, polyethylene was most rigorously studied, ever since changes in the intensity of some bands by annealing were originally pointed out by Brown.[1] The analysis was applied by Koenig and Witenhafer[2] for the quantitative analysis of chain folds in lamellar specimens and many works followed.

For polyoxymethylene (POM), a trigonal form consisting of chains in helical conformation is common, though an orthorhombic modification is another form found in some specimens. By now, the assignment of infra-red bands has been almost established by reference to theoretical calculations. The fact that the infra-red spectrum of the trigonal form changes with crystallinity/regularity in the 1200-900 cm^{-1} region, was first reported by Zamboni and Zerbi.[3] Bands in this region were studied in detail by Oleinik

and Enikolopyan[4] by bringing in a series of oligomeric homologues : it was assumed that the bands at 903 and 1238 cm^{-1} were "regularity bands" characteristic of longer *gauche* helix, whereas "additional" bands at 985 and 1130 cm^{-1} were affiliated to planar zig-zag chains in non-crystalline part. Terlemezyan *et al.*[5,6] studied the effect of temperature and mechanical force on the *gauche* conformation fraction of the sample and reached a conclusion that the infra-red spectra are related to conformational defects of helical chain in crystalline part. However, results obtained in these studies were rather qualitative, partly due to the lack of standard, as only the pressure-crystallized highly crystalline samples were made available for the study of polyethylene.

Needle-like, trigonal single crystals of POM developed by Iguchi *et al.*[7,8] consist of fully extended helical chains and their perfection has been proved by X-ray and various other measurements.[9-11] Infra-red spectroscopic study of this specimen has been of interest. As expected, preliminary experiment gave a spectrum having only five infra-red bands in the 1300-550 cm^{-1} region, whereas up to seven bands were observed for conventional POM samples.

In this chapter, measurement of infra-red spectra in the 1300-550 cm^{-1} region has been made for various POM specimens of different origin and/or processing. From the analysis of the infra-red spectra of various POM specimens, an attempt has been made to classify infra-red absorption bands into sample-insensitive and sample-sensitive ones and systematic relationships have been obtained between the intensities of the latter bands.

2.2 **Experimental**

2.2.1 *Samples*

Needle-like crystals were grown in a cationic polymerization system of trioxane under similar conditions as described in literature[8] and subjected to boron trifluoride etching[9] to disrupt the original radial assembly.

Feather-shaped crystals were prepared in a similar system during the polymerization of trioxane.[12,13]

Fibrillar crystals were prepared by the cationic solid-state polymerization method[10] and reflexed in an ethanol/water mixture containing a small amount of triethylamine to remove the traces of catalytic species.

A heterogeneous as-polymerized sample was obtained by polymerizing trioxane in nitrobenzene (3.3mol / l) with boron trifluoride catalyst (1m mol / l).[14]

A melt crystallized sample, in the form of a thin film, was prepared from POM diacetate (Delrin 500X from E. I. du Pont de Nemours & Co.). The polymer was dissolved in hexafluoroacetone sesquihydrate and cast on a glass plate. After washing out the solvent with acetone and drying, the polymer was melted at 180°C and allowed to cool to room temperature. The film comprised spherulites in its morphology.

A precipitate from Delrin 500X was obtained by dissolving 0.1g polymer in 10 ml hexafluoroacetone sesquihydrate and pouring in a large amount of acetone. The precipitate was freeze-dried with benzene.

Lamellar crystals were prepared, with both needle-like crystals and Delrin 500X, from 0.3% bromobenzene solution containing 0.4% 2,6-di-*tert*-butyl-*p*-cresol at 130°C and, after filtration, freeze-dried using

benzene. Since the needle-like crystals were insoluble in boiling bromobenzene, they had to be dissolved in hexafluoroacetone sesquihydrate to destroy their highly crystalline structure and precipitated in acetone prior to the solution crystallization. The lamellar crystals also served for measurements after annealing at various temperatures, between 155°C and 170°C, for 2h.

2.2.2 *Measurement of Infra-red Spectra and Data Processing*

A diffraction grating infra-red spectrometer, Jasco Model 701G, was used. For measurement, powder samples were mulled with Nujol and sandwiched between two KBr windows. Some samples were ground and pelletized with KBr powder and served for measurement.

FACOM/HITAC M160-II computer was employed for data processing. Recorded spectra of 1300-550cm^{-1} region were manually digitized at 5 cm^{-1} intervals and, after smoothing by the seven-point cubic method,[15] the spectra were converted into the absorbance unit. For the data of the Nujol mull method, subtraction of background was based on reference to the band at 720 cm^{-1}. All spectra were normalized based upon the intensity of 1240cm^{-1} band, which seemed to be common to and invariant for all specimens. In order to separate overlapped bands and to measure their area intensities, a curve resolver, Model 301 of E. I. du Pont de Nemours and Co., was used.

2.3 **Results and Discussion**

2.3.1 *Infra-red Spectra of Polyoxymethylene Specimens*

Spectra of various specimens measured by the Nujol mull method, or by the film method for film specimens, have been processed to convert the percent transmission to the absorbance unit according to the procedure described in Experimental Section and typical spectra in the 1300–550 cm^{-1} region are shown in *Figure 2–1*. The difference in the spectra of different specimens is clearly illustrated. It should be remarkable that the curves from the specimens of the extended chains with higher crystalline perfection, *i.e.*, the needle–like and feather–shaped crystals, are rather simple with five bands, whereas those from other specimens are more complicated, as usually observed, with up to seven bands or shoulders in the present wavenumber region. (It has come to the author's notice that a spectrum reported earlier by Zamboni and Zerbi[3] for a crystalline sample is similar to that of the needle–like or feather–shaped crystals. The sample might have been of similar character, although the details are not clear.) It should be noted that the spectra for two solution–grown crystals from different sources, Delrin and needle–like crystals, are almost identical, showing that the difference of terminal groups, acetoxy and hydroxy, has hardly affected these spectra.

Figure 2–2 shows spectra of some specimens obtained by the KBr pellet method. The measurement was primarily aimed at testing the effect of the sample orientation which could have been significant for the Nujol mull method in which anisotropic samples are sandwiched in a thin layer, despite the latter method's advantage of avoiding damage to samples. This was not the case, however, and the spectra of needle–like and feather–shaped crystals,

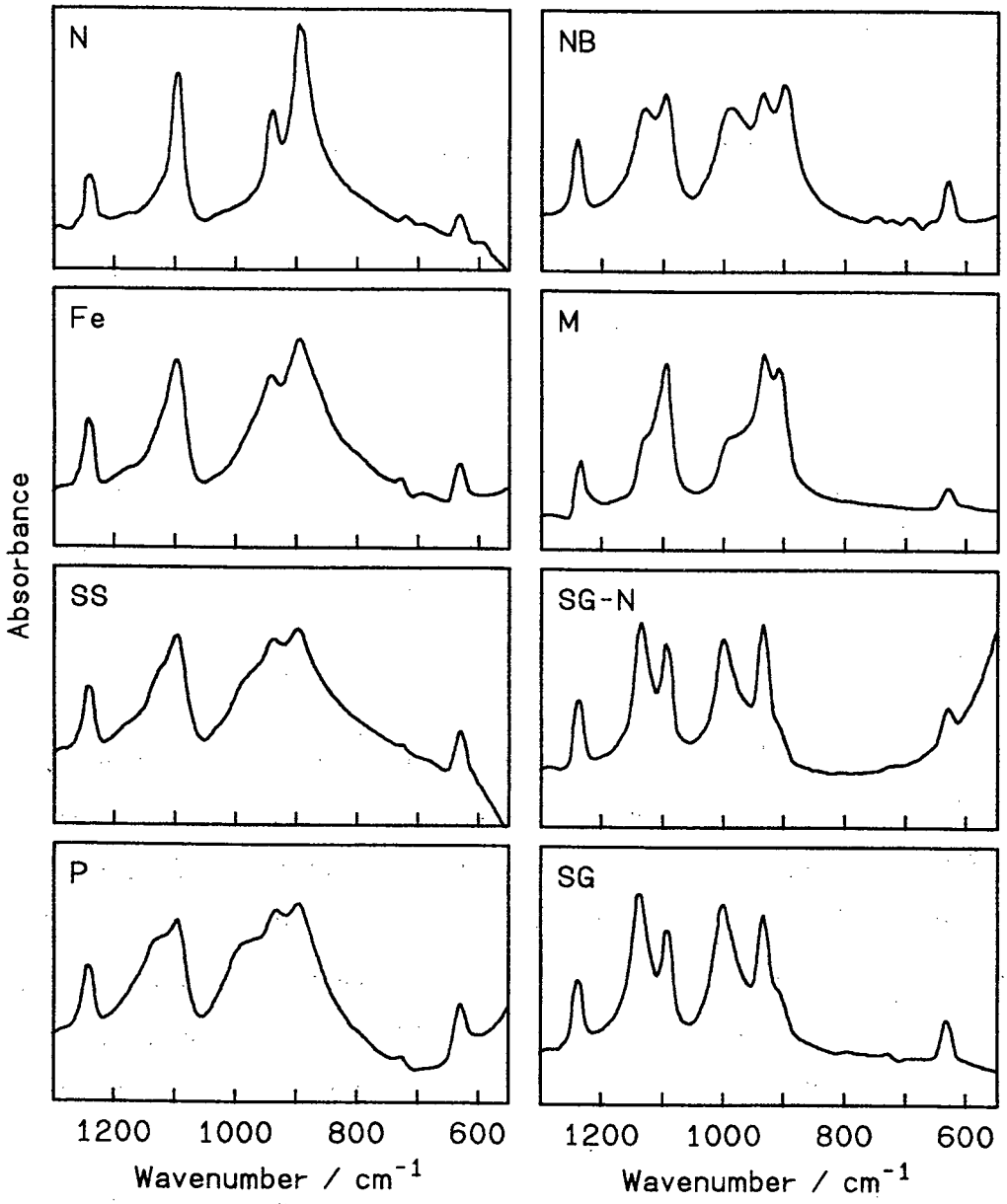

Figure 2–1 Infra–red spectra of various polyoxymethylene specimens.

N:needle–like, Fe:feather–shaped, SS:solid–state polymerized, P:precipitated, NB:polymerized in solution, M:melt crystallized film, SG–N:solution–grown from needle, SG:solution–grown from Delrin. All spectra except M are measured by Nujol mull method.

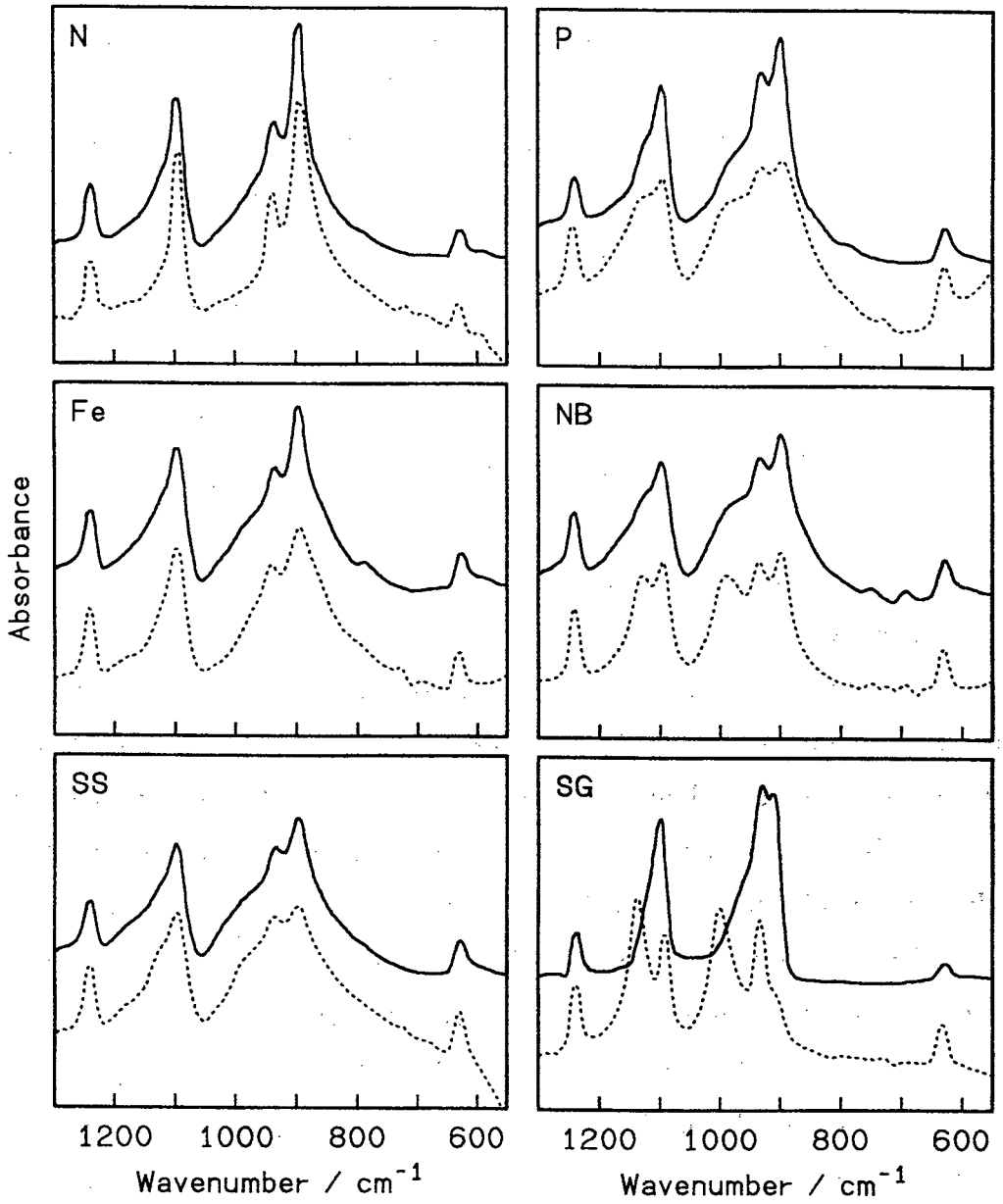

Figure 2–2 Infra–red spectra of various polyoxymethylene specimens measured by KBr pellet method. (Broken lines reproduce spectra by Nujol mull method.)

Notations are the same as in *Figure 2–1*.

as well as that of fibrillar crystal, were almost the same as those obtained by the Nujol mull method. Instead, the spectra of other specimens comprising folded-chains or more or less imperfect structures changed dramatically, reflecting the effect of mechanical deformation[5] caused by pelletization. The spectra of the heterogeneous polymer polymerized in nitrobenzene and the precipitated are found to be changed and become similar to the spectrum of the fibrillar specimen (*Figure 2-1 : SS*). The change of spectra of the solution-grown and the melt crystallized specimens are rather complicated, however, the spectra are closer to that of the needle-like crystal than those measured by the Nujol mull method.

For these spectra, the wavenumbers of bands for different specimens are scanned to fall almost at the same positions, with a minor deviation, less than 7 cm^{-1} in this region. The intensity of bands has been classified into five levels and listed in *Table 2-1*. Three bands at 1240, 935 and 635 cm^{-1} are present in all spectra and their intensities seem to be constant, suggesting that these bands are independent of the higher-order structure of the sample. The other four bands around 1140, 1095, 1000 and 900 cm^{-1} are changeable in intensity and, in some cases, the bands at 1140 and 1000 cm^{-1} have completely disappeared from the spectra. The band around 900 cm^{-1} seems to be characteristic of the regular structure of helical conformation as has been concluded before.[4] The band is outstanding for extended-chain type specimens and also it tends to increase for folded-chain type specimens in consequence of annealing. That the band at 1095 cm^{-1} is dependent on the nature of samples, being stronger for the extended-chain needle-like crystals, is clear from the present results, though it has not been pointed out before. The bands at 1140 and 1000 cm^{-1} are absent from the spectra of extended-chain specimens and their affiliation to the folded-chain structure has been

Table 2-1 Intensity of absorption bands for various polyoxymethylene specimens in 1300–550 cm^{-1} region.

Specimen	Wavenumber (cm^{-1})						
	1240	1140	1095	1000	935	900	635
Needle–like		m	–	vs	–	m	vs	w
Feather–shaped		m	–	s	–	m	vs	w
Solid–state polymerized		m	sh	s	sh	m	s	w
Polymerized in bromobenzene		m	m	m	m	m	m	w
Melt crystallized film		m	w	s	w	s	m	w
Precipitate		m	w	s	w	m	s	w
Solution grown (Delrin)		m	s	m	s	s	sh	w
Solution grown (Needle)		m	s	m	s	s	sh	w
Solution grown (Delrin), annealed at 155°C		m	s	m	s	m	sh	w
Solution grown (Delrin), annealed at 160°C		m	s	m	s	m	sh	w
Solution grown (Delrin), annealed at 165°C		m	s	m	s	m	w	w
Solution grown (Delrin), annealed at 170°C		m	s	m	s	m	w	w
Needle(KBr)		m	–	vs	–	m	vs	w
Feather(KBr)		m	–	s	–	m	vs	w
Solid–state polymerized(KBr)		m	sh	s	sh	m	vs	w
Polymerized in nitrobenzene(KBr)		m	sh	s	w	m	s	w
Precipitate(KBr)		m	sh	vs	sh	s	vs	w
Solution grown (Delrin)(KBr)		m	–	vs	–	s	vs	w
Melt crystallized (KBr)		m	s	s	s	vs	–	w

confirmed. Of course, the validity of these interpretations rests on the assumption that the 1240 cm^{-1} band is consistent and useful for the normalization of spectra, as was actually done, but the assumption is not unreasonable in the light of a previous report.[4)]

2.3.2 *Band Intensity of Each Infra-red Spectrum*

When the bands in *Figures 2-1* and *2-2* were examined carefully, it was deduced that the two absorption bands at 1140 and 1000 cm^{-1} changed in intensity in parallel. The relation between the bands at 1095 and 900 cm^{-1} was not so simple but it seemed that the former band is a superposition of two modes, variable and constant ones, and the variable part was proportional to the intensity of the band of 900 cm^{-1}. In order to make it quantitative, the band area intensity was measured by means of a curve resolver. Plots have been made in *Figure 2-3* and linear relationships were obtained as expected. Here, the normalization of the area intensity was carried out referring to the 1240 cm^{-1} band. Similar linearities were also obtained when the 935 cm^{-1} band was adopted as reference.

Assignments of infra-red bands for trigonal POM crystals are given by Matsui *et al.*[17)] with reference to theoretical calculation and Raman data. (The interpretation is slightly different from a preceding report by Zerbi and Hendra,[16)] but the following discussion is made on the basis of the former assignments.) For seven absorption bands in the present wavenumber region, correspondence to the calculation is found for five bands observed in common with all spectra but for two bands unobserved in those of extended-chain highly crystalline specimens. Four bands at 1240, 935, 900 and 635 cm^{-1} are assigned to [CH_2 rock. + COC bend. + COC sym. str.], [COC sym. str. + CH_2

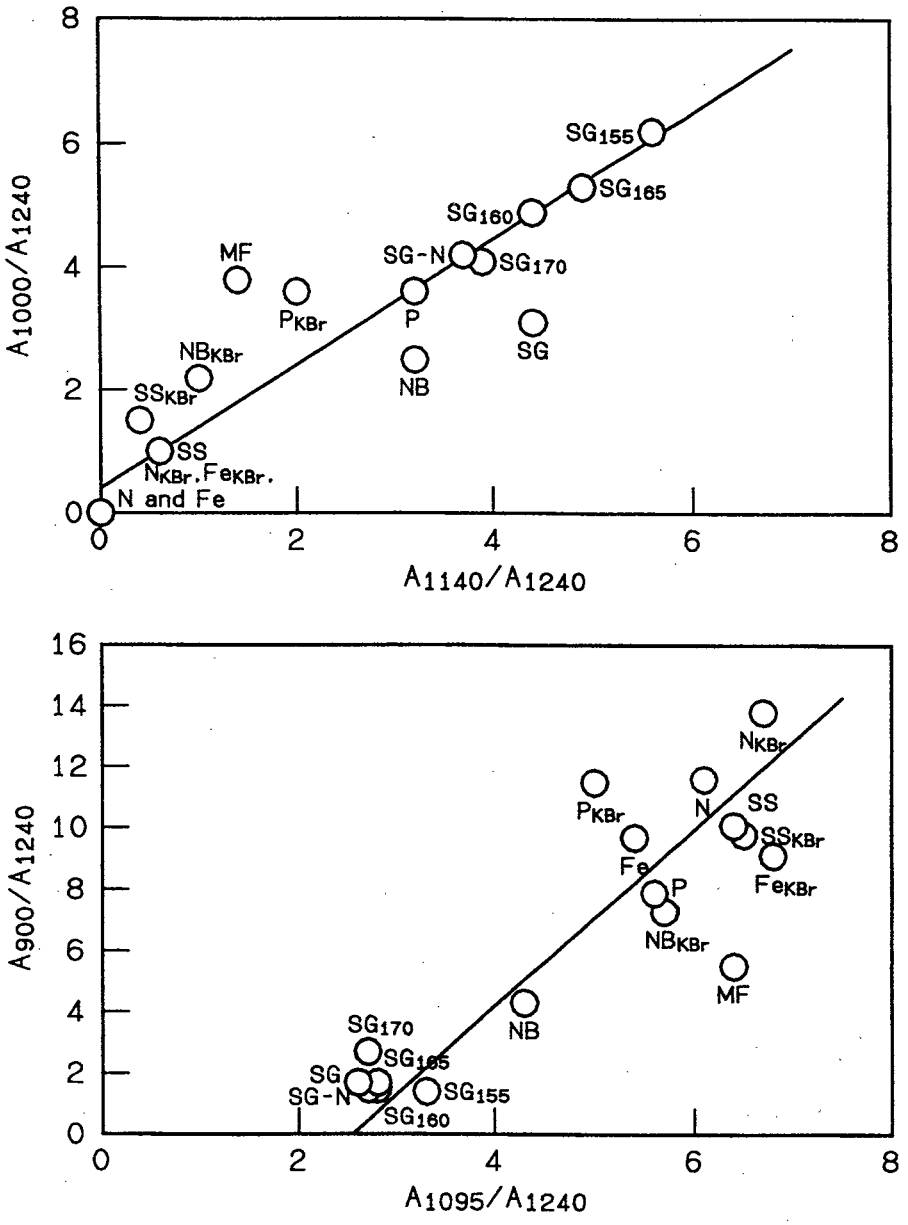

Figure 2–3 Plot of relative absorption intensities. Upper:A_{1000}/A_{1240} vs. A_{1140}/A_{1240}. Lower:A_{900}/A_{1240} vs. A_{1095}/A_{1240}.

Notation; N:needle–like, Fe:feather–shaped, SS:solid–state polymerized, P:precipitated, NB:polymerized in solution, MF:melt crystallized film, SG–N:solution–grown from needle, SG:solution–grown from Delrin, SGxxx:solution–grown annealed at xxx°C.

rock.], [CH_2 rock. + COC antisym. str.] and [COC bend.+ COC antisym. str.], respectively. At around 1095 cm^{-1}, correspondences are found to [COC antisym. str. + OCO bend.] and [COC antisym. str. + CH_2 rock.]. From the knowledge of these assignments and the results described above, it is assumed that the bands at 1095 and 900 cm^{-1} are sample–sensitive and the unassigned bands at 1000 and 1140 cm^{-1} are also sample–sensitive and have resulted from the shift of 900 and one component of 1095 cm^{-1} bands, respectively. (According to Oleinik and Enikolopyan,[4] these new bands are affiliated to planar zig–zag conformation, though there has been no theoretical explanation.)

If this assumption is valid, complementary relationships might exist between the intensities of 1095 and 1140 cm^{-1} bands and between those of 900 and 1000 cm^{-1} bands. The plots have been made in *Figure 2–4*. Although the points are scattered considerably, it should not be unreasonable to approximate them with straight lines for both plots. That the ratios of extinction coefficients for two pairs of vibrations, *i.e.*, the slopes in *Figure 2–4*, are not far from unity, at least, supports the assumption of the band shift. In the course of these analyses, it became clear that the broadness as well as the shape of bands at the same band regions was variable between samples. The reason is not clear, except that an effect by the environment surrounding any particular conformation is conceivable.

The cause of the scattering of data is not simple. Firstly, the effect of the scattering of the incident beam would not have been the same for all measurements, since it was inevitable that samples used were either in the form of powders with different grain sizes or films. Secondly, errors are inevitably introduced during the resolving of curves, particularly for those comprising heavily overlapped bands.

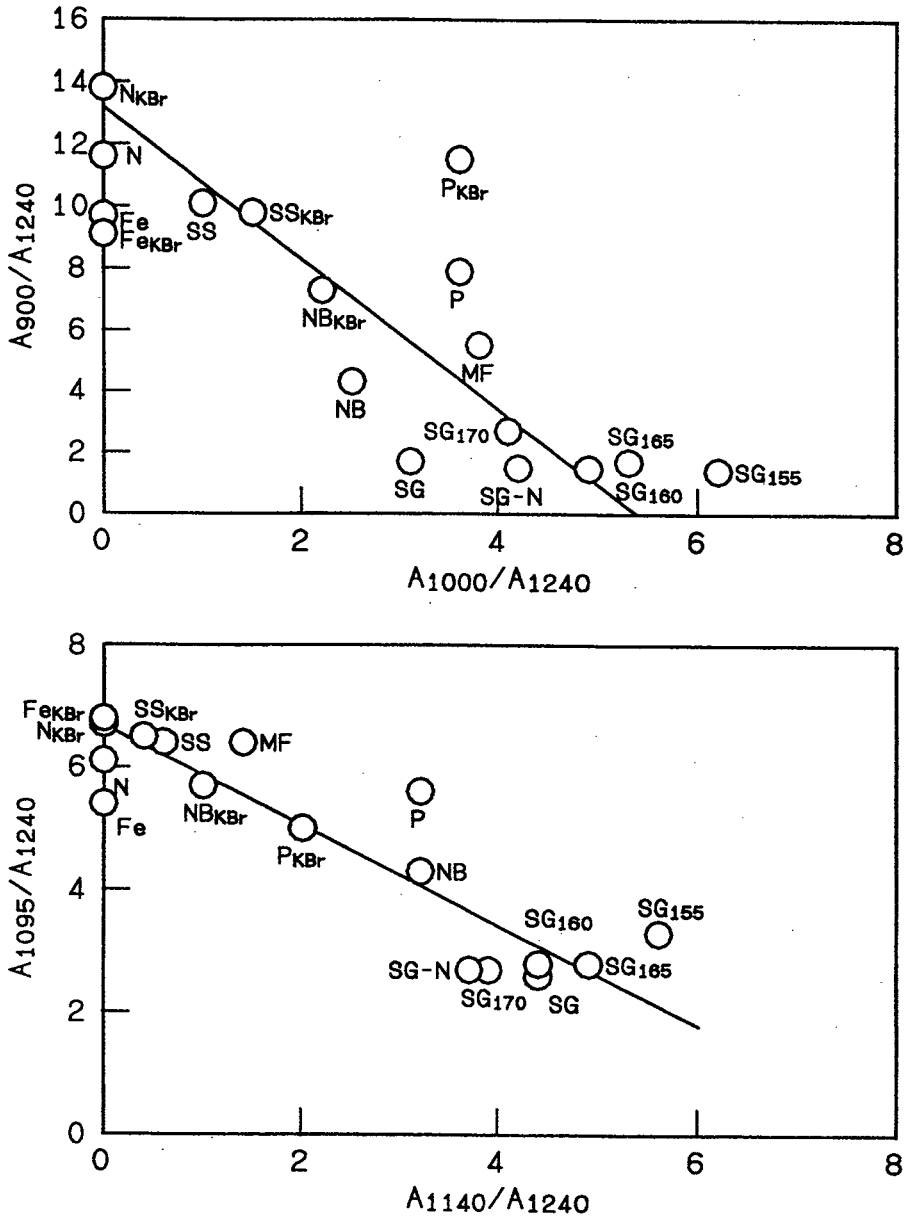

Figure 2–4 Plot of relative absorption intensities. Upper:A_{900}/A_{1240} vs. A_{1000}/A_{1240}. Lower:A_{1095}/A_{1240} vs. A_{1140}/A_{1240}.

Notations are the same as in *Figure 2–3*

Leaving aside these problems, the way of plotting in *Figure 2–4* might be a semi–quantitative measure for higher–order structure of POM crystals. Polyoxymethylene ranks with the most highly crystalline polymers, and its degree of crystallinity, determined by the X–ray method, would not be less than 60%. In *Figure 2–4*, the plots are distributed over a wide range on the slopes. It could be said that the band shifts are not related to the usual crystallinity.

2.4 Conclusion

In this chapter, the infra–red spectra of various POM specimens of different origin and/or sample processing are surveyed in the 1300–550 cm^{-1} region. Infra–red bands are separated for each spectrum and changes of their intensity characterize each bands. Thus the infra–red bands of POM are classified into two types, *i.e.*, sample–sensitive and sample–insensitive. Relationships among the sample–sensitive bands suggest the change of spectra is caused by the frequency shifts of those bands, even though such a large frequency shift has never been seen so far.

References

1 R. G. Brown, *J. Appl. Phys.*, **34**, 2382 (1963)

2 J. L. Koenig and D. E. Witenhafer, *Makromol. Chem.*, **99**, 193 (1966)

3 V. Zamboni and G. Zerbi, *J. Polym. Sci. (C)*, **7**, 153 (1964)

4 E. F. Oleinik and N. S. Enikolopyan, *J. Polym. Sci. (C)*, **16**, 3677 (1968)

5 L. Terlemezyan, M. Mihailov, P. Schmidt and B. Schneider, *Makromol. Chem.*, **179**, 807 (1978)

6 L. Terlemezyan, M. Mihailov, P. Schmidt and B. Schneider, *Makromol. Chem.*, **179**, 2315 (1978)

7 M. Iguchi, *Br. Polym. J.*, **5**, 195 (1973)

8 M. Iguchi and I. Murase, *J. Crystal Growth*, **24/25**, 596 (1974)

9 M. Iguchi, I. Murase and K. Watanabe, *Br. Polym. J.*, **6**, 61 (1974)

10 M. Iguchi, *Makromol. Chem.*, **177**, 549 (1976)

11 T. Mashimoto, T. Sakai and M. Iguchi, *J. Phys. (D)*, **12**, 1567 (1979)

12 M. Iguchi, H. Kanetsuna and T. Kawai, *Makromol. Chem.*, **176**, 63 (1975)

13 M. Iguchi and I. Murase, *Makromol. Chem.*, **176**, 2113 (1975)

14 M. Iguchi, *J. Polym. Sci. (A-1)*, **8**, 1022 (1970)

15 P. G. Guest in K. C. Chang and R. Y. M. Huang, *J. Appl. Polym. Sci.*, **13**, 1459 (1969), Numerical Methods of Curve Fitting, Cambridge University Press, (1961)

16 G. Zerbi and P. J. Hendra, *J. Mol. Spectrosc.*, **27**, 17 (1968)

17 Y. Matsui, T. Kubota, H. Tadokoro and T. Yoshihara, *J. Polym. Sci. (A)*, **3**, 2275 (1965)

Chapter 3

Vibrational Spectra of Polyoxymethylene and Polyoxymethylene-d_2 Single Crystals

3.1 Introduction

Polyoxymethylene (POM) is known as trigonal crystalline polymer consisting of chains basically of a 9/5 helical conformation.[1-3] Another modification, metastable orthorhombic POM (*o*-POM) crystal consisting of 2/1 helical chains, was first obtained by Mortillario *et al.*, through polymerization of formaldehyde in aqueous solution[4] and was recently found in a cationic polymerization system of trioxane in cyclohexane solution.[5] Needle-like crystals of POM[6,7] are known as trigonal single crystals having ultra-high perfection, consisting of extended 9/5 helical chains. Their highly ordered structure has been proved by X-ray diffraction, DSC and other measurements.[8-10] Other typical trigonal single crystals are lamellar crystals, recrystallized from dilute solution, which consist of regularly folded-chains.[11,12]

Vibrational spectra of trigonal POM (*t*-POM), as well as those of *o*-POM, have been of interest and a number of studies have been published. The assignment of the infra-red and Raman bands has by now been almost established, with reference to a normal modes analysis.[13] It was reported first by Zamboni and Zerbi that the infra-red spectrum of *t*-POM changes with specimen treatment in the 1200-900 cm^{-1} region.[14] Bands in this region were studied in detail by Oleinik and Enikolopyan by bringing in a series of oligomeric homologues[15]: it was assumed that the bands at 1238 and 903 cm^{-}

[1] were sensitive to the regular structure and were characteristic of a long *gauche* sequence, whereas "additional" bands at 985 and 1130 cm^{-1} were affiliated to a planar zig-zag conformation in non-crystalline part. Terlemezyan *et al.* studied the structure of the specimen obtained from cationic polymerization systems of trioxane in various solvents.[16-18] Infra-red spectra were classified into two types. It was concluded that these changes in the infra-red spectra were related to conformational defects in helical chains.

The infra-red spectral changes between the needle-like and solution-grown crystals and other specimens of *t*-POM were investigated by Shimomura and Iguchi.[19] All of the infra-red bands of the needle-like crystals were assignable to the optically active fundamentals of the regular 9/5 helix of the POM molecule, and no additional bands appeared in the spectrum. For other POM specimens, on the contrary, the spectral pattern in the 1200-900 cm^{-1} region exhibited substantial variation depending on the state and/or the route of processing of the samples. These remarkable spectral changes were thought to be related to some difference in the crystalline part.

Fawcett proposed another interpretation of the changes in the infra-red spectra.[20] These spectral changes were due to a difference in the chain packing, *i.e.*, some molecules slid along the *c*-axis and intermolecular interactions were different as a result. Terlemezyan *et al.*[21] argued against Fawcett's interpretation using copolymer of trioxane and dioxolane in which slides along the *c*-axis always exist. In spite of these works, interpretation of the difference in the infra-red spectra of *t*-POM is not clear so far.

In this chapter, infra-red and Raman spectra of two typical *t*-POM single crystals, *i.e.*, extended-chain needle-like crystals and folded-chain solution-grown single crystals, are discussed in detail from a spectroscopic

viewpoint. The characteristics of the sample-sensitive bands of *t*-POM mentioned in Chapter 2 will be clarified. Vibrational spectra of the needle-like and the solution-grown crystals of deuterated polyoxymethylene (POM-d_2) are also measured and discussed.

3.2 Experimental

3.2.1 *Samples*

Needle-like crystals were prepared in a cationic polymerization system of trioxane in cyclohexane solution under similar conditions as described in literature.[7] Some samples were subjected to boron trifluoride etching[8] to disrupt the original radial assembly.

Solution-grown crystals were prepared from the needle-like crystals, Delrin 500 of E. I. Du Pont de Nemours & Co. and other commercial acetal resins. Folded-chain crystals were recrystallized from dilute bromobenzene solution at various temperatures, typically from 0.5 wt% solution at 130°C. After filtration, crystals were washed and freeze-dried using benzene. Since the needle-like crystals were insoluble in boiling bromobenzene, they had to be dissolved first in hexafluoroacetone sesquihydrate to destroy their highly crystalline structure and precipitated in acetone prior to the recrystallization from bromobenzene solution. Lamellar crystals grown from cyclohexanol solution were also examined.

Deuterated paraformaldehyde was used as the starting material of POM-d_2 synthesis. Trioxane-d_6 was prepared from deuterated paraformaldehyde and heavy water catalyzed by silicotungstic acid. Needle-like crystals of POM-d_2 were prepared from trioxane-d_6 through the same

procedures as in the case of the normal POM needle-like crystals. The boron trifluoride etching was not performed in this case. Solution-grown crystals of POM-d_2 were prepared from bromobenzene solution of the polymer obtained in the cationic polymerization system described above.

3.2.2 *Measurement of Infra-red, Far Infra-red and Raman Spectra and Wide Angle X-ray Diffraction*

A Jasco Model 701G infra-red spectrometer was used. Sampling was performed by the Nujol mull method in order to avoid mechanical deformation during sample preparation, since by grinding with KBr powder, the solution-grown crystals transform very easily to another structure having different morphology, causing a significant spectral change. The recorded infra-red spectra were converted to absorbance scale and the background due to the mulling reagent was subtracted using a personal computer.

A Hitachi Model FIS-3 far infra-red spectrometer was used. Powder samples were mixed with paraffin wax, spread on a silicon plate, and subjected to measurement.

Powder samples were sealed in glass ampoules and Raman spectra were measured with a Jasco Model R-500 double monochromator using the 514.5 nm line from an Ar^+ laser as the excitation source.

A Phillips Model PW1700 system with a graphite monochromator was used to record wide angle X-ray diffraction. Data were also processed using the personal computer.

3.3 Results and Discussion

3.3.1 *Needle-like and Solution-grown Crystals of Polyoxymethylene*

In ref. 19, it was found that the infra-red spectrum of the needle-like crystals was in good accordance with the results of the normal mode analysis,[13] while some bands of the solution-grown crystals shifted substantially from the positions of the corresponding bands of the needle-like crystals. Rather complicated spectral profiles of other *t*-POM specimens were able to be explained as the superposition of these two extreme spectra. In *Figure 3-1*, the infra-red spectra (1300-400 cm^{-1} region) of *t*-POM in the two extreme crystalline morphologies, *i.e.* the extended-chain (needle-like) crystals (ECC) and the folded-chain (solution-grown) crystals (FCC), are compared with each other. Since the solution-grown crystals are very easy to change by mechanical deformation during pelletization into KBr pellet, the Nujol mull method was adopted in this study.

The difference in spectra between the two cases is quite obvious. In the spectrum of the solution-grown crystals (lower), the 1093 and 895 cm^{-1} bands of the needle-like crystals (upper) almost disappear and, instead, new bands appear at 1138 and 1000 cm^{-1}. The other bands are common in both spectra. Solution-grown crystals recrystallized from the needle-like crystals and other commercial acetal resins give almost the same infra-red spectra as that shown in *Figure 3-1* (lower). The spectrum of the solution-grown crystals recrystallized from cyclohexanol solution is also the same as those of the other solution-grown crystals. From these facts, it is evident that the spectral change between the needle-like and solution-grown crystals can be ascribed not to a difference in chemical structure but to a difference in

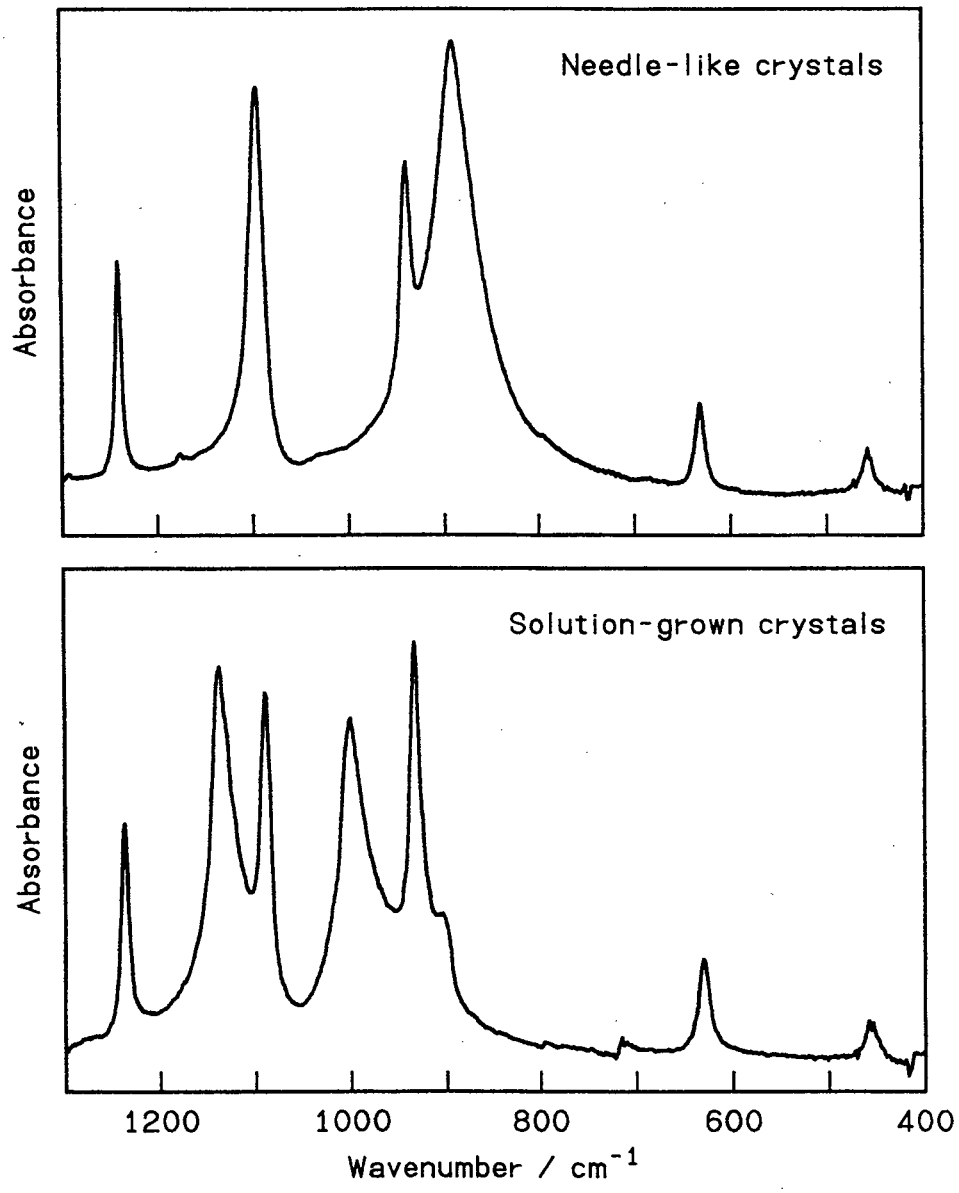

Figure 3–1 Infra–red spectra of polyoxymethylene crystals.

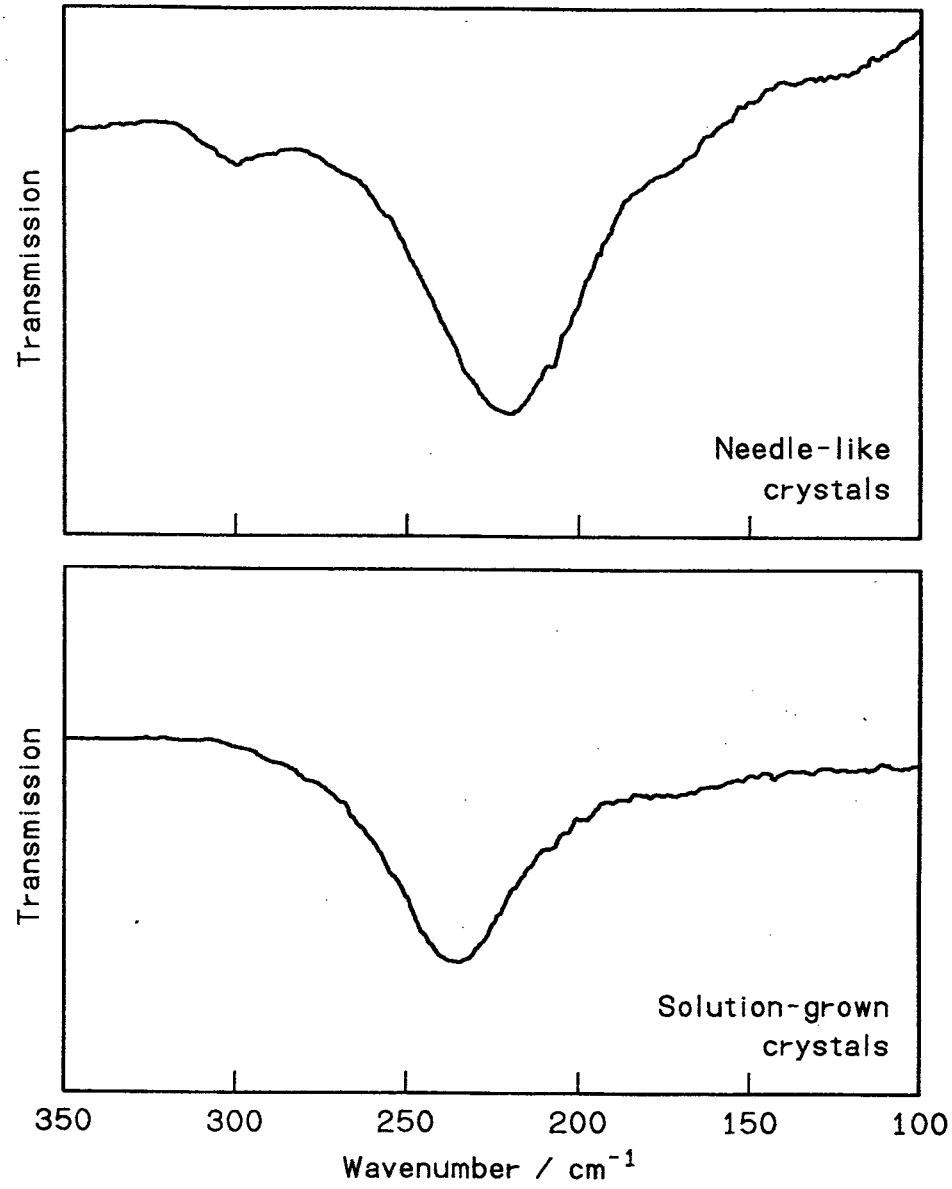

Figure 3–2 Far infra-red spectra of polyoxymethylene crystals.

morphological structure. The same comparison has been made also for the far infra-red region (*Figure 3-2*). The difference is also clear. The band at 220 cm^{-1} of the needle-like crystals shifts to 234 cm^{-1} in the spectrum of the solution-grown crystals. The weak bands around 300 cm^{-1} in the needle-like crystals are due to a small amount of orthorhombic form contained (a few mol%).

Raman spectra of these two samples are reproduced in *Figure 3-3*. In contrast to the infra-red spectra, no significant difference is found so far as the peak positions are concerned.

Figure 3-4 shows the wide angle X-ray diffraction patterns of these two crystals. The sharpness of the X-ray diffraction peaks of the needle-like crystals proves the very high crystalline perfection. The crystallinity of the solution-grown crystals is also nearly as high as for polymer crystals, as is recognized from the small background scattering due to the amorphous part. Although the sharpness of the peaks is not the same, the reflections of the two crystals are basically identical. This means that as far as the unit cell structure is concerned these two crystals are of the same trigonal phase consisting of 9/5 helices.

The optically active (or the zone-centre) molecular vibrations of the 9/5 helix are classified into A_1, A_2, E_1, E_2, E_3 and E_4 species, where the A_2 and E_1 modes are infra-red-active, the A_1, E_1 and E_2 modes are Raman-active and the E_3 and E_4 are inactive in both infra-red and Raman spectra. The vibrational spectra of the needle-like crystals are readily assignable in accordance with the established normal mode calculations,[13] which have been based on the spectral data measured on highly crystalline and highly oriented POM resins. In *Table 3-1*, the observed wavenumbers of the infra-red bands and the corresponding calculated frequencies of the A_2 and E_1 species are

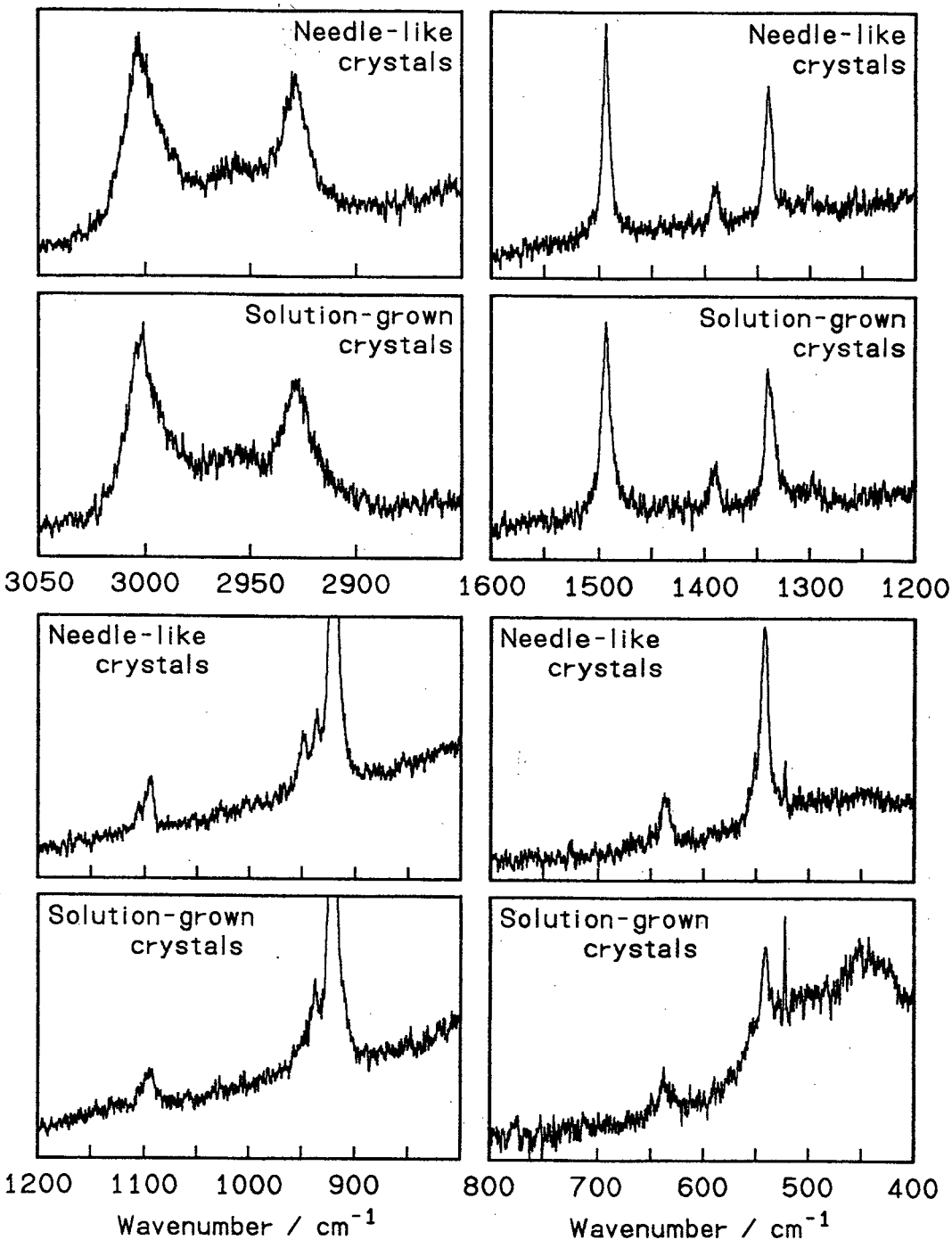

Figure 3–3 Raman spectra of polyoxymethylene crystals.

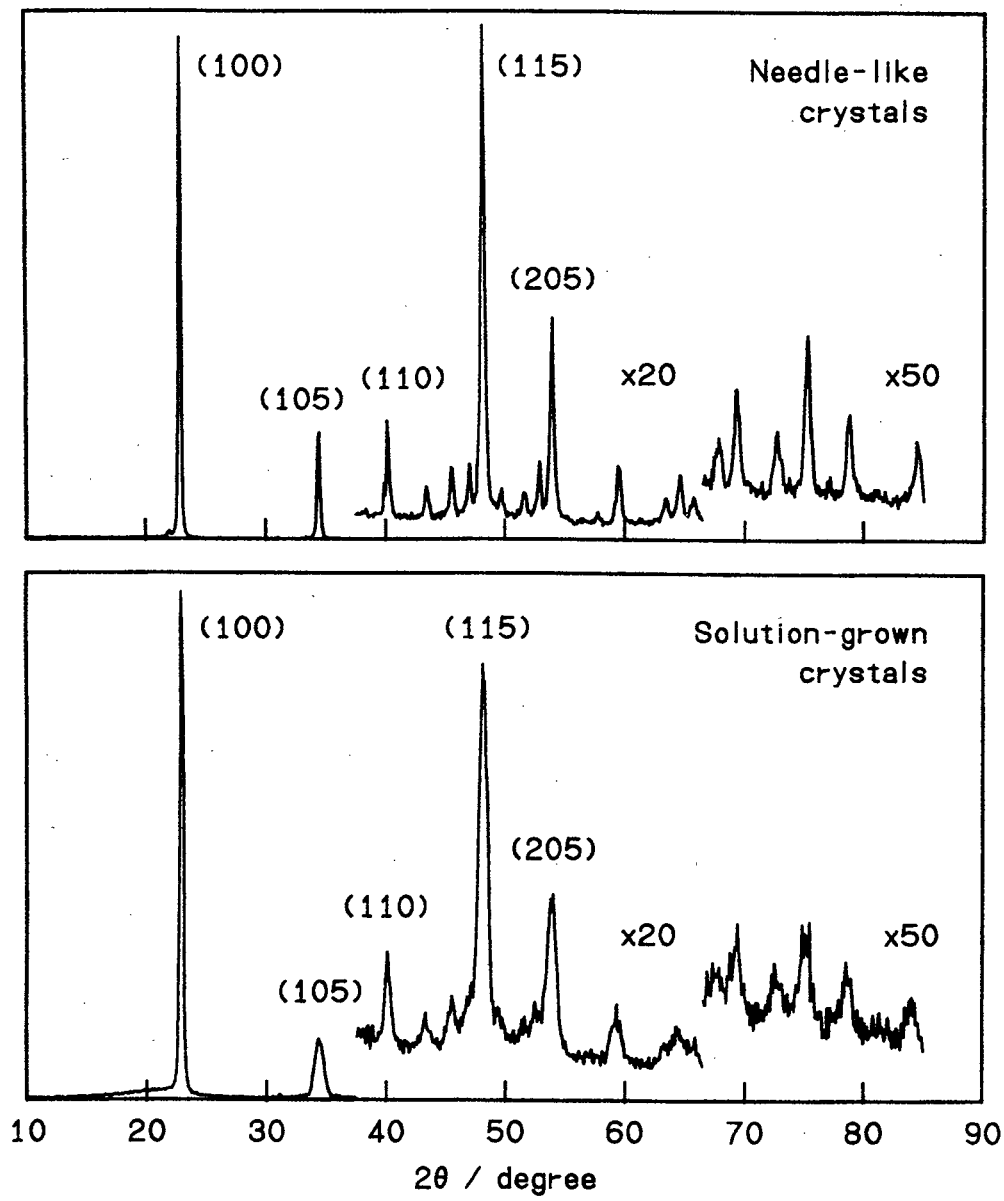

Figure 3–4 X–ray diffraction diagrams of polyoxymethylene crystals. The indices of main reflections of the trigonal lattice are described.

Table 3–1 Vibrational bands of trigonal polyoxymethylene

Species	Calculated (cm^{-1})	Observed (cm^{-1})			
		Infra–red		Raman	
		Needle–like	Solution–grown	Needle–like	Solution–grown
A_1	2924	Inactive		2928 s	2928 s
	1508			1493 s	1493 s
	1330			1339 m	1339 m
	916			921 vs	922 vs
	587			542 m	540 w
A_2	2977	—	—	Inactive	
	1425	1385 vw	1385 vw		
	—	—	1138 s		
	1118	1093 s	—		
	—	—	1000 s		
	922	895 vs	(905 vw)		
	—	—	234		
	237	220	—		
E_1	2982	2999 w	2998 w	3003	3003
	2936	2928 m	2926 m	—	—
	1506	1470 vw	1470 vw	—	—
	1407	1435 vw	1435 vw	—	—
	1318	—	—	1300 w	1298 vvw
	1169	1240 m	1240 m	—	—
	1072	1093 s	1093 m	1095 m	1095 m
	930	938 m	935 m	937 w	937 w
	634	633 w	633 w	636 w	636 w
	483	457	460	—	—
	22	—	—	—	—

summarized. The observed and calculated frequencies of the Raman-active A_1 and E_1 modes are also listed (E_2 modes are omitted here). No significant difference is found between the A_1 and E_1 bands of the two samples. In Chapter 2, complementary relationships of the intensities for the 1138 and 1093 cm^{-1} band pair and the 1000 and 895 cm^{-1} band pair in the infra-red spectra have been found among various POM specimens different in origin as well as in history of sample processing.[19] From this fact and the result given in *Table 3-1*, the infra-red spectral changes of *t*-POM might be explained as follows. The 895 and 220 cm^{-1} bands and one of the overlapping components around 1093 cm^{-1} of the needle-like crystals shift, respectively, to 1000, 234 and 1138 cm^{-1} in the solution-grown crystals; on going from the needle-like to the solution-grown crystals, some of the A_2 bands shift towards the high-frequency side, while the other bands remain unshifted. The symmetry species of the infra-red bands of the needle-like crystals have been determined by polarization measured on highly oriented film specimens. In contrast, the above-mentioned infra-red bands characteristic of solution-grown crystals remain unassigned because of the lack of polarization data.

To check the species of the unassigned, shifted bands of the solution-grown crystals, the infra-red spectra of random and plane-oriented solution-grown crystals were measured. The latter sample was prepared by pressing a powder of the solution-grown crystals between two KBr windows with a small amount of liquid paraffin. In this process, the plate-shaped crystals are partly oriented with *c*-axis directing normal to the window surface (a plane-orientation). On measuring the transmission spectrum of this sample, the incident infra-red radiation is nearly parallel to the *c*-axis, so that the *c*-polarized A_2 bands should diminish compared with the spectrum taken on a randomly oriented powder sample. The degree of plane orientation decreases

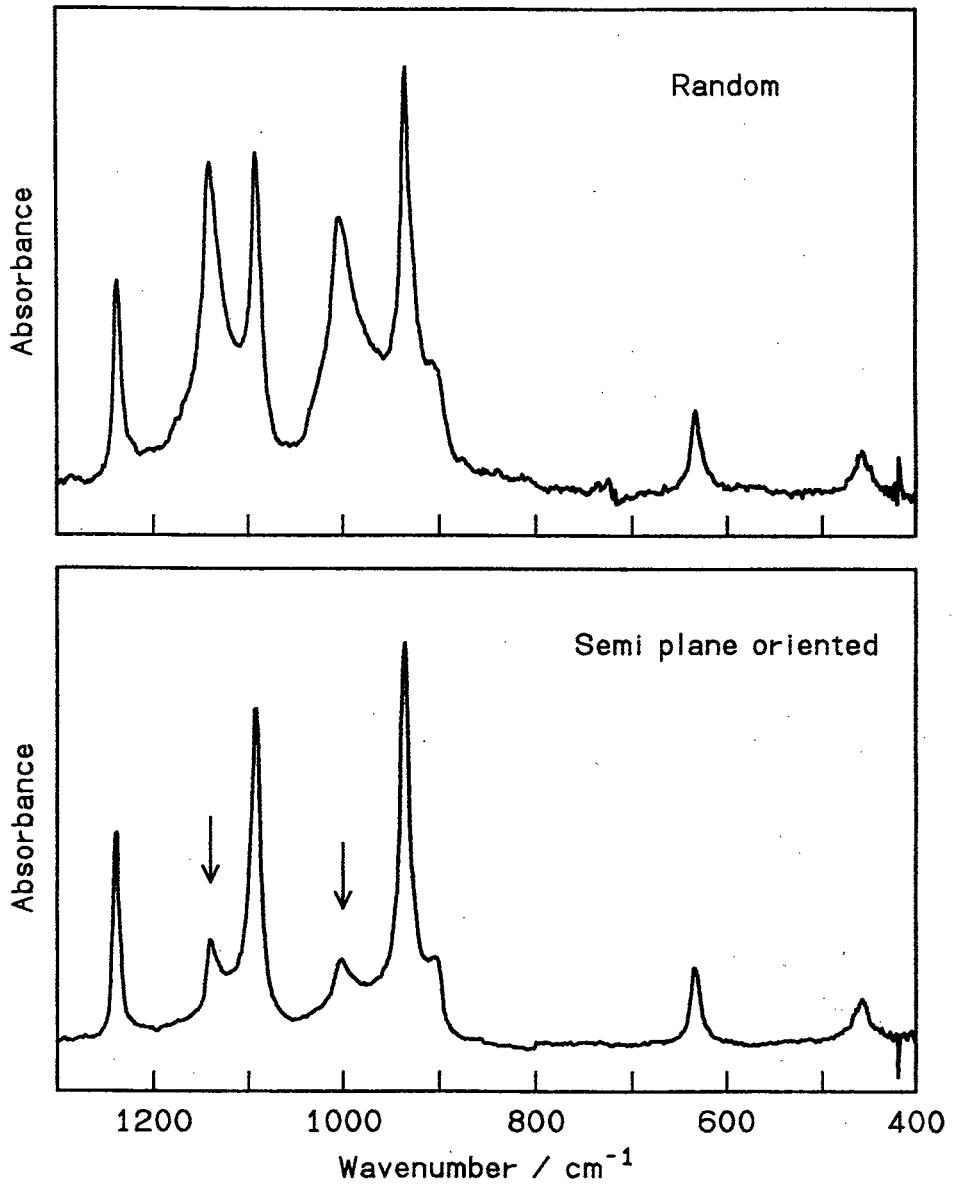

Figure 3–5 Infra–red spectra of random and plane–oriented solution–grown crystals of polyoxymethylene.

with increasing thickness of mulled powder between the windows. By insertion of a spacer of sufficient thickness, randomly oriented sample was prepared.

Figure 3–5 shows the infra–red spectra of the solution–grown crystals in a random and a semi–plane orientation. The absorption bands of the semi–oriented sample at 1138 and 1000 cm^{-1} are much weaker than those of the random sample compared with the other five E_1 bands. This means that the unassigned bands at 1138 and 1000 cm^{-1} should be classified to the A_2 mode. This result also supports the hypothesis that the difference in the infra–red spectrum among various *t*–POM samples is caused by significant frequency shifts of some of the A_2 bands on changing the morphology between the ECC and the FCC types.

It should be noted that the magnitude of the frequency shift of the A_2 band is closely related to the band intensity. Namely, the stronger is the band the greater is the bandshift (see *Table 3–1*).

3.3.2 *Needle–like and Solution–grown Crystals of Polyoxymethylene–d_2*

In order to get other spectral evidence, deuterated POM samples were synthesized and their vibrational spectra were examined. During the synthesis of the needle–like crystals, an orthorhombic modification was sometimes generated as a by–product.[22] Though the X–ray diffraction pattern of the needle–like crystals of POM–d_2 indicates contamination of a few per cent of the orthorhombic form, it does not interfere with the analysis of the vibrational spectra.

Figure 3–6 shows the infra–red spectra of *t*–POM–d_2. As expected, a remarkable difference is found between the two crystals. Although the

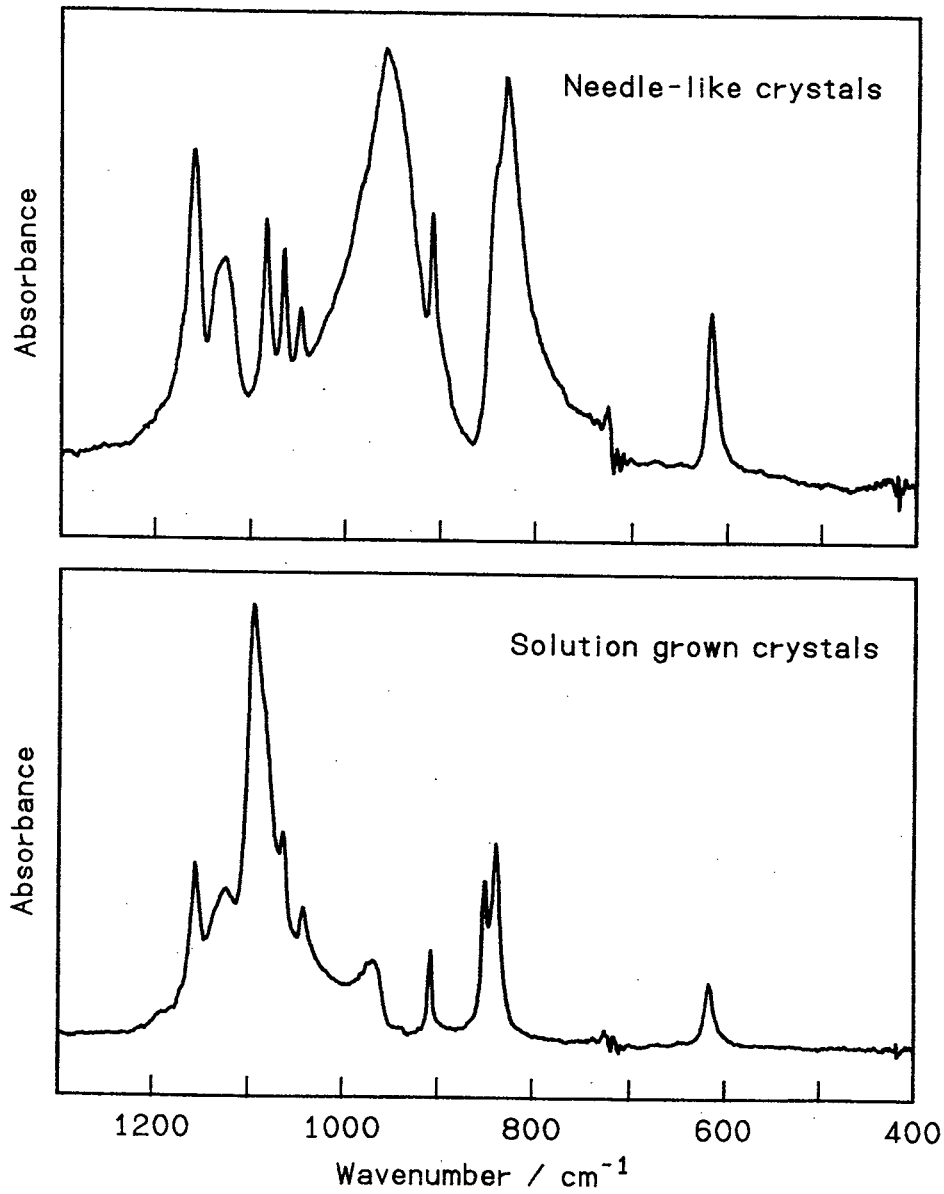

Figure 3–6 Infra–red spectra of polyoxymethylene–d_2 crystals.

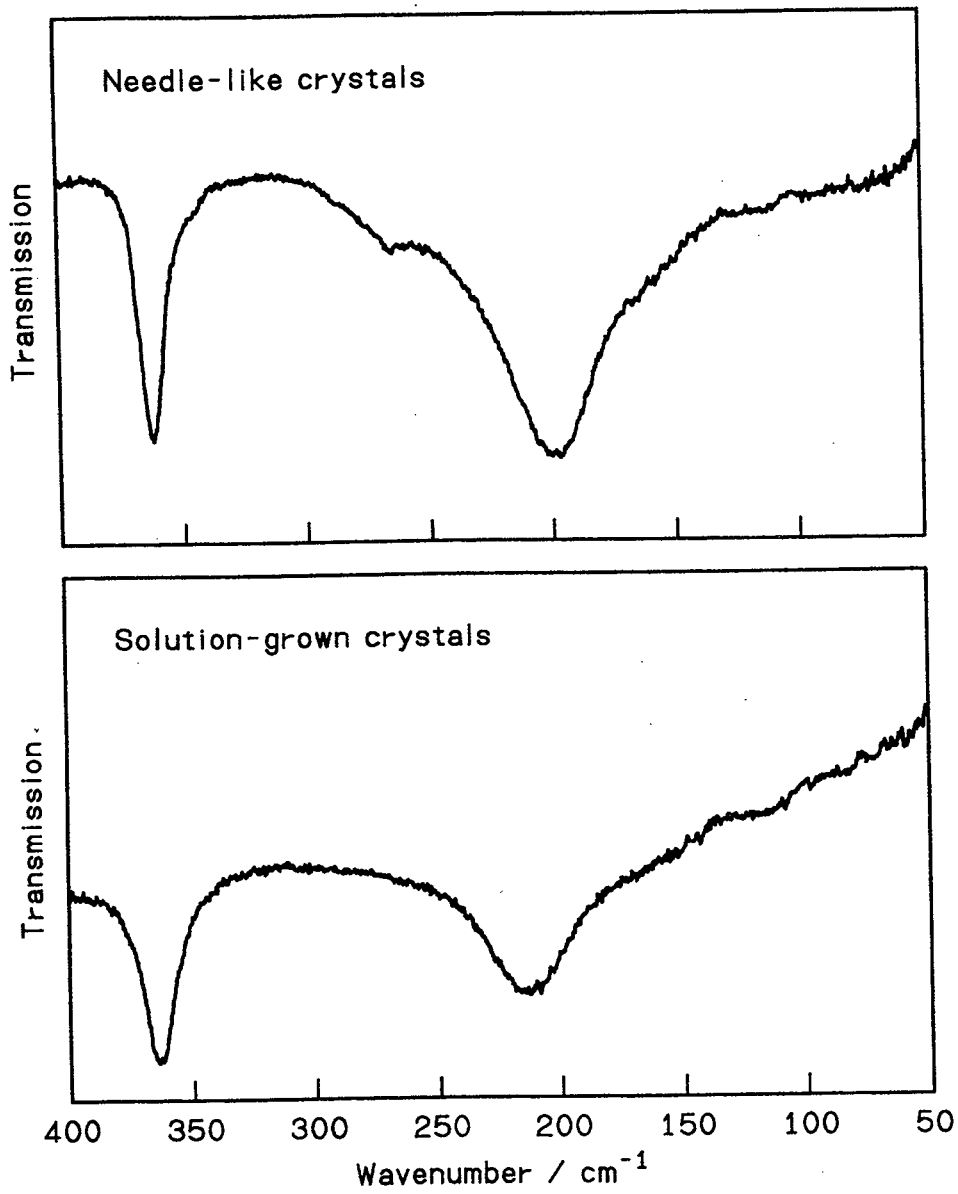

Figure 3–7 Far infra–red spectra of polyoxymethylene–d_2 crystals.

spectra are more complicated than those of normal POM, the bands of the needle-like crystals are readily assignable with reference to the literature.[13] The far infra-red spectra of both samples were also measured (*Figure 3-7*). Here the difference is rather simple, that is, the band at 365 cm^{-1} is common and the 199 cm^{-1} of the needle-like crystals shifts to 214 cm^{-1} in the solution-grown crystal. *Figure 3-8* shows the Raman spectra of *t*-POM-d_2. Like normal POM, the bands of the two crystals appear at the same positions.

The observed frequencies of the infra-red bands and the corresponding calculated values are listed in *Table 3-2*. The Raman bands of *t*-POM-d_2 are also listed (E_2 modes are omitted). The bands assigned to the A_2 modes, at 958, 830 and 199 cm^{-1} of the needle-like crystals, almost disappear in the solution-grown crystals and new bands appear at 1095, 850 and 214 cm^{-1}. In contrast, the bands of the A_1 and E_1 modes appear at the same positions.

Figure 3-9 shows the infra-red spectra of random and plane-oriented solution-grown crystals of *t*-POM-d_2. The bands at 1095 and 850 cm^{-1} diminish remarkably in the semi-oriented sample and are assigned to the A_2 species. There is an unassigned band at 969 cm^{-1} in both crystals. This band may be due to the amorphous or folding part. Because of overlapping, weak bands at around 1048-1042 cm^{-1} cannot be assigned. Thus, it is concluded that the A_2 bands of the POM-d_2 needle-like crystals (958, 830 and 199 cm^{-1}) shift to 1095, 850 and 214 cm^{-1}, respectively, in the spectra of the solution-grown crystals. For the deuterated POM, the A_2 bandshifts are proportional to the band intensities, as is seen in normal POM.

From these results, the changes in the vibrational spectra of *t*-POM, and *t*-POM-d_2 as well, are summarized as follows. Two extreme crystals, the ECC and the FCC, give quite different infra-red spectra, though they give essentially the same X-ray diffraction. The infra-red spectra of other POM

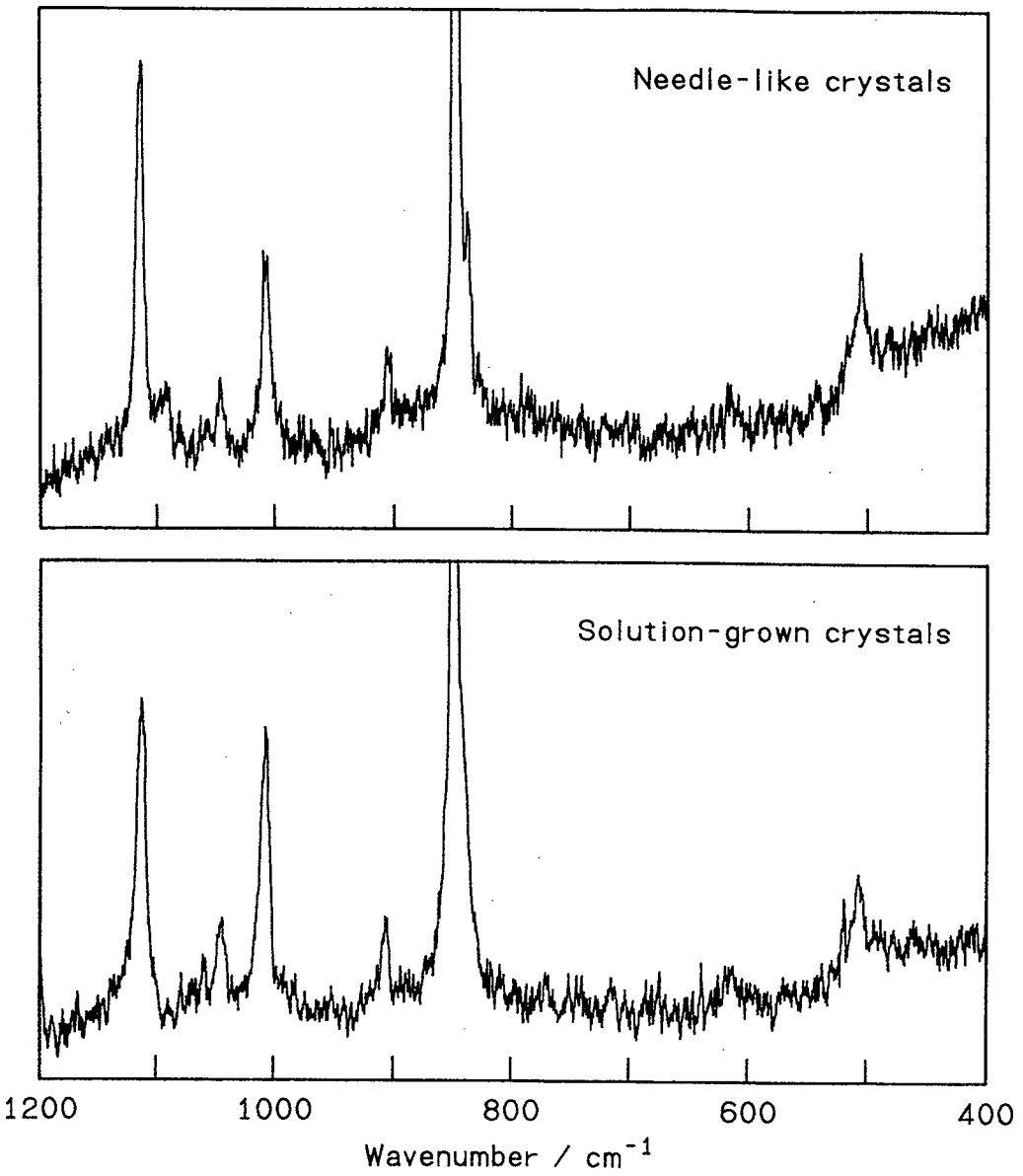

Figure 3–8 Raman spectra of polyoxymethylene–d_2 crystals.

Table 3–2 Vibrational bands of trigonal polyoxymethylene–d_2

Species	Calculated (cm^{-1})	Observed (cm^{-1}) Infra–red		Raman	
		Needle–like	Solution–grown	Needle–like	Solution–grown
A_1	2121	Inactive		—	—
	1126			1115 s	1114 s
	1013			1009 m	1008 s
	828			850 vs	850 vs
	557			506 m	507 w
A_2	2193	—	—	Inactive	
	—	—	1095 vs		
	1154	1048 w	1042 w		
	—	—	969 m		
	1026	958 vs	—		
	—	—	850 m		
	769	830 vs	—		
	—	—	214		
	212	199	—		
E_1	2207	—	—	—	—
	2121	—	—	—	—
	1178	1159 s	1156 m	—	—
	1145	1127 m	1124 m	—	—
	1047	1083 m	1083 sh	—	—
	1044	1065 m	1063 m	—	—
	916	908 m	907 m	907 w	907 m
	810	840 sh	839 s	838 w	— sh
	618	617 m	616 m	617 vvw	616 vvw
	372	365	364	—	—
	21	—	—	—	—

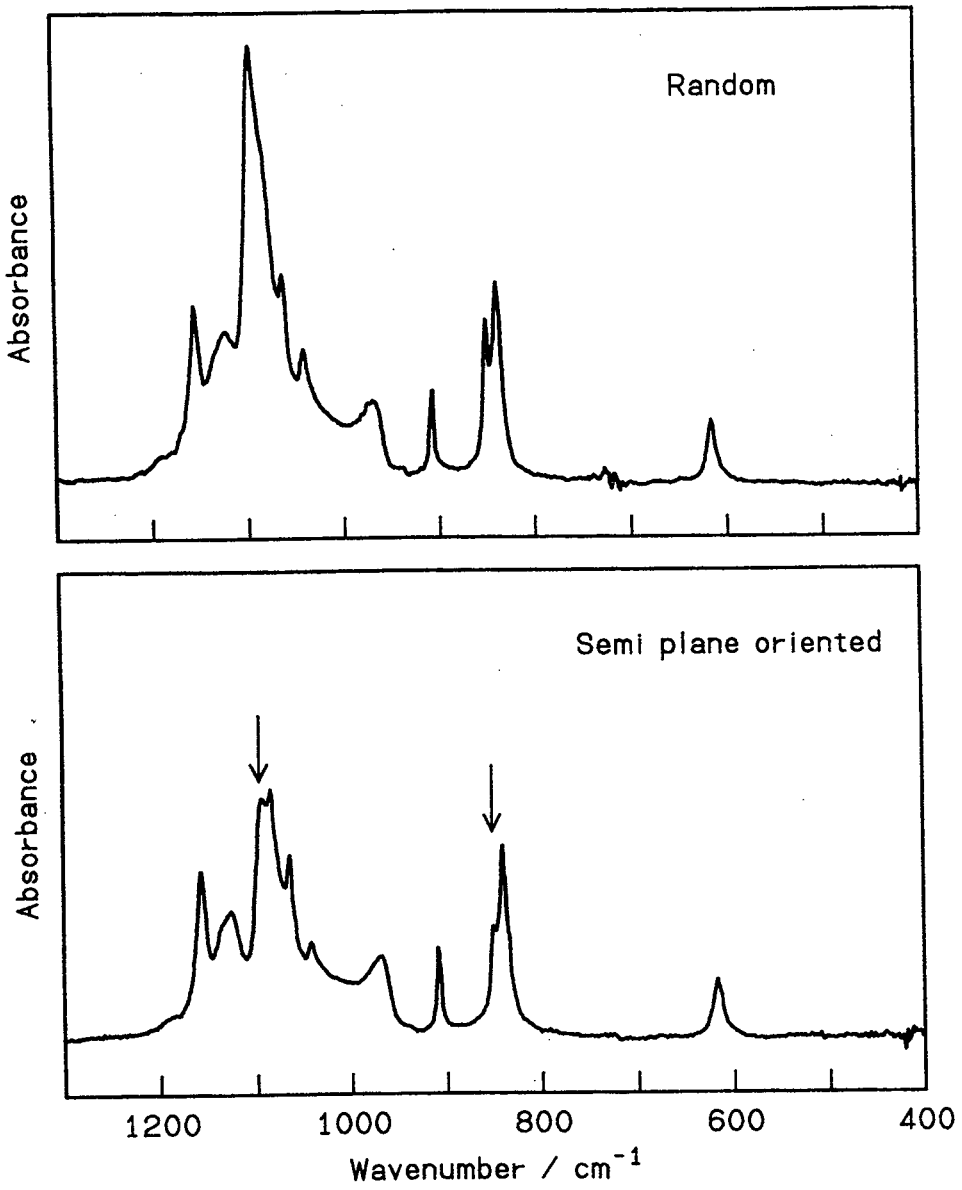

Figure 3–9 Infra–red spectra of random and plane–oriented solution–grown crystals of polyoxymethylene–d_2.

samples are reproduced by the superposition of the spectra of the two extremes. Only the A_2 modes of the ECC shift towards the high-frequency side in the FCC and the other modes, A_1, E_1 and E_2, show no difference among specimens.

In considering the origin of the specific infra-red spectrum of the FCC, possibility of another crystal modification other than the previously known trigonal and orthorhombic forms must be checked first. The X-ray diffraction pattern and the Raman spectrum of the solution-grown crystals are of the typical trigonal form.

Fawcett proposed a model of structural inhomogenities in *t*-POM,[20] where some chains in the lattice slid by half of the pitch of the repeating unit along the *c*-axis. He supposed that the difference in intermolecular interactions caused the changes in the infra-red spectrum. Terlemezyan and Mihilov denied this possibility using trioxane-dioxolane copolymer.[21] Solution-grown crystals of ethylene oxide copolymer and tetramethylene oxide copolymer were also examined by the author. In the crystalline part of the copolymers, chains in some parts are well-aligned and chains in other parts slid each other. Thus, the spectra of copolymers should be different from that of ECC nor FCC. However, in the infra-red spectra of the FCC of the copolymers, the bands at 1138 and 1000 cm^{-1} were observed and only a shoulder was found at about 900 cm^{-1}. These results mean that Fawcett's interpretation of the spectral change is not appropriate. Also, conformational defects in the $\{CH_2\}_2$ or $\{CH_2\}_4$ unit cannot make the shifts of the A_2 modes.

Oleinik and Enikolopyan[15] thought that the bands at 1138 and 1000 cm^{-1} were due to defects such as planar zig-zag conformations in non-crystalline parts. Because of its high crystallinity and small amount of non-crystalline part, this cannot explain the shift in the FCC.

Terlemezyan *et al.*[18] explained the bands as follows. The bands at 1128 and 988 cm^{-1} arise from short regular *gauche* conformations, in other words, from a high content of conformational defects such as *trans* form in helix. The band at 900 cm^{-1} was related to long regular *gauche* conformations. Such defects might change the selection rules and the appearance of new bands might be expected, but the disappearance of the 900 cm^{-1} band and the diminishing of the 1093 cm^{-1} band could not be explained. From the other point of view, fewer defects would exist in the solution–grown crystals than in melt–crystallized film, since the solution–grown crystals were prepared by isothermal crystallization from dilute solution and were expected to have better perfection than the melt film. Experimentally, the melt crystallized film and other defective specimens showed stronger absorption bands at 1093 and 900 cm^{-1}. Thus the spectral change among various POM specimens could not be interpreted by conformational defects such as planar zig–zag forms in the crystalline part.

By the normal–mode calculations, a small difference of helical pitch (or conformation), which is not detected by X–ray diffraction, cannot make such large shifts (up to about 100 cm^{-1}) of the A_2 modes but have to cause small shifts for all species to both high– and low–frequency sides. Such differences cannot explain the spectral change of the FCC *t*–POM.

Another possibility of spectral change, namely splitting of bands, should be considered. The extent of the frequency shifts of *t*–POM are much larger than those of splittings due to interchain interactions observed in the orthorhombic form. All three A_2 bands shifted to the high–frequency side and no bands appeared in the lower region in the spectrum of the FCC. From these facts, it is difficult to interpret the spectral change as the splitting of the A_2 bands. Then next possibility was a mixing with modes of other species. If

mixing of modes did occur in the FCC, some A_1 bands should be found in the infra-red spectrum and A_2 bands should be found in the Raman spectrum. However, in the vibrational spectra of the FCC, as well as the ECC, the selection rule is kept and mixing of modes does not occur.

3.4 Conclusion

The changes in the vibrational spectra of *t*-POM and *t*-POM-d_2 are very interesting phenomena. The needle-like and solution-grown crystals, which give the same X-ray diffraction patterns, show quite different vibrational spectra. In the spectra of the FCC, only the A_2 bands having transition dipole parallel to the chain axis shift to the high-frequency side and all bands of other species, A_1 and E_1, are the same as those of the ECC. The spectra of the POM specimens between the two extremes could be reproduced as the superposition of the two spectra.

This specific bandshift cannot be explained within the framework of conventional vibrational spectroscopy, and it might be caused by the difference in morphology. A new concept, *e.g.*, an interaction between transition dipole moments, might be necessary to explain the spectral changes of *t*-POM and *t*-POM-d_2.

References

1 H. Tadokoro, S. Yasumoto, S. Murahashi and I. Nitta, *J. Polym. Sci.*, **44**, 266 (1960)

2 T. Uchida and H. Tadokoro, *J. Polym. Sci. (A-2)*, **5**, 63 (1967)

3 G. Carazzolo, *J. Polym. Sci. (A)*, **1**, 1573 (1963)

4 L. Mortillario, G. Galliazzo and S. Bessi, *Chem. Ind. (Milan)*, **46**, 139 (1964), *ibid* **46**, 144 (1964)

5 M. Iguchi, *Polymer*, **24**, 915 (1983)

6 M. Iguchi, *Br. Polym. J.*, **5**, 195 (1973)

7 M. Iguchi and I. Murase, *J. Crystal Growth*, **24/25**, 596 (1974)

8 M. Iguchi, I. Murase and K. Watanabe, *Br. Polym. J.*, **6**, 61 (1974)

9 M. Iguchi, *Makromol. Chem.*, **177**, 549 (1976)

10 T. Mashimoto, T. Sakai and M. Iguchi, *J. Phys. (D)*, **12**, 1567 (1979)

11 D. C. Bassett, F. R. Dammont and R. Salovey, *Polymer*, **5**, 579 (1964)

12 D. R. Carter and E. Baer, *J. Appl. Phys.*, **37**, 4060 (1966)

13 H. Tadokoro, M. Kobayashi, Y. Kawaguchi, A. Kobayashi and S. Murahashi, *J. Chem. Phys.*, **38**, 703 (1063)

14 V. Zamboni and G. Zerbi, *J. Polym. Sci. (C)*, **7**, 153 (1964)

15 E. F. Oleinik and N. S. Enikolopyan, *J. Polym. Sci. (C)*, **16**, 3677 (1968)

16 L. Terlemezyan, M. Mihailov, P. Schmidt and B. Schneider, *Makromol. Chem.*, **179**, 807 (1978)

17 L. Terlemezyan, M. Mihailov, P. Schmidt and B. Schneider, *Makromol. Chem.*, **179**, 2315 (1978)

18 L. Terlemezyan and M. Mihailov, *Eur. Polym. J.*, **17**, 1115 (1981)

19 M. Shimomura and M. Iguchi, *Polymer*, **23**, 509 (1982)

20 A. H. Fawcett, *Polym. Commun.*, **23**, 1865 (1982)

21 L. Terlemezyan and M. Mihailov, *Polym. Commun.*, **25**, 80 (1984)

22 M. Kobayashi, Y. Itoh, H. Tadokoro, M. Shimomura and M. Iguchi, *Polym. Commun.*, **24**, 38 (1983)

Chapter 4

Vibrational Spectra of Low Molecular Weight Polyoxymethylene

4.1 Introduction

Polyoxymethylene (POM) is known as a typical crystalline polymer and appears in two crystal modifications, the stable trigonal form consisting of the chains in the 9/5 helical conformation[1-3] and the metastable orthorhombic form of a 2/1 helix.[4,5] Vibrational spectra of both modifications, especially of the trigonal form, have been the subject of many studies for years.[6-12] The extended-chain crystal of orthorhombic form was found as a by-product of the synthesis of the needle-like crystals of trigonal POM (*t*-POM).[5,13] Using the newly found orthorhombic single crystal, vibrational spectroscopic studies have been performed on the molecular aggregation state and the solid-state phase transition.[14,15] For the trigonal crystal, the assignment of the infra-red absorption bands and the Raman scattering bands has been established with reference to the normal mode analysis of an infinitely extended polymer chain.[16] Zamboni and Zerbi[6] first reported that the infra-red spectrum in the 1200-900 cm^{-1} region of the *t*-POM changes with processing of the specimens. Infra-red spectral differences among various specimens of *t*-POM, different in origin and/or history of processing, were also investigated by Shimomura and Iguchi.[11]

In Chapter 3, the vibrational spectra of two typical single crystals of *t*-POM were examined and discussed in relation to their morphological structure.[17] One typical crystal is the needle-like crystal,[18,19] which is known as a polymer whisker. It consists of fully extended molecular chains,

and its high crystalline perfection has been proved by various measurements, such as wide angle X-ray diffraction, d.s.c. and thermoluminescence.[20-22] The other typical trigonal crystal is the lamellar crystal, crystallized isothermally from dilute solution, in which molecular chains are folded periodically.[23,24] The infra-red spectra of these two single crystals are quite different from each other and the infra-red spectra of the other *t*-POM specimens are essentially the superposition of these two extreme spectra.[11,17] Though the molecular mechanism was not clear so far, it was concluded phenomenologically that the spectral difference between the extended-chain crystal (ECC) and the folded-chain crystal (FCC) results from the anomalously large shifts of the bands assigned to the infra-red active A_2 symmetry species towards the high-frequency side in the FCC (solution-grown crystal). On the other hand, the vibrations assigned to the other species, Raman active A_1 and E_2 and infra-red and Raman active E_1, show no significant shift among various samples of *t*-POM. Thus, the significant frequency shifts take place only in the infra-red bands with the transition dipole parallel to the chain axis. The wide angle X-ray diffraction patterns of the two crystals were identical, indicating that these trigonal single crystals had the same unit cell structure.

In this chapter, the infra-red and the Raman spectra of low molecular weight POM diacetates (LMW-POM) are presented and discussed in comparison with those of the ECC and FCC of high molecular weight POM. The molecular weight dependence of the spectra of the LMW-POM was examined. The role of the chain folding and/or lamellar structure in the morphology-dependent bandshifts will be discussed. Spectral changes during mechanical deformation of the samples by milling with KBr powder and during the melt crystallization were also examined and discussed.

4.2 Experimental

4.2.1 *Samples*

The needle-like crystal was synthesized in a cationic polymerization system of trioxane.[19] The solution-grown crystal of high molecular weight POM was prepared under the same condition as described in *Chapter 3*.[17]

The LMW-POM samples were prepared from paraformaldehyde.[25] A mixture of commercial paraformaldehyde and acetic anhydride was heated in an autoclave and acetylated LMW-POM was extracted and crystallized using ether, chloroform, benzene or xylene.

As oligomers of lower molecular weight are soluble in $CDCl_3$, n.m.r. spectra were measured and the degrees of polymerization were determined from the signal intensities due to the methyl protons of the acetoxy terminal groups and the methylene protons in the main chain. The degrees of polymerization of the LMW-POM with rather high molecular weight were determined from the intensities of the Raman bands and the infra-red bands due to the terminal groups. The degrees of polymerization of the LMW-POM were determined as 12 to 30 in $\{CH_2O\}$ units, which were in good accordance with the literature.[25]

4.2.2 *Measurement of Infra-red and Raman Spectra, Wide Angle X-ray Diffraction and D.S.C.*

A Jasco model 701G diffraction grating infra-red spectrometer was used. Sampling methods were the Nujol mull and the KBr pellet methods. Since the solution-grown crystal of *t*-POM transforms very easily to another

crystal form and/or another morphology, giving rise to a significant change in the infra-red spectrum, all samples were mixed carefully with Nujol to avoid mechanical deformation and subjected to the measurement. The background due to the mulling reagent was removed by the spectral subtraction technique. Some sample powders were also ground well with KBr powder, pelletized and measured. The KBr pellets were heated at about 200°C on a hot plate and measured again after cooling to room temperature.

For the measurement of Raman spectra, the samples were sealed in glass ampoules and measured with a Jasco model R-500. The 514.5 nm line of an Ar^+ laser was used as the excitation source.

A Philips model PW1700 system with a graphite monochromator was used for wide angle X-ray diffraction measurements. D.s.c. curves were measured by a Perkin-Elmer model DSC-2.

4.3 **Results and discussion**

4.3.1 *Spectra of Low Molecular Weight Polyoxymethylene*

Figure 4-1 shows the wide angle X-ray diffraction patterns of the needle-like crystals, the solution-grown crystals and the LMW-POM specimens. (DP denotes the degree of polymerization.) It is evident that all oligomeric samples were crystalline as well as the high molecular weight POM samples, though the widths of diffraction peaks, which reflect their crystalline perfection, etc., were different from each other. It could be said that the unit cell structure of the LMW-POM was very close to that of the needle-like crystals and the solution-grown crystals, *i.e.*, the trigonal modification consisting of basically 9/5 helical molecules. The Bragg angles

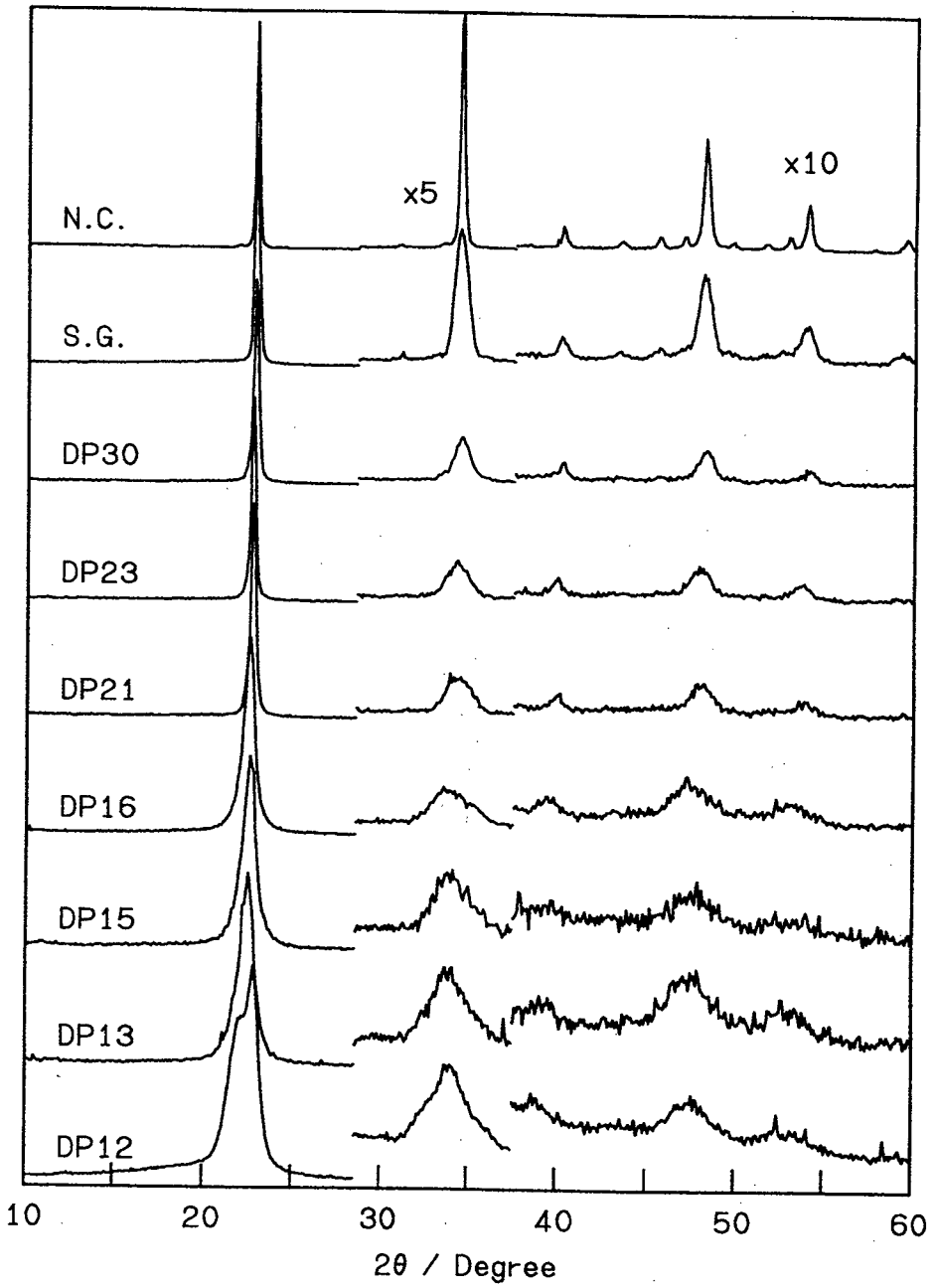

Figure 4-1 X-ray diffraction of various polyoxymethylene specimens.

N.C.:needle-like crystals; S.G.:solution-grown crystals;
DP denotes degree of polymerization

of the diffraction peaks of the LMW–POM, especially of lower degree of polymerization, were a little smaller than those of the high molecular weight POM crystals and the LMW–POM might have a larger unit cell dimension.

D.s.c. curves of the low and high molecular weight POM crystals are reproduced in *Figure 4–2*. Melting point of the LMW–POM specimens were, qualitatively at least, in a good accordance with the degree of polymerization determined by n.m.r. and vibrational spectra. This also indicated that all samples were more or less crystalline, as was found by the wide angle X–ray diffraction. The curve of DP30 showed that this sample had a wide molecular weight distribution compared with the other LMW–POM specimens.

As mentioned in Chapter 3, the changes in the vibrational spectra of the *t*–POM crystals were summarized as follows.[17] Only bands assigned to the A_2 symmetry species of the needle–like crystal (ECC) shift towards the high–frequency side in the spectrum of the solution–grown crystal (FCC). Namely, the bands at 895 and 220 cm^{-1} and one of the overlapping components at 1093 cm^{-1} of the ECC shifted to 1000, 234 and 1138 cm^{-1}, respectively, and the other bands, assigned to the A_1, E_1 and E_2 symmetry species, appeared at the same wavenumbers in both crystals. The spectral change was once ascribed to the effect of the chain folding,[11] *i.e.*, molecular distortion caused by the chain folding penetrates deep into the crystallite and, as a result, disturbs the molecular as well as crystalline structure. It was difficult, however, to explain the spectral change in terms of disorders or defects.[17] In order to obtain more spectral data, the vibrational spectra of the LMW–POM specimens were measured.

In *Figure 4–3*, the infra–red spectra of the LMW–POM specimens measured by the Nujol mull method are compared with those of the two

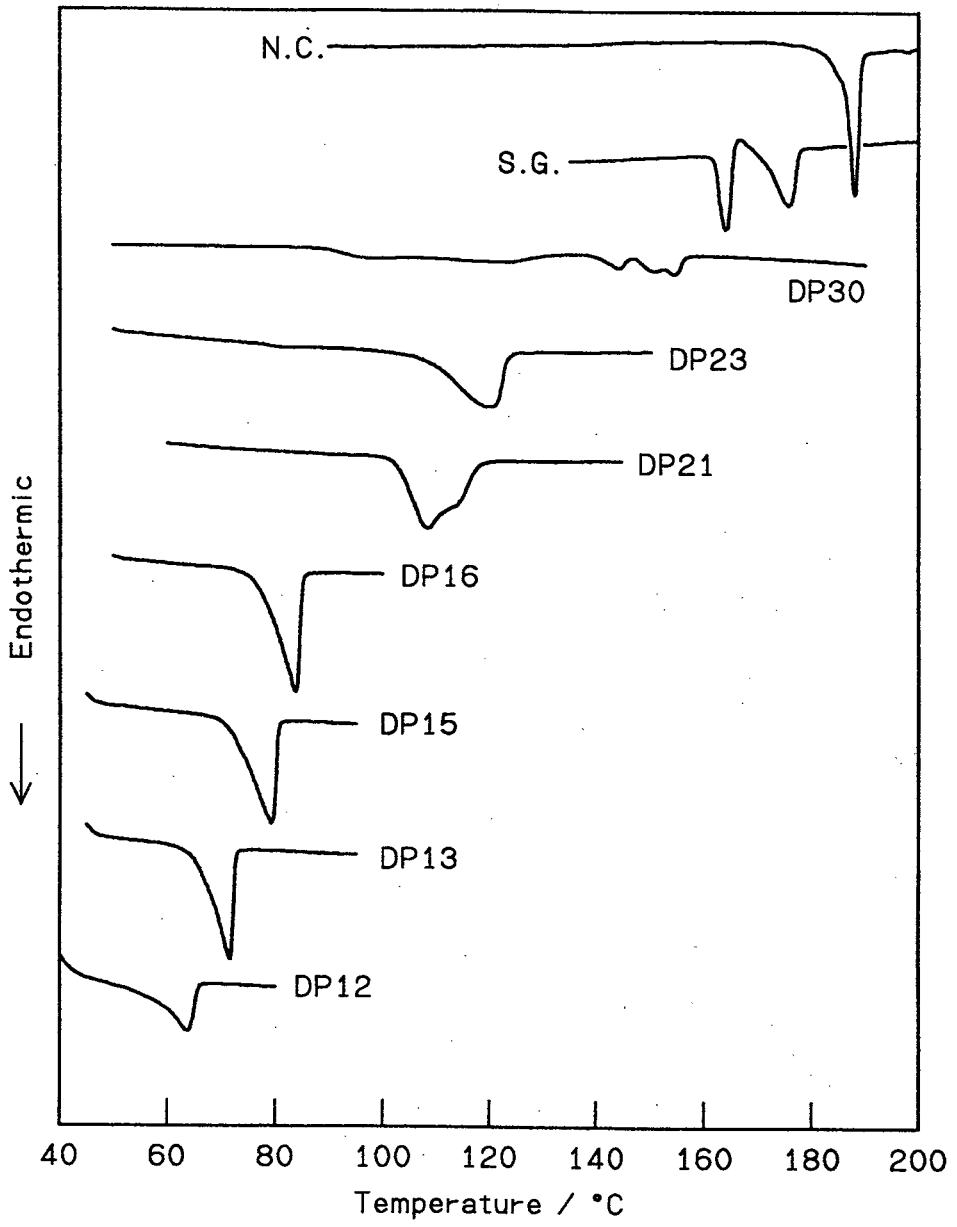

Figure 4–2 D.s.c. curves of various polyoxymethylene specimens.

Notations are the same as in *Figure 4–1*.

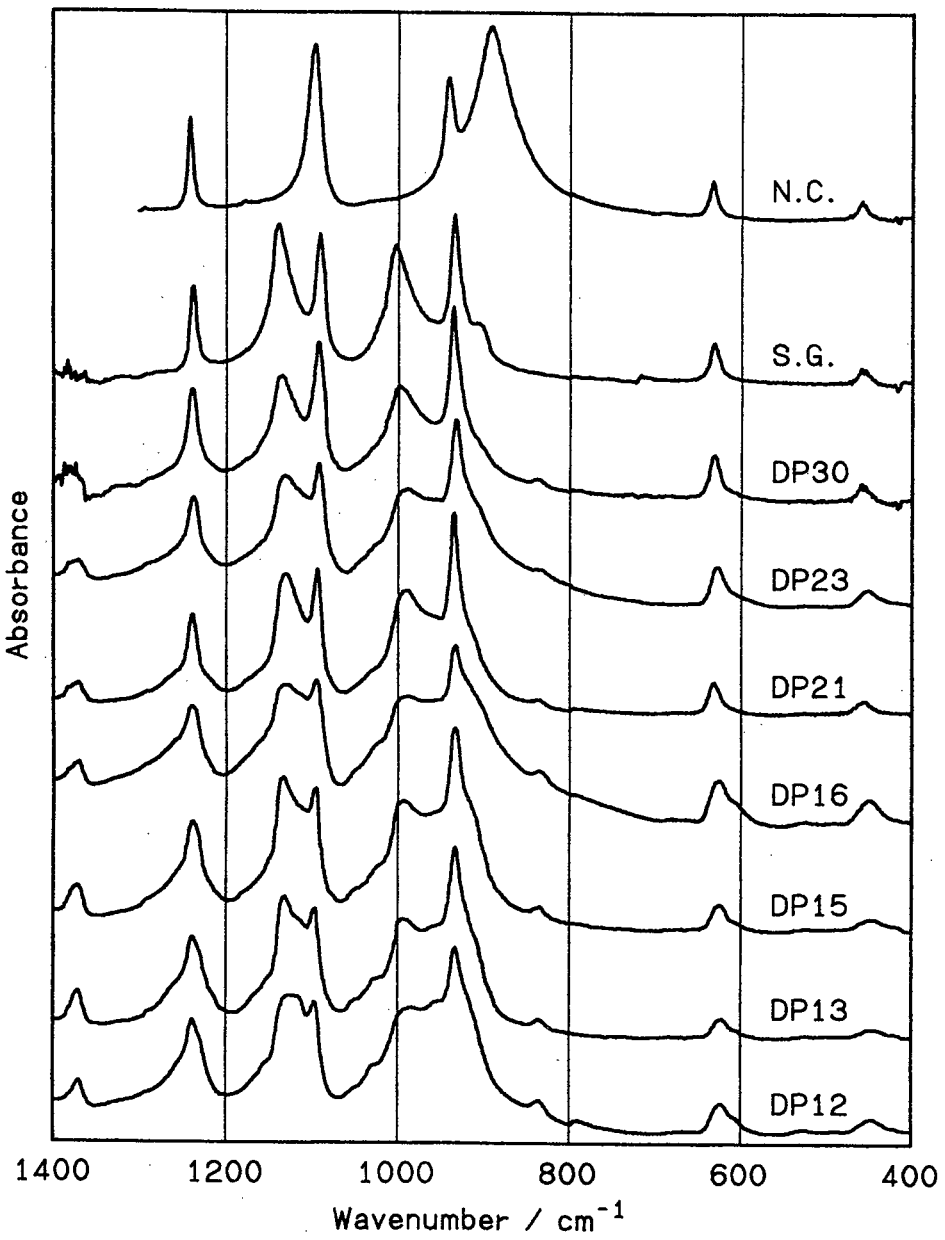

Figure 4–3 Infra–red spectra of various polyoxymethylene specimens.

Notations are the same as in *Figure 4–1*.

extreme crystals of high molecular weight POM. The spectral change between the needle-like crystals (ECC, *Figure 4-3 N.C.*) and the solution-grown crystals (FCC, *Figure 4-3 S.G.*) is very clear. The infra-red spectra of the LMW-POM were quite different from that of the ECC, which is thought to be the "normal" or "standard" crystal of *t*-POM, and resembled that of the FCC, though some minor discrepancies exist. In fear of mechanical deformation and resulting spectral change, the samples were not ground well enough with mulling reagent and the dispersion of the sample powder in Nujol was not fully satisfactory. Thus, the infra-red spectra of the LMW-POM were not clear enough to be discussed in detail.

The Raman spectra of the high and low molecular weight POM samples are shown in *Figures 4-4a* and *4-4b*. As mechanical deformation can be avoided easily during sample preparation, the Raman spectra of the LMW-POM were clearer than the infra-red spectra. In *Figures 4-4a* and *4-4b*, Raman bands at 2948 and 841 cm^{-1} are due to the acetoxy terminal group and the other bands, assigned to the A_1, E_1 and E_2 species, were basically the same as those of the high molecular weight POM crystals.

The infra-red and the Raman spectra of the LMW-POM specimens (DP12-30) were essentially the same as those of the FCC of high molecular weight POM, *i.e.*, only the bands assigned to A_2 species exhibited a large shift towards the high frequency side. The estimated length of the LMW-POM chain was less than 5nm, while the thickness of the solution-grown crystals, the period of the chain folding measured by the small angle X-ray diffraction, was about 9 nm. Such short molecules as LMW-POM might be extended in a crystal as was found with *n*-alkane crystals. On the other hand, the vibrational spectra of the LMW-POM were basically the same as those of the FCC. This result suggests that the infra-red spectral change between the ECC

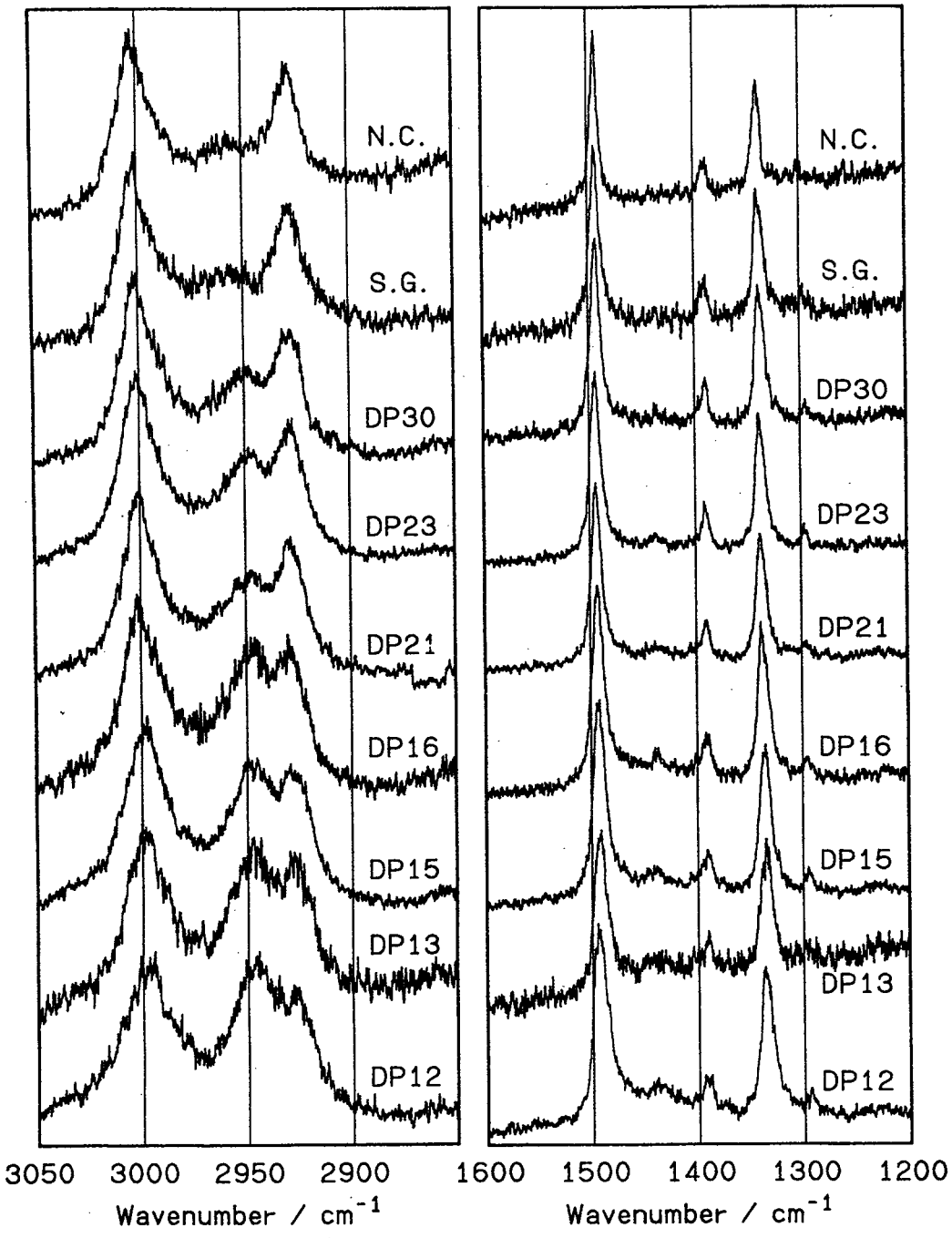

Figure 4–4a Raman spectra of various polyoxymethylene specimens.

Notations are the same as in *Figure 4–1*.

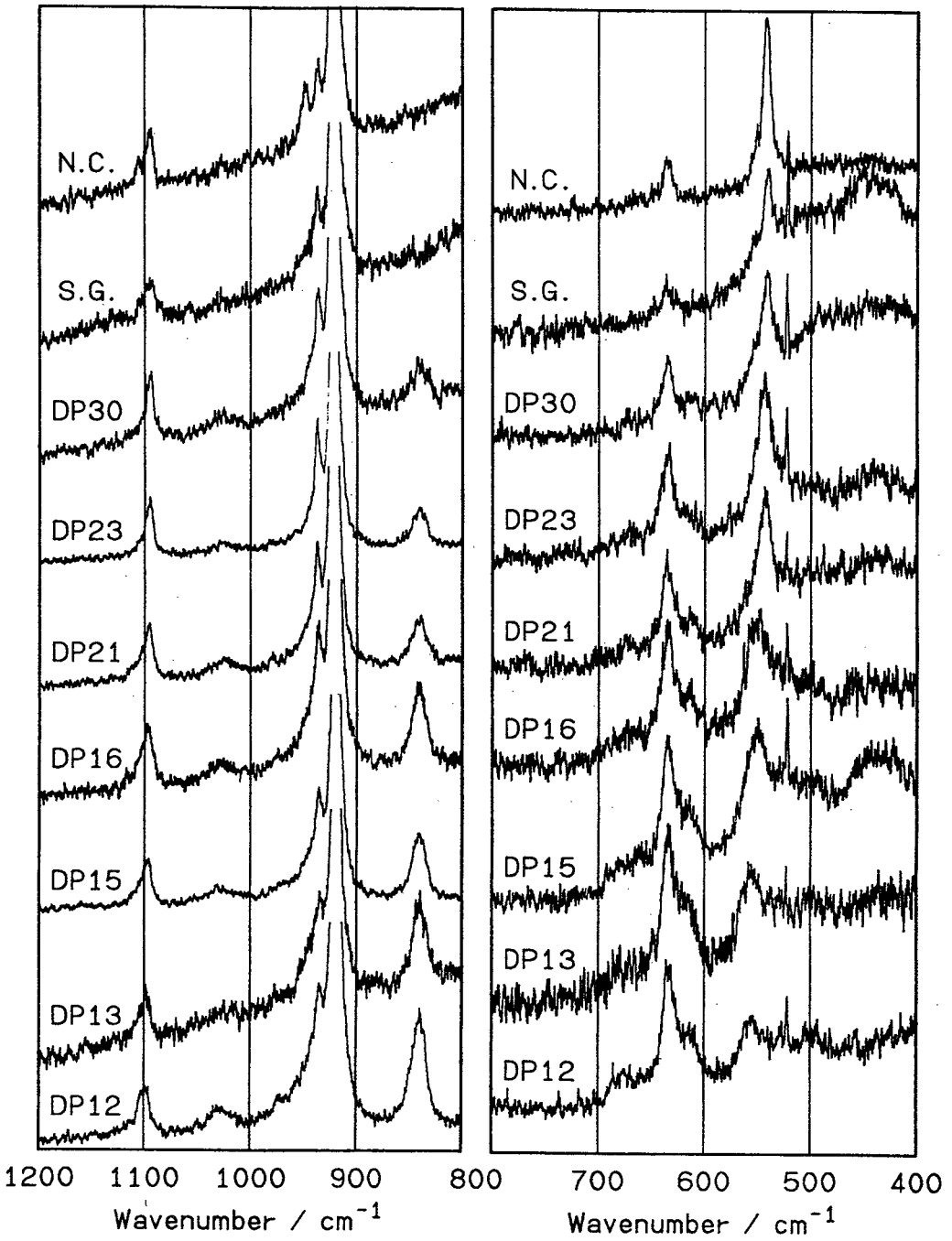

Figure 4–4b Raman spectra of various polyoxymethylene specimens.

Notations are the same as in *Figure 4–1*.

and FCC is related to the crystallite size along the *c*–axis.

In the Raman spectra of the LMW–POM, minor variations in wavenumber and in relative intensity were observed among the samples. The wavenumber of the Raman bands, with their symmetry species, are listed in *Table 4–1* (bands due to the terminal group are omitted here). For bands at 3004, 1340, 1096 and 542 cm^{-1} of the needle–like crystals, small frequency shifts among the LMW–POM specimens were found. The symmetry species of these shifted bands are both E_1 and A_1. The directions of the shifts were both to high– and low–frequency sides, as was predicted by the dispersion curves of *t*–POM.[26] The amount of the shifts changed continuously with the molecular weight and the maximum value of the shift was only 15 cm^{-1} for the 542cm^{-1} band. The shifts in the Raman spectra of the LMW–POM might be due to the molecular weight and/or a small difference in the conformation (unit cell size), as was detected by the wide angle X–ray diffraction measurement.

The behaviour of the bandshifts observed in the Raman spectra of the LMW–POM were quite different from that of the infra–red bands of the ECC and FCC. In the infra–red spectra, the symmetry species of the shifted bands was limited to A_2, and the direction of the shifts was always towards high frequency side on going from the ECC to the FCC and also the band shifts occur discretely. The behaviour of both types of shifts showed that the molecular mechanism of the large shifts of the A_2 bands is quite different from that of the minor shifts found in the Raman spectra of the LMW–POM. The shifts in the Raman spectra of the LMW–POM samples might be interpreted as minor deviations in the conformations and/or effects of the finite length of the molecular chain. In contrast, the small difference in the conformations of chains cannot explain such a large shift of the A_2 bands

Table 4–1 Raman bands of various polyoxymethylene specimens

species	observed wavenumbers (cm^{-1})								
	NC	SG	DP30	DP23	DP21	DP16	DP15	DP13	DP12
E_1	3004	3003	3002	3002	3001	3002	2999	2999	2999
		2949	2948	2947	2947	2947	2948	2947	
A_1	2929	2928	2929	2929	2930	2930	2930	2927	2928
A_1	1494	1495	1494	1496	1495	1494	1494	1494	1495
			1439		1440	1442		1440	
E_2	1391	1392	1391	1392	1392	1391	1391	1392	1392
A_1	1340	1340	1339	1340	1340	1339	1337	1336	1337
	1296	1297		1296	1295		1294		
E_2	1106								
E_1	1096	1096	1096	1096	1097	1099	1099	1101	1102
		1027	1027	1025	1030	1031		1032	
E_2	949								
E_1	938	938	937	938	938	938	937	936	937
A_1	921	922	921	922	922	921	921	921	921
		842	841	841	841	841	842	841	
E_1	637	637	636	636	637	636	636	636	636
					625			615	
A_1	542	541	542	544	543	552	550	557	557

between the ECC and the FCC.

4.3.2 *Spectral Change of Low Molecular Weight Polyoxymethylene by Mechanical Deformation and Heat Treatment*

It has been known that the infra-red spectra of the needle-like crystals taken with the Nujol mull and the KBr pellet methods show no significant difference.[11] *Figure 4-5* shows the infra-red spectra of the solution-grown crystals of *t*-POM. On the top is shown the spectrum of as-grown crystals measured by the Nujol mull method. Lower curves are spectra of the crystals measured on KBr pellets prepared by grinding under different mechanical conditions, being aligned in the order of increasing mechanical deformation. The spectral change induced by the treatment is obvious. As the mechanical deformation increases, intensities of the bands around 1095 and 900 cm^{-1} are increased and those of the bands around 1140 and 1000 cm^{-1} are diminished with the mechanical treatment, the infra-red spectra go from the FCC type to the ECC type. It is worth noted that positions of the bands are basically unchanged and their intensities change gradually.

Figure 4-6 shows wide angle X-ray diffraction of an as-grown solution-grown sample and that of the mechanically deformed one. After the mechanical deformation, the starting trigonal form remains unchanged, while the diffraction intensities, especially those for wide angle, are decreased and the half widths of the peaks are broadened. This means that the mechanical deformation produces defects and/or disorder in the crystal. If the FCC type spectrum is caused by such crystal defects, as Terlemezyan suggested, the 1138 and 1000 cm^{-1} bands should get stronger in the deformed sample. However, the observed spectrum of a more defective sample becomes closer

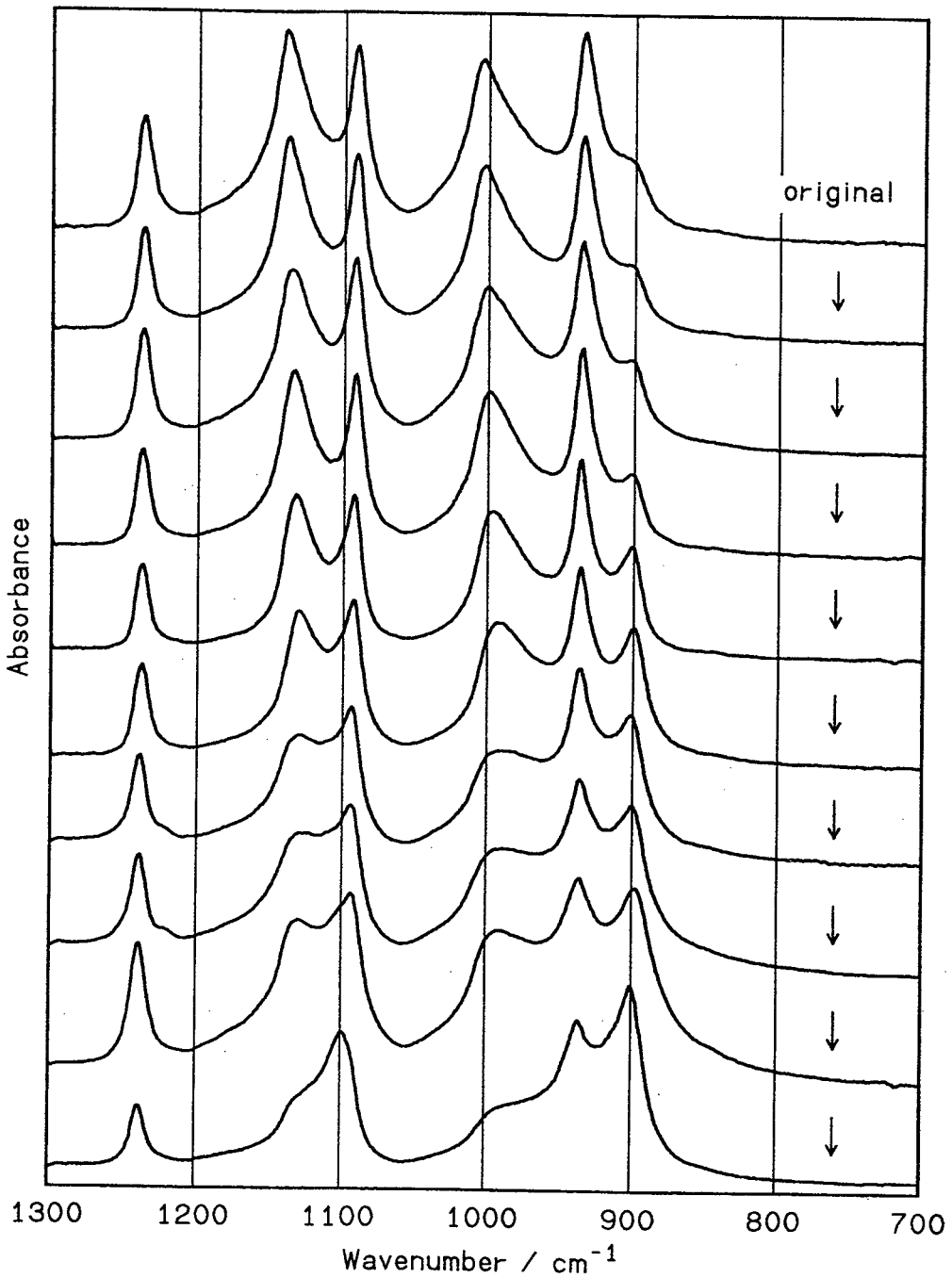

Figure 4–5 Infra-red spectra of polyoxymethylene solution-grown crystals.

Original and milled samples.

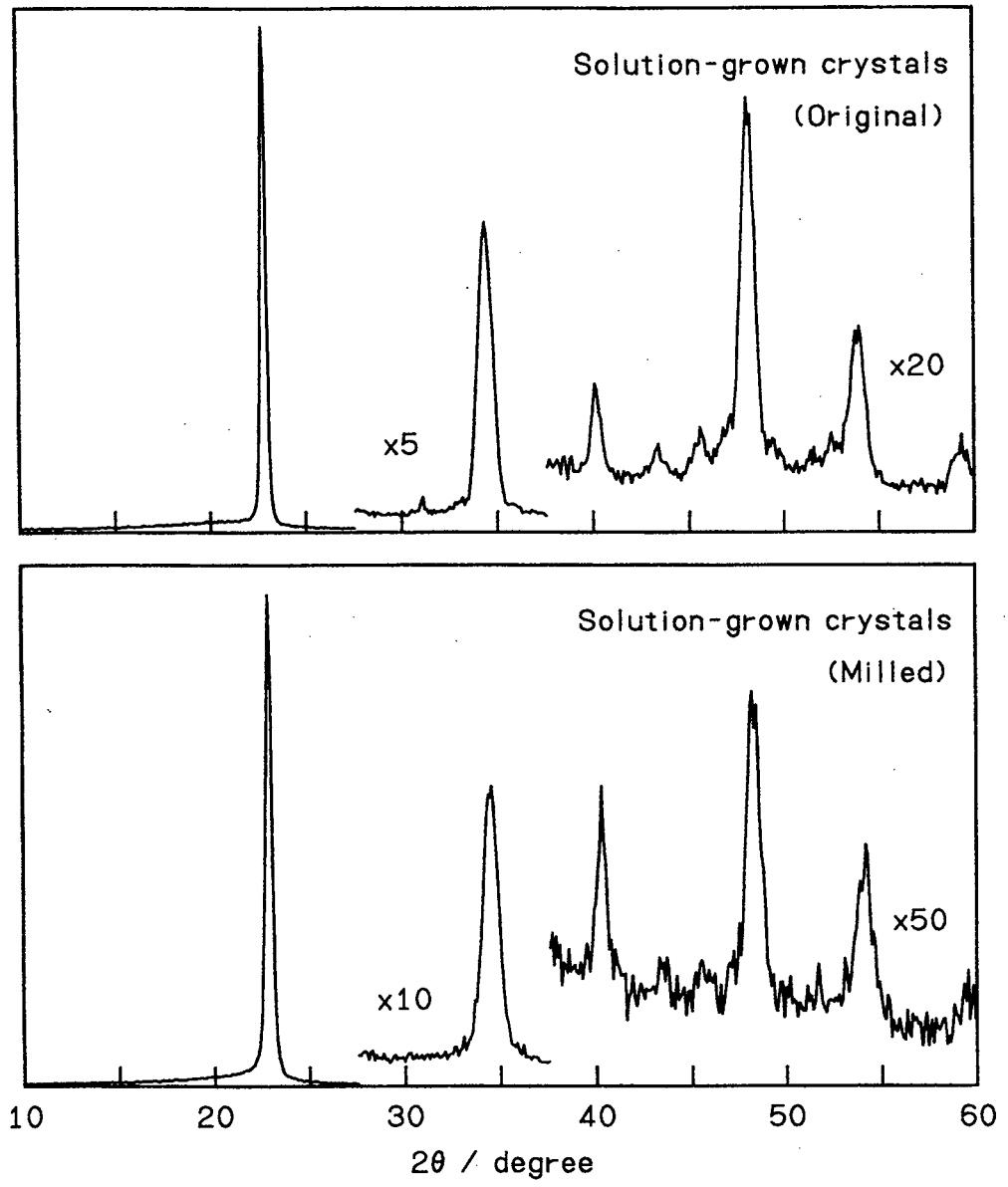

Figure 4–6 X–ray diffraction of polyoxymethylene solution–grown crystals.

to the ECC type. This support the consideration made in Chapter 3, saying that crystal defects are not the origin of the morphology-dependent infra-red spectral changes of *t*-POM.

Figure 4-7 shows the infra-red spectra of the LMW-POM specimens and the solution-grown crystals of high molecular weight POM measured by the Nujol mull method (A) and the KBr method (B). The infra-red spectra of the LMW-POM measured by the both methods showed no significant difference. The spectrum of DP30, a specimen with a wide distribution of the chain lengths and rather high molecular weight, showed minor changes like that of the solution-grown crystals with the mechanical treatment during pelletization.

In *Figure 4-8*, the infra-red spectra of POM specimens before (A) and after (B) melt crystallization, heated up to 200°C and cooled, are shown. Though the spectral change of the solution-grown crystals was not so drastic as was found in *Figures 4-5* and *4-7*, the spectrum after melt crystallization was like the spectrum of a melt crystallized film[11] and could be considered as the superposition of the spectrum of the ECC and the original spectrum of the FCC. For the LMW-POM, basically the same spectra were obtained before and after melt crystallization.

These behaviours of the infra-red spectra of the LMW-POM with KBr pelletization and subsequent melt crystallization could be summarized as follows. The infra-red spectrum of the solution-grown crystals of high molecular weight POM changes very easily with treatments that effect the morphology, while the infra-red spectra of the LMW-POM showed no significant change with those treatments. Also LMW-POM containing long molecular chains (DP30) showed the same tendency as the solution-grown crystals of high molecular weight POM.

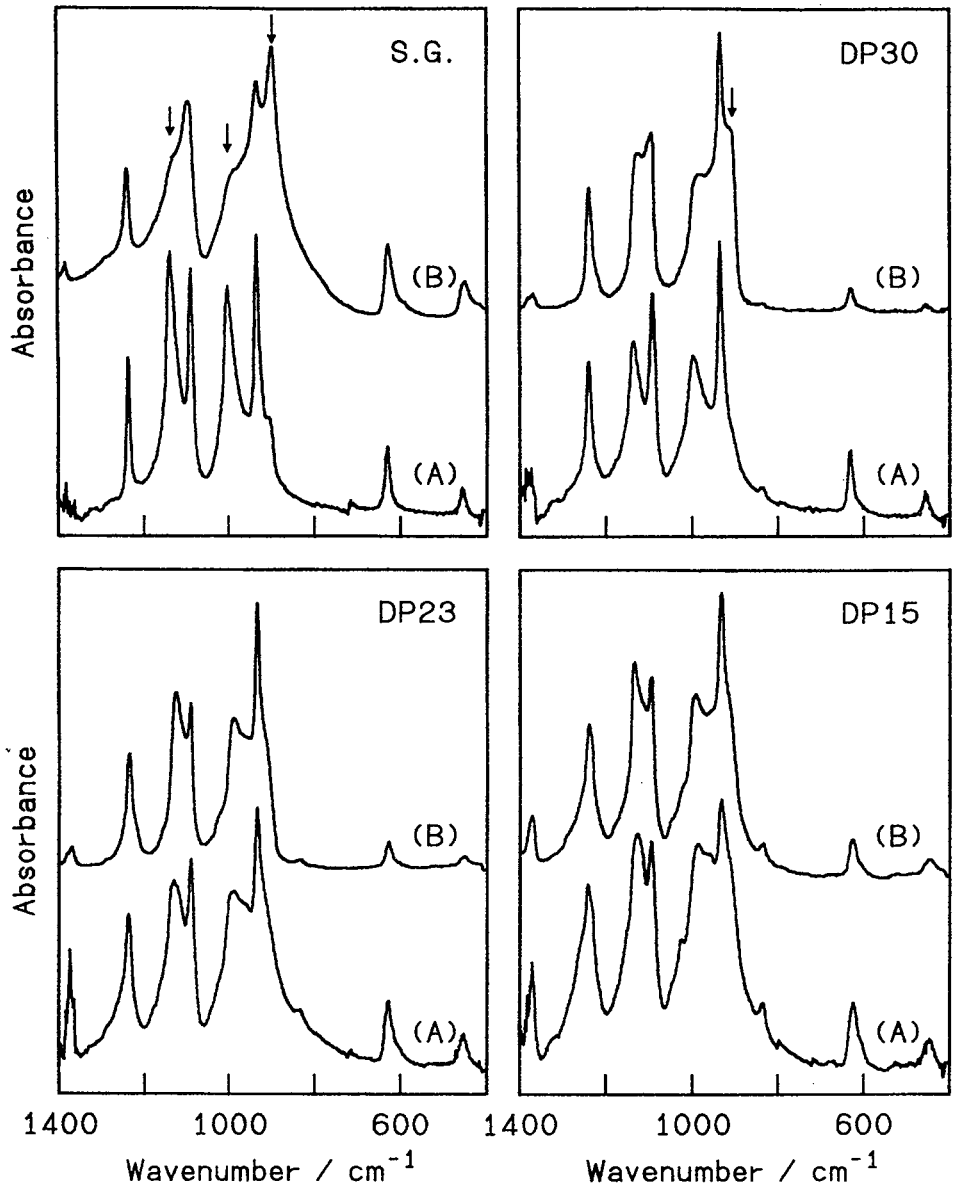

Figure 4–7 Infra–red spectra of solution–grown crystals of polyoxymethylene and low molecular weight polyoxymethylene. (A):Nujol mull method; (B):KBr pellet method.

Notations are the same as in *Figure 4–1*.

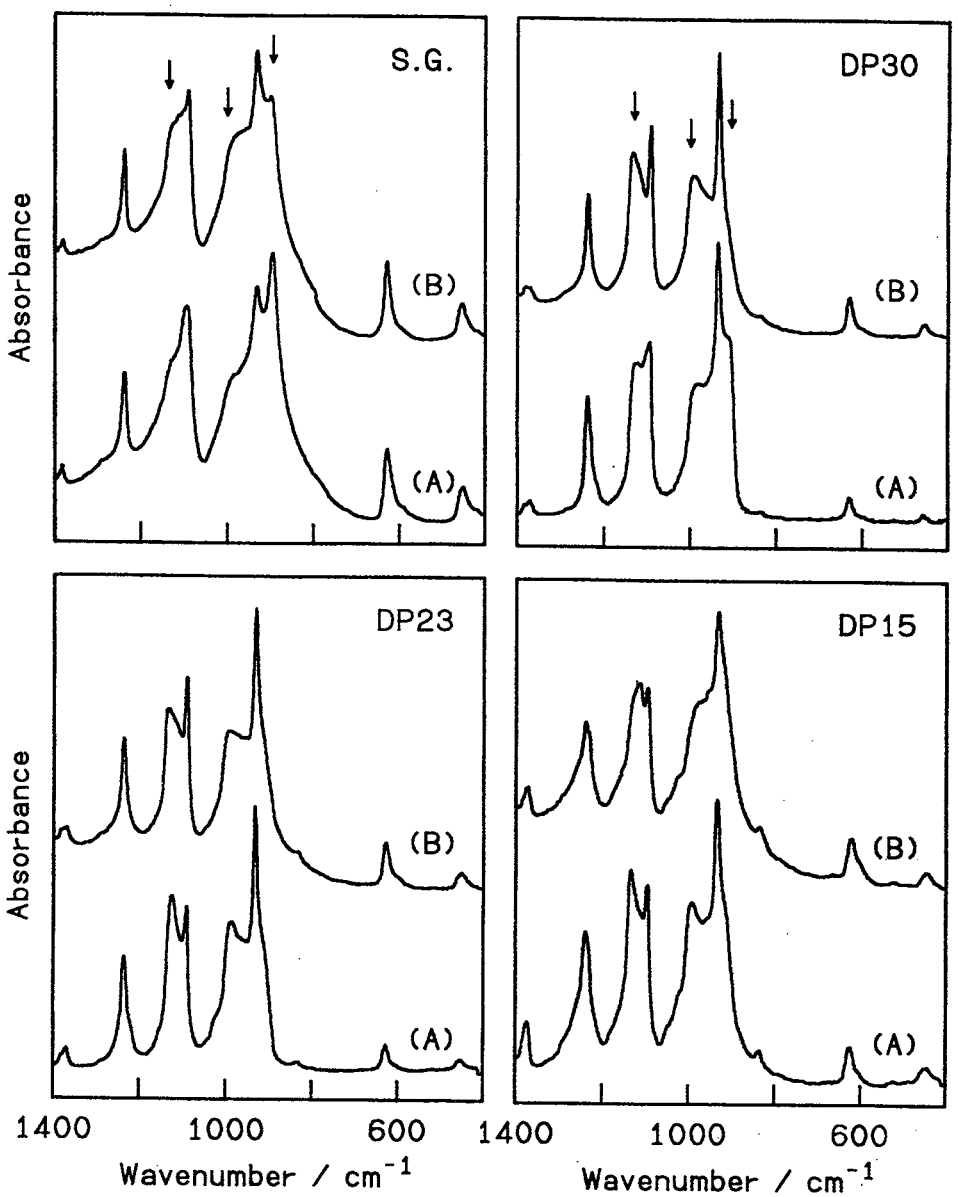

Figure 4–8 Infra–red spectra of solution–grown crystals of polyoxymethylene and low molecular weight polyoxymethylene. (A):before melt crystallization; (B):after melt crystallization.
Notations are the same as in *Figure 4–1*.

These phenomena could be interpreted in terms of the new hypothesis as follows. Through the milling of the sample, the long molecular chains of the solution–grown crystals were extended with shear stress and the spectrum changes to that of the ECC. In the course of subsequent melt crystallization, long molecular chains could not fold regularly and both long extended and folded parts would coexist in the sample. The resulting infra–red spectrum could be thought as the superposition of those of the ECC and FCC. On the contrary, molecular chains in the LMW–POM specimens are too short to have long extended part and the spectra remain unchanged through the milling and subsequent melt crystallization.

4.4 Conclusion

Infra–red and Raman spectra of LMW–POM are discussed in comparison with the ECC and FCC of high molecular weight *t*–POM from the spectroscopic viewpoint. Bands of LMW–POM assigned to the A_2 symmetry species shifted towards the high–frequency side as was found in the spectrum of FCC. Since the LMW–POM samples have no chain folding, the infra–red spectrum of the FCC sample should be ascribed not to folded–chain structure but to lamellar type morphology. Minor shifts of Raman lines of the LMW–POM were also found, however, the mechanism of the shift is clearly different from that of the shifts of A_2 bands. Behaviours of the infra–red spectra of LMW–POM with mechanical deformation and subsequent melt crystallization are different from those of FCC of high molecular weight POM. From these observations, it can be concluded that the large anomalous high–frequency shifts of the A_2 bands are related to the crystallite size along the *c*–axis.

References

1 H. Tadokoro, S. Yasumoto, S. Murahashi and I. Nitta, *J. Polym. Sci.*, **44**, 266 (1960)

2 G. Carazzolo, *J. Polym. Sci. (A)*, **1**, 1573 (1963)

3 T. Uchida and H. Tadokoro, *J. Polym. Sci. (A-2)*, **5**, 63 (1967)

4 L. Mortillario, G. Galliazzo and S. Bessi, *Chem. Ind. (Milan)*, **46**, 139 (1964), *ibid* **46**, 144 (1964)

5 M. Iguchi, *Polymer*, **24**, 915 (1983)

6 V. Zamboni and G. Zerbi, *J. Polym. Sci. (C)*, **7**, 153 (1964)

7 E. F. Oleinik and N. S. Enikolopyan, *J. Polym. Sci. (C)*, **16**, 3677 (1968)

8 L. Terlemezyan, M. Mihailov, P. Schmidt and B. Schneider, *Makromol. Chem.*, **179**, 807 (1978)

9 L. Terlemezyan, M. Mihailov, P. Schmidt and B. Schneider, *Makromol. Chem.*, **179**, 2315 (1978)

10 L. Terlemezyan and M. Mihailov, *Eur. Polym. J.*, **17**, 1115 (1981)

11 M. Shimomura and M. Iguchi, *Polymer*, **23**, 509 (1982)

12 L. Terlemezyan and M. Mihailov, *Polym. Commun.*, **25**, 80 (1984)

13 M. Kobayashi, Y. Itoh, H. Tadokoro, M. Shimomura and M. Iguchi, *Polym. Commun.*, **24**, 38 (1983)

14 M. Kobayashi, H. Morishita, T. Ishioka, M. Iguchi and M. Shimomura, *J. Mol. Struc.*, **146**, 155 (1986)

15 M. Kobayashi, H. Morishita, M. Shimomura and M. Iguchi, *Macromolecules*, **20**, 2453 (1987)

16 H. Tadokoro, M. Kobayashi, Y. Kawaguchi, A. Kobayashi and S. Murahashi, *J. Chem. Phys.*, **38**, 703 (1963)

17 M. Shimomura, M. Iguchi and M. Kobayashi, *Polymer*, **29**, 351 (1988)

18 M. Iguchi, *Br. Polym. J.*, **5**, 195 (1973)

19 M. Iguchi and I. Murase, *J. Crystal Growth*, **24/25**, 596 (1974)

20 M. Iguchi, I. Murase and K. Watanabe, *Br. Polym. J.*, **6**, 61 (1974)

21 M. Iguchi, *Makromol. Chem.*, **177**, 549 (1976)

22 T. Mashimoto, T. Sakai and M. Iguchi, *J. Phys. (D)*, **12**, 1567 (1979)

23 D. C. Bassett, F. R. Dammont and R. Salovey, *Polymer*, **5**, 579 (1964)

24 D. R. Carter and E. Baer, *J. Appl. Phys.*, **37**, 4060 (1966)

25 H. Staudinger, R. Signer, H. Johner, M. Luthy, W. Kern, D. Russidis and O. Schweitzer, *Ann. Chem.*, **474**, 145 (1929)

26 L. Piseri and G. Zerbi, *J. Chem. Phys.*, **48**, 3561 (1968)

Chapter 5

Identification of Orthorhombic Polyoxymethylene Generated in a Cationic Polymerization System and Its Spectral Change

5.1 Introduction

Needle-like single crystals of trigonal polyoxymethylene (*t*-POM) were prepared by Iguchi[1] as the polymer whiskers, through cationic polymerization of trioxane. Thereafter, the relationship between the polymerization conditions and the crystallographic as well as morphological structures of the resultant polymers has been investigated extensively by his group.[2-5] In the course of vibrational spectroscopic studies of the needle-like crystals of *t*-POM and other samples from various origins,[6] as was described in Chapter 2, a special case was found. One sample obtained by cationic polymerization of trioxane exhibited unusual bands in both the far infra-red and Raman spectra in addition to those associated with *t*-POM. The positions of these bands suggested that orthorhombic polyoxymethylene (*o*-POM) was generated as a by-product in the polymerization system originally designed to prepare the needle-like crystals of *t*-POM. The orthorhombic form of POM was first obtained by an Italian group through polymerization of formaldehyde in aqueous solution.[7] For the new crystal modification, the structure determination by X-ray diffraction[8,9] and the vibrational analyses[10-13] were performed. However, the mechanism of formation of *o*-POM still remains unsettled, and procedures whereby the *o*-POM crystals were prepared inevitably have not been established yet.

In this chapter, the formation of *o*-POM in a cationic polymerization

system of trioxane will be investigated by vibrational spectroscopy.[14,16] Vibrational spectral changes induced by the difference in crystal morphology of *o*–POM will be also considered.

5.2 Experimental

Two samples were subjected to investigation. They were synthesized by cationic polymerization of trioxane according to the procedures reported by Iguchi *et al.*[1-5] Sample I was identified as consisting of the typical needle–like crystals of *t*–POM. Sample II was obtained as an exceptional case via the same polymerization procedure, though no significant difference in condition was recorded.

In addition to samples I and II, fibrillar crystals obtained by a cationic solid–state polymerization of trioxane (sample III),[17] solution-grown lamellar crystals from Delrin resin (E. I. du Pont de Nemours & Co.) (sample IV), and pellets of Delrin resin were also investigated for comparison.

For Raman measurement, powder samples were sealed in glass ampoules and Delrin pellets were cut in a suitable size. Raman spectra were measured using a Jasco R–500 double monochromator. The 514.5 nm line from an Ar^+ laser was used as the excitation source. The microfocus Raman technique was also applied, using a Jasco Raman microscope, by the courtesy of Japan Spectroscopic Co. Ltd.

The absorption spectra in the mid infra–red region were measured with a Jasco 5MP Fourier–transform spectrometer. Far infra–red spectra were taken on powders of samples I – IV dispersed in a paraffin matrix using a Hitachi FIS–3 far infra–red spectrophotometer.

Figure 5-1 Optical micrograph of sample II

5.3 Results and Discussion

In the optical micrograph of sample II, thin plate-shaped crystals are found to be mingled with the usual needle-like crystals (*Figure 5-1*). They appear mostly in a "moth-like" shape, or sometimes in a "bamboo-leaf" shape, with dimensions as large as 100 μm diameter. Identification of the crystals having such a characteristic appearance is the main subject of this chapter.

The Raman spectra (in the fingerprint region) of samples I and II, and a Delrin pellet are reproduced in *Figure 5-2*. The bands due to *t*-POM are commonly observed in these samples.[12,18,19] In sample II, contrary to the other samples, several additional bands appear in the spectrum (marked by arrows). The frequencies and the relative intensities of the extra bands coincide with those of the bands characteristic of *o*-POM.[12] In the low-frequency region, sample II exhibits the Raman bands at 79 and 37 cm^{-1} associated with the lattice vibrations of *o*-POM,[13] besides that of *t*-POM at 64 cm^{-1} (*Figure 5-3*).[11,19]

In the far infra-red spectrum of sample II (*Figure 5-4* (B)), there are absorption bands at 296 and 130 cm^{-1} in addition to the strong band at 220 cm^{-1} associated with *t*-POM.[18,20] These extra bands are very weak but are still detectable in sample I too(*Figure 5-4*(A)), while they disappear completely in the solution-grown and solid-state polymerized polymers (*Figures 5-4*(C) and *5-4*(D)) and they correspond to the absorption bands characteristic of *o*-POM.[11]

From the above spectroscopic results, it is evident that sample II contains a significant amount of the orthorhombic crystals besides the trigonal form. In the X-ray diffraction diagram of sample II there are weak but

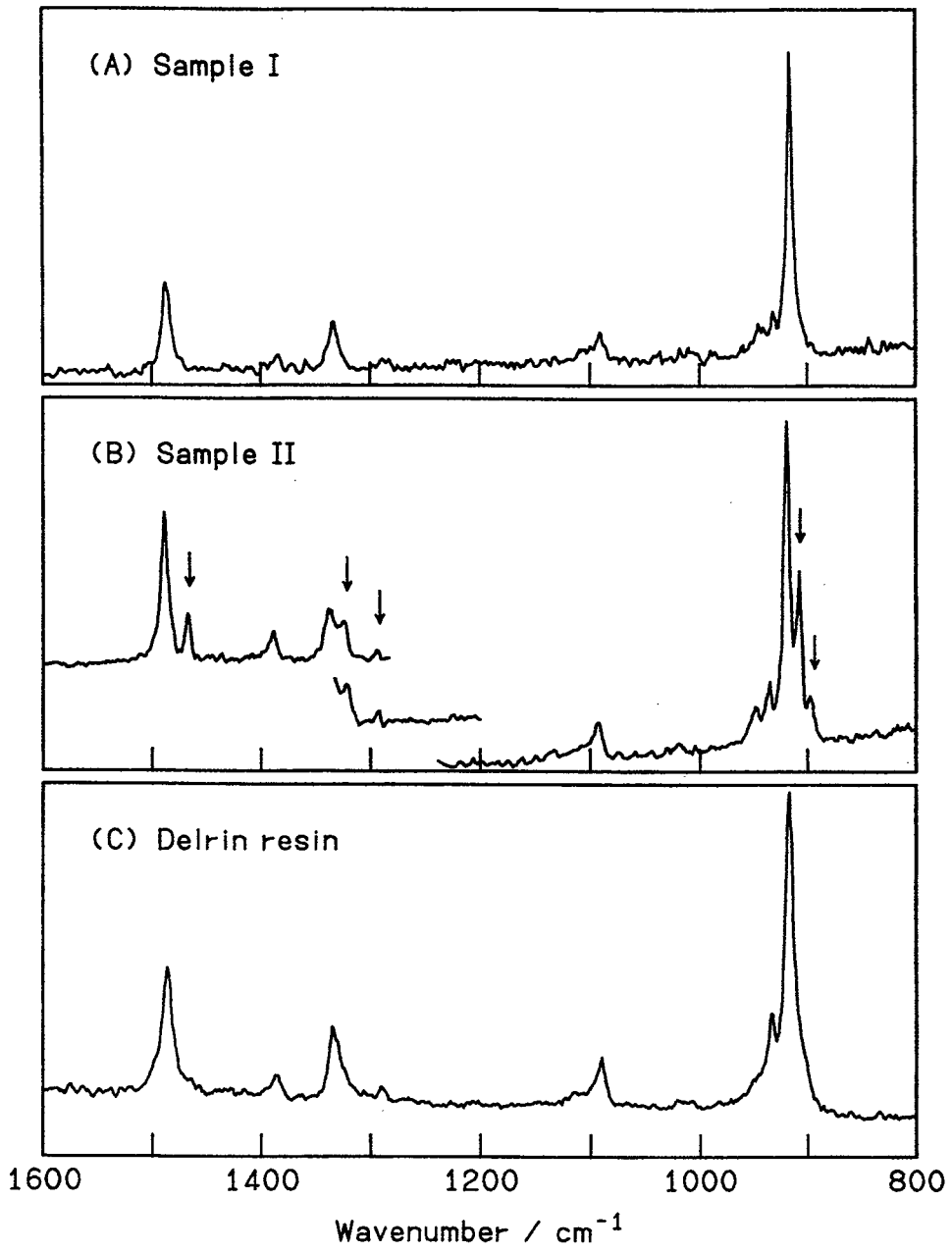

Figure 5–2 Raman spectra of Sample I (A), Sample II (B), and Delrin resin (C). The bands marked by arrows are due to orthorhombic polyoxymethylene.

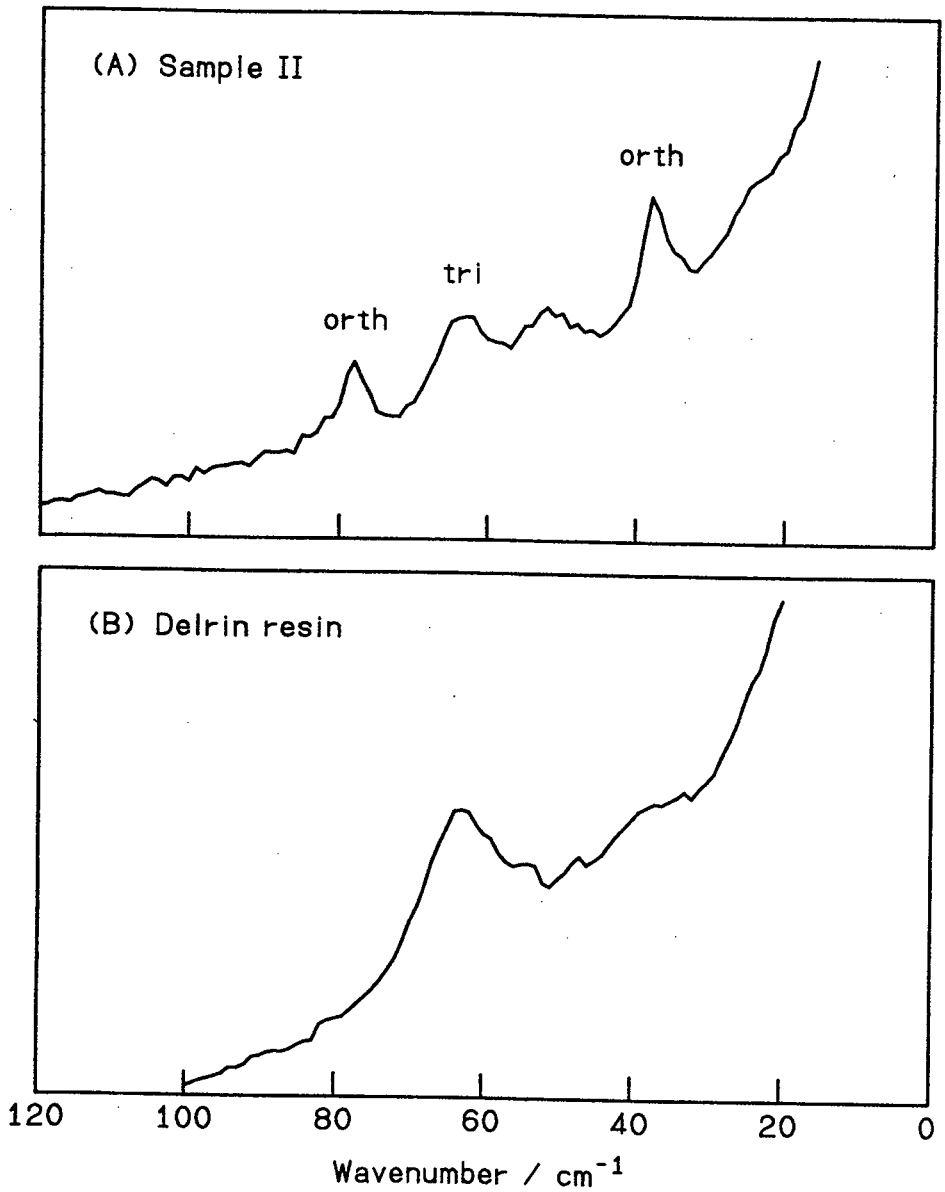

Figure 5–3 Low-frequency Raman spectra of Sample II (A) and Delrin resin (B). The bands marked orth and tri are due to the lattice vibrations of orthorhombic and trigonal polyoxymethylene, respectively.

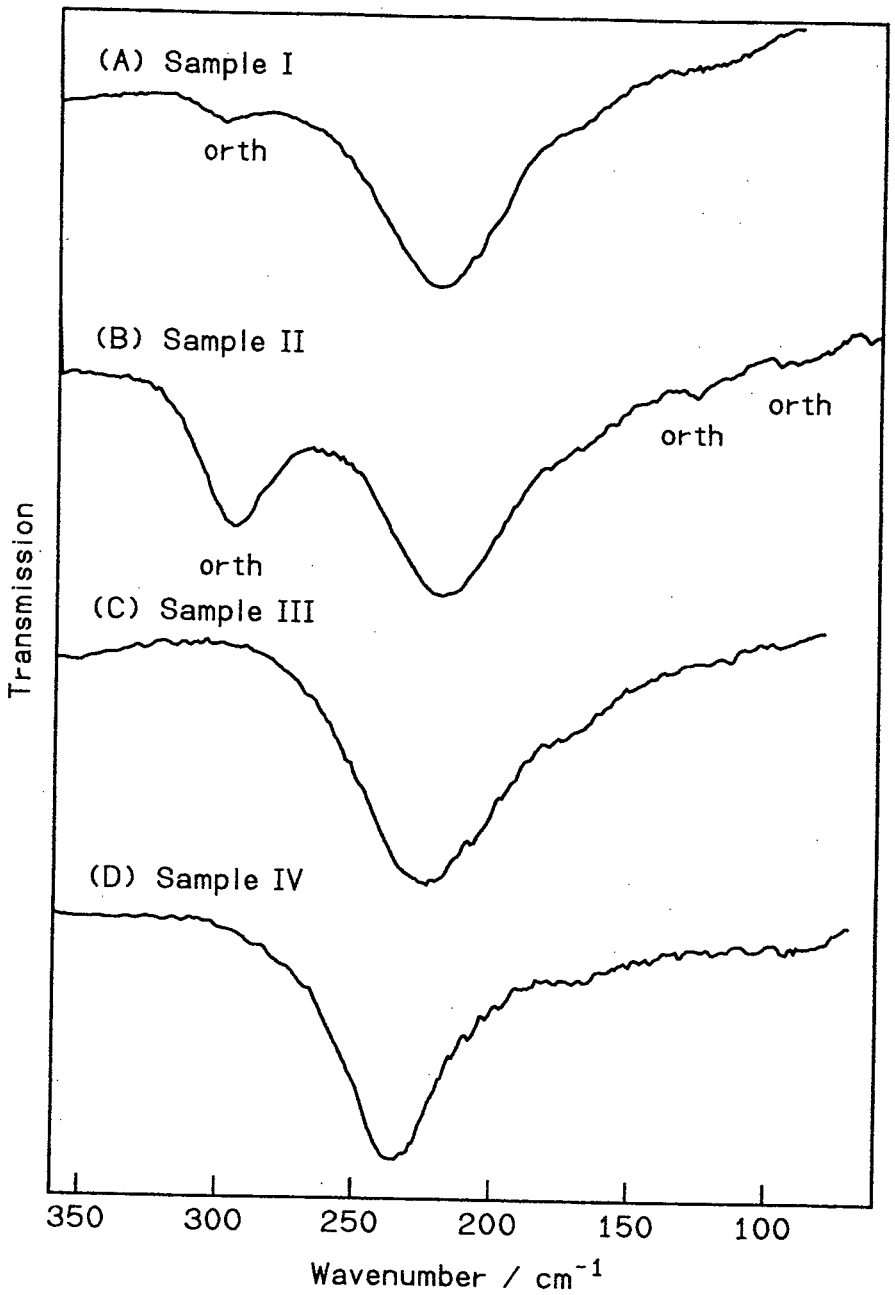

Figure 5–4 Far infra–red spectra of various polyoxymethylene samples. The bands marked orth are due to orthorhombic polyoxymethylene.

distinct peaks due to the (110) (2θ : 22.0°) and (111) (33.6°) reflections of *o*–POM in vicinity of the strong (100) (22.9°) and (105) (34.6°) reflections of *t*–POM, respectively (*Figure 5–5*). Judging from the intensity ratios of these pairs of reflections, the amount of the orthorhombic modification contained in sample II is estimated as 10% or less. Also in sample I, far less *o*–POM was detected by X–ray diffraction and far infra–red spectra. Here, it should be noted that the presence of *o*–POM in sample II could not be detected by the absorption spectrum in the mid infra–red region. Both samples I and II gave rise to essentially the same spectrum in which all the observed bands were assigned to the fundamentals of the *t*–POM molecules.[18] The disappearance of the *o*–POM bands is caused by occurrence of the phase transition of the metastable orthorhombic to the stable trigonal form during the sampling process. The spectra in this region were measured on Nujol paste or KBr pellets of the powder samples. Because of strong absorption intensities in this frequency region, a hard grinding of the samples was necessary in order to prepare the specimens with suitable absorbance. During this process, strong shear applied to the *o*–POM crystals brought about the phase transition.

The next stage of this work was to elucidate the morphology of the *o*–POM crystals present in sample II. As described above, the major component of sample II consists of the *t*–POM crystals which appear in the well–defined needle–like crystals. Then, the "moth–like" plates found in the optical micrograph (*Figure 5–1*) were anticipated at a glance to be *o*–POM portion whose existence was proved by X–ray diffraction and vibrational spectroscopy. In order to confirm this idea, the microfocus Raman technique was applied to this system. *Figure 5–6* reproduces the microscopic view of the sample stage, in which both the needle–like and moth–like crystals are observed. The size of the laser spot (~3μm diameter) is indicated. The

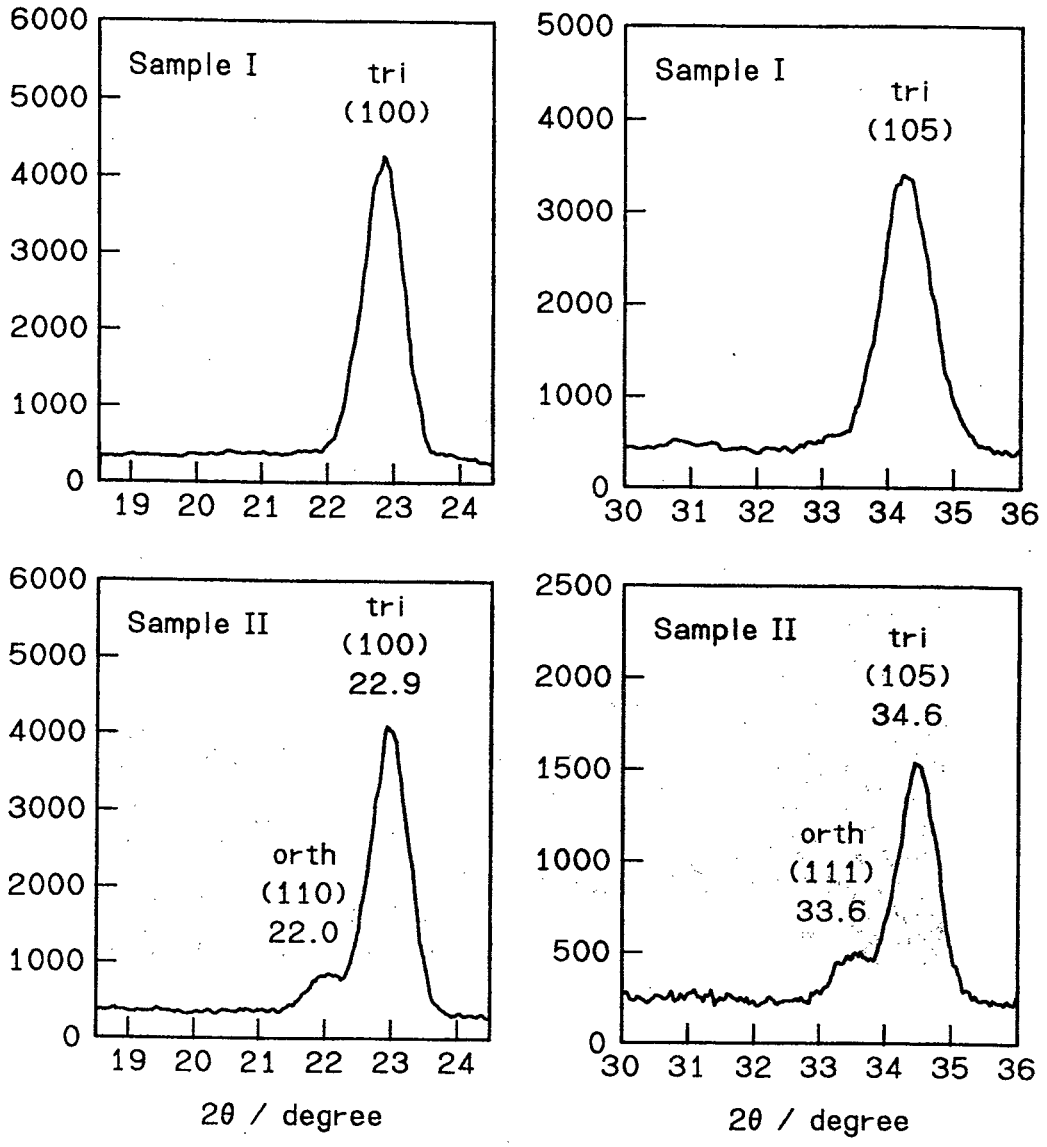

Figure 5-5 X-ray diffraction diagrams of samples I and II

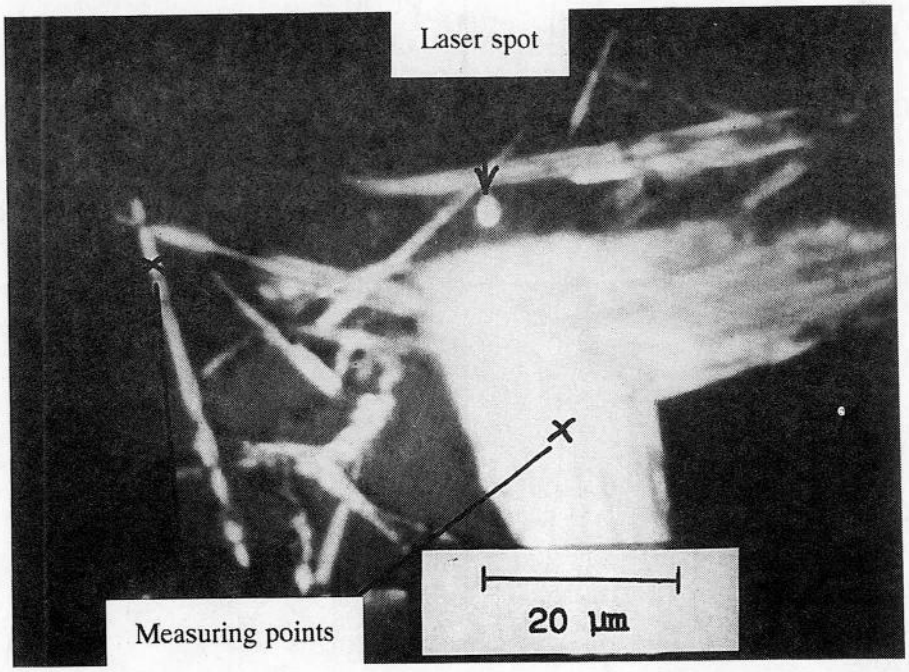

Figure 5–6 Micrograph of sample II on the sample stage of Raman microscope. The size of the laser spot and the positions where the Raman spectra were taken are indicated.

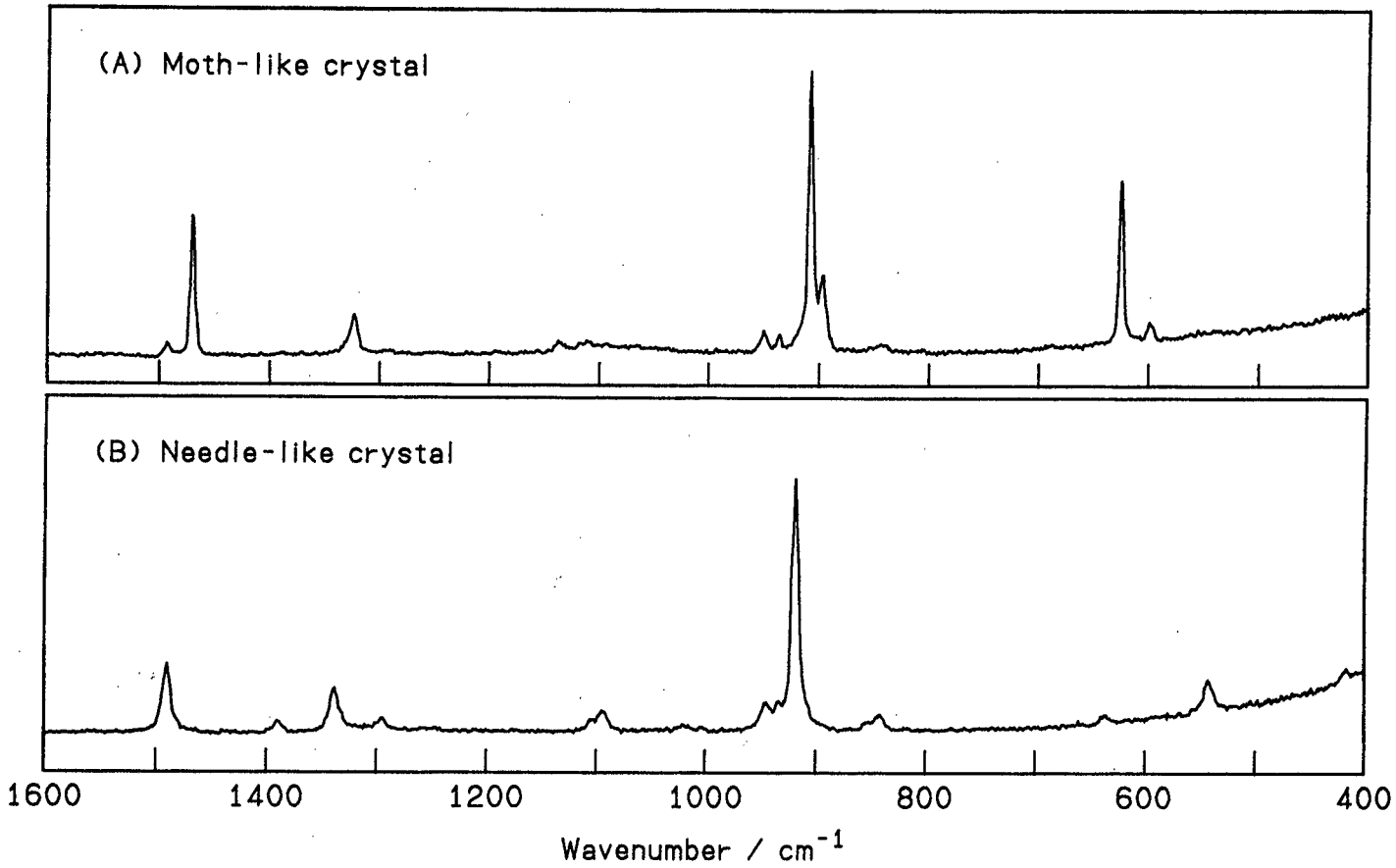

Figure 5–7 Microfocus Raman spectra of the needle–like (*t*–POM) and moth–like (*o*–POM) crystals.

crosses indicate the positions where the laser beam was focused for measuring the Raman spectra of the limited areas. As shown in *Figure 5-7*, the limited area on a needle-like crystal gave the microfocus Raman spectrum characteristic of the trigonal form, while that of a moth-like crystal gave the spectrum consisting exclusively of the bands to be assigned to the orthorhombic form. Therefore, it became evident that the moth-like crystals were of the orthorhombic modification.

Thus, the formation of *o*-POM via cationic polymerization of trioxane was proved. As for the route of contamination with *o*-POM crystals in Sample II, Iguchi showed that *o*-POM crystals were formed on the inner wall of the reaction vessel in contact with the vapor phase. He succeeded in preparing sample consisting essentially of orthorhombic crystals from the cationic polymerization of trioxane.[21)]

Because *o*-POM is the metastable phase in ambient condition, it is transformed to *t*-POM by heating or mechanical deformation.[22)] Recently, it was found that solid-state phase transition from *t*-POM to *o*-POM is induced by compressing *t*-POM samples.[23,24)] It was also confirmed that the morphologies of starting *t*-POM were maintained during the pressure-induced phase transition by comparing the spectrum of "moth-like" crystal in which the chains are extended and that of *o*-POM obtained from extended-chain crystal of *t*-POM. Thus, both extended- and folded-chain crystals of *o*-POM were obtained by the phase transition, although the transition is partial and the content of *o*-POM is limited to 10 - 20 % at most. Concerning the origin of the morphology-dependent spectral change found in *t*-POM, it is important to confirm whether the specific spectral change is limited to the case of *t*-POM or it is a generally observable phenomenon for a group of materials including *o*-POM. Infra-red spectra of extended- and

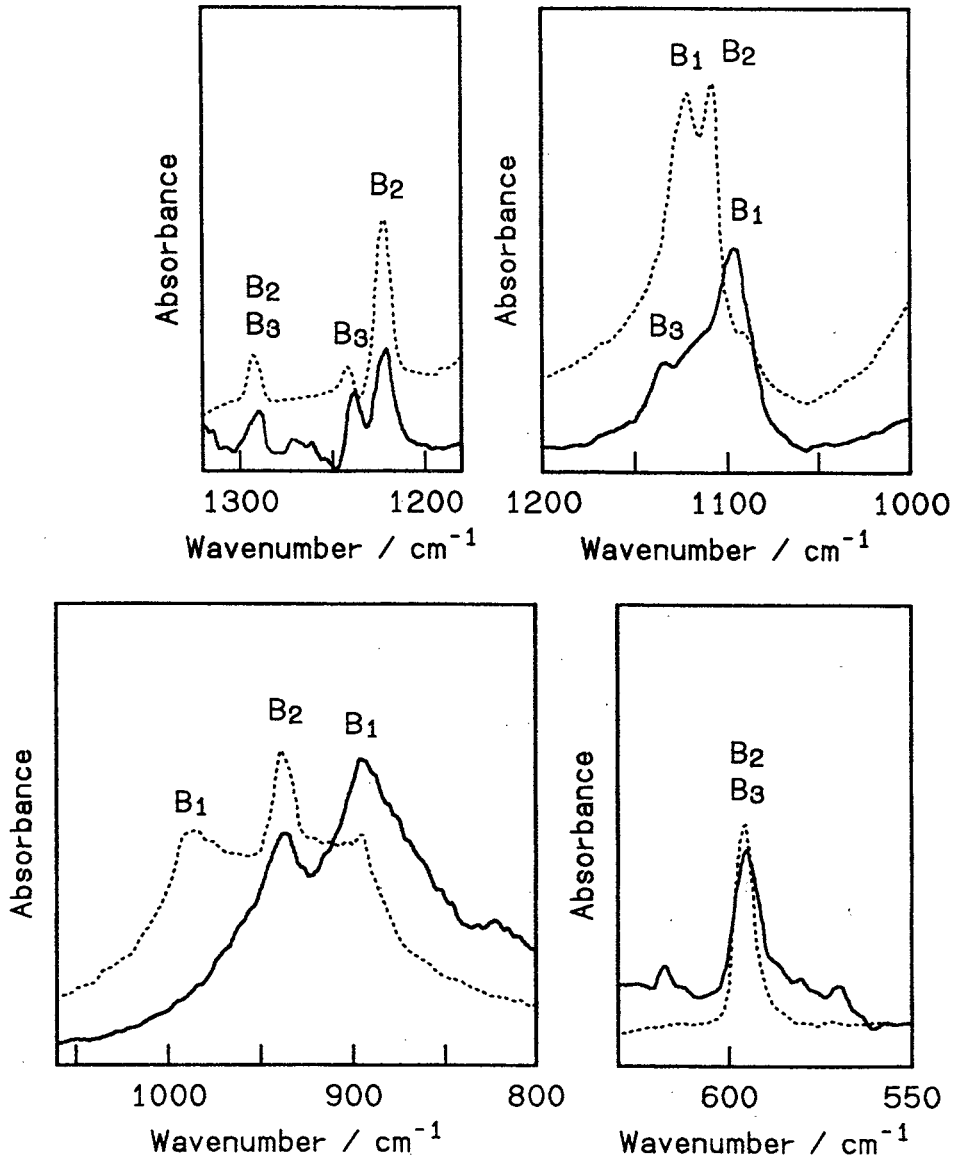

Figure 5-8 Infra-red spectra of orthorhombic polyoxymethylene generated by the pressure-induced phase transition form trigonal polyoxymethylene.

(——) : extended-chain crystals ; (·····) : folded-chain crystals

Table 5–1 Infra–red bands of orthorhombic polyoxymethylenes

Species	Wavenumber (cm^{-1})		
	Folded–chain, ν_A	Extended–chain, ν_B	$\nu_A-\nu_B$
$B_2(5)+B_3(5)$	1287 m	1287 m	0
$B_3(6)$	1240 m	1240 m	0
$B_2(6)$	1220 s	1220 s	0
$B_3(7)$	*	1133 s	—
$B_2(7)$	1108 vvs	*	—
$B_1(6)$	1121 vvs	1096 vvs	25
$B_1(8)$	987 vvs	895 vvs	92
$B_2(8)$	936 vvs	936 vvs	0
$B_2(9)+B_3(9)$	595 vs	595 vs	0
$B_2(10)$	434 m	434 m	0
$B_3(10)$	428 m	428 m	0
$B_1(10)$	316 m	304 m	12

*) Overlapped band.

folded–chain crystals of pure *o*–POM are shown in *Figure 5–8*. Here, the subtraction technique is used to remove the interference by strong absorptions associated with the remaining *t*–POM. *Table 5–1* shows the observed wavenumbers, symmetry species and frequency gaps between two crystals.[25] It is clear that only the B_1 bands having the transition dipoles parallel to the chain axis shift towards high–frequency side in the spectrum of folded–chain *o*–POM crystal, while the B_2 or B_3 bands having perpendicular polarization appear at the same positions. From *Figure 5–8*, we can see that the strongest B_1 band (at 895 cm^{-1} for ECC) gives rise to the largest bandshift, as in the cases of normal and deuterated *t*–POM. Thus, for the orthorhombic modification, the infra–red parallel bands show large frequency shifts induced by change in crystal morphology. The spectral change should arise from the same origin as that observed in *t*–POM and *t*–POM–d_2.

5.4 **Conclusion**

It is confirmed that the metastable orthorhombic modification is generated via cationic polymerization of trioxane by vibrational spectroscopy and X–ray diffraction. Microfocus Raman measurement clarifies that the *o*–POM crystals appear in "moth–like" shape.

Using the "moth–like" crystal, extended– and folded–chain crystals of *o*–POM produced by pressure–induced phase transition, morphology–dependent changes in infra–red spectra were found. The B_1 bands of the folded–chain crystals with transition moment parallel to the molecular axis shifted as large as 90 cm^{-1} towards high–frequency side as the parallel A_2 bands of *t*–POM and *t*–POM–d_2, while the perpendicular bands (B_2 and B_3) are unshifted like the A_1 and E_1 bands of *t*–POM. The spectral change of *o*–

POM is morphology–dependent, and have the same characteristics and molecular mechanism as those of *t*–POMs.

References

1 M. Iguchi, *Br. Polym. J.*, **5**, 195 (1973)

2 M. Iguchi and I. Murase, *J. Crystal Growth*, **24/25**, 596 (1974)

3 M. Iguchi, I. Murase and K. Watanabe, *Br. Polym. J.*, **6**, 61 (1974)

4 M. Iguchi, H. Kanetsuna and T. Kawai, *Makromol. Chem.*, **128**, 63 1969)

5 M. Iguchi and I. Murase, *Makromol. Chem.*, **176**, 2113 (1975)

6 M. Shimomura and M. Iguchi, *Polymer*, **23**, 509 (1982)

7 L. Mortillario, G. Galliazzo and S. Bessi, *Chem. Ind. (Milan)*, **46**, 139 (1964), *ibid* **46**, 144 (1964)

8 G. Carazzolo and G. Putti, *Chem. Ind. (Milan)*, **45**, 771 (1963)

9 G. Carazzolo and M. Mammi, *J. Polym. Sci. (A)*, **1**, 965 (1964)

10 V. Zamboni and G. Zerbi, *J. Polym. Sci. (C)*, **7**, 153 (1964)

11 G. Zerbi and G. Masetti, *J. Mol. Spectrosc.*, **22**, 284 (1967)

12 G. Zerbi and P. J. Hendra, *J. Mol. Spectrosc.*, **27**, 17 (1968)

13 F. J. Boerio and D. D. Cornell, *J. Chem. Phys.*, **56**, 1516 (1972)

14 M. Kobayashi, Y. Itoh, H. Tadokoro, M. Shimomura and M. Iguchi, *Polym. Commun.*, **24**, 38 (1983)

15 M. Kobayashi, H. Morishita, T. Ishioka, M. Iguchi and M. Shimomura, *J. Mol. Struc.*, **146**, 155 (1986)

16 H. Morishita, M. Kobayashi, M. Shimomura and M. Iguchi, *Sci. Bull. Fac. Educ., Nagasaki Univ.* **39**, 47 (1988)

17 M. Iguchi, *Makromol. Chem.*, **177**, 549 (1976)

18 H. Tadokoro, M. Kobayashi, Y. Kawaguchi, A. Kobayashi and S. Murahashi, *J. Chem. Phys.*, **38**, 703 (1063)

19 H. Sugeta, T. Miyazawa and T. Kajiura, *Polym. Lett.*, **7**, 251 (1979)

20 H. Tadokoro, M. Kobayashi, S. Murahashi, A. Mitsuishi and H. Yoshinaga, *Bull. Chem. Soc. Jpn.*, **25**, 1429 (1963)

21 M. Iguchi, *Polymer*, **24**, 915 (1983)

22 M. Kobayashi, H. Morishita, M. Shimomura and M. Iguchi, *Macromolecules*, **20**, 2453 (1987)

23 M. Kobayashi, H. Morishita and M. Shimomura, *Rep. Prog. Polym. Phys. Jpn.*, **31**, 473 (1988)

24 H. Morishita, M. Kobayashi, M. Shimomura, M. Iguchi and H. Kuwahara, *Sci. Bull. Fac. Educ., Nagasaki Univ.* **41**, 1 (1989)

25 M. Kobayashi, H. Morishita and M. Shimomura, *Macromolecules*, **22**, 3726 (1989)

Chapter 6

Vibrational Spectra of Poly(ethylene oxide) Crystals

6.1 Introduction

The vibrational spectra of trigonal polyoxymethylene (*t*–POM) crystals[1–3] have been of interest as well as those of another modification, metastable orthorhombic form (*o*–POM),[4,5] and a number of studies have been published.[6–15] It has been found that the infra–red spectra of *t*–POM are very dependent on the state and/or the route of processing of the specimens measured.[13] Though the absorption profiles are rather complicated, the infra–red spectra of some *t*–POM specimens could be reproduced by the superposition of the spectra of two extreme samples. One is a needle–like crystal known as a polymer whisker,[16,17] in which the molecular chains are fully extended and arranged in extremely high perfection.[18–20] The other is a lamellar crystal grown isothermally from dilute solution, with molecular chains folded periodically.[21,22] The infra–red spectra of these two extreme crystals are quite different, though both crystals show the same wide angle X–ray diffraction patterns, *i.e.* both crystals have the same unit cell structure. The infra–red spectrum of the needle–like crystals is very close to that of a well oriented and highly crystalline film sample and the assignment of the bands has been established by normal mode analysis.[6] On the contrary, some bands of the solution–grown crystals shifted substantially from the positions of the corresponding bands of the needle–like crystals. In previous chapters, the symmetry species of the shifted bands of the solution–grown crystals was determined to be A_2, which has transition dipole parallel to the chain axis.[23,24]

In the clear contrast, the bands of the other symmetry species, infra-red- and Raman-active E_1 and Raman-active A_1 and E_2, showed no frequency difference between these two extreme crystals. The same phenomenon was also observed with deuterated samples of trigonal polyoxymethylene (*t*-POM-d_2).[23]

Recently, an extended-chain crystal of *o*-POM was obtained in a cationic polymerization system of trioxane as a by-product of the needle-like crystal synthesis,[25,26] and spectroscopic studies have been performed.[27,28] Folded- and extended-chain crystals of *o*-POM were obtained by a pressure-induced solid-state phase transition.[29,30] These *o*-POM crystals exhibited the same spectral change caused by the difference in morphology. In this case, only the bands assigned to the B_1 species with transition dipole parallel to the chain axis shift towards the high-frequency side in the spectrum of the folded-chain crystals, while B_2 and B_3 bands having transition dipoles perpendicular to the chain axis remain unshifted.

In this chapter, another polar polymer, the monoclinic form of poly(ethylene oxide) (PEO), was investigated in order to obtain more experimental information on the anomalous behaviour of the vibrational spectra of the POM crystals depending on the morphology. PEO is a crystalline polymer with 7/2 helical conformation[31,32] and contains oxygen atom in the main chain like in POM. Unfortunately, PEO crystals consisting of fully extended-chain structure like the needle-like crystals of *t*-POM cannot be obtained at the moment. A well-drawn film of PEO was used in this study, because the drawn film of *t*-POM shows the ECC type infra-red spectrum. The infra-red and Raman spectra of the solution-grown (folded-chain) crystals and drawn film of PEO were measured and the behaviour of the morphology-dependent spectral changes was investigated in comparison

with the cases of *t*–POM and *o*–POM.

6.2 Experimental

6.2.1 *Samples*

Commercial PEO with the weight average molecular weight of $3x10^5$ g/mol was used. Film samples with appropriate thickness for the infra–red measurement were cast from methanol solution. After drying in air, the film was drawn at room temperature. Draw ratios of the films were about eight.

The solution–grown crystals were prepared from the same resin. The folded–chain crystals were crystallized from dilute (0.5wt%) xylene solution at room temperature.[33,34] After filtration, the crystals were dispersed in benzene and freeze–dried. To avoid the effect of water, the solvents were dried with calcium sulfate before the crystallization or freeze–drying operations.

6.2.2 *Measurement of Infra–red and Raman Spectra and Wide Angle X–ray Diffraction*

A Fourier transform infra–red spectrometer, Perkin–Elmer model 1800, was used. Sampling for the solution–grown crystals was performed by the Nujol (liquid paraffin) mull method in order to avoid mechanical deformation, since the folded–chain structure is destroyed very easily by grinding with KBr powder, causing a significant spectral change just like the *t*–POM solution–grown crystals. Measurements on KBr pellets of the same sample were also performed for comparison. The bands due to water in the atmosphere were

subtracted carefully. In the case of the Nujol mull method, the background due to the mulling reagent was also subtracted.

Raman spectra were measured using a Jasco model R-800S spectrometer. Samples were rotated during the measurements to avoid damage (melting) caused by the laser light. The 488nm line of an Ar^+ laser was used as the excitation source.

A Philips model PW1700 system with a graphite monochromator was used for the powder pattern measurement.

6.3 **Results and Discussion**

6.3.1 *Spectra of Drawn Film and Solution-grown Crystals*

Figure 6-1 shows the wide angle X-ray diffraction patterns of the PEO samples. The drawn film was cut into small pieces and a randomly oriented sample was prepared and measured. As the solution-grown crystals were rather fine powder, no orientation is expected for the X-ray diffraction measurement. Both patterns of the drawn film and the solution-grown crystals were identical. This means that these samples have the same unit cell structure. The diffraction patterns also indicate that the both samples have enough crystallinity.

Infra-red spectra of the PEO drawn film and the solution-grown crystals were measured. It was confirmed that the effect of the humidity in the air can be ignored in this work. Though the difference in the spectrum between the two samples was not so large as was found in the spectra of POMs, small but distinct differences can be found. In order to enhance the difference and to determine the symmetry species of the infra-red bands,

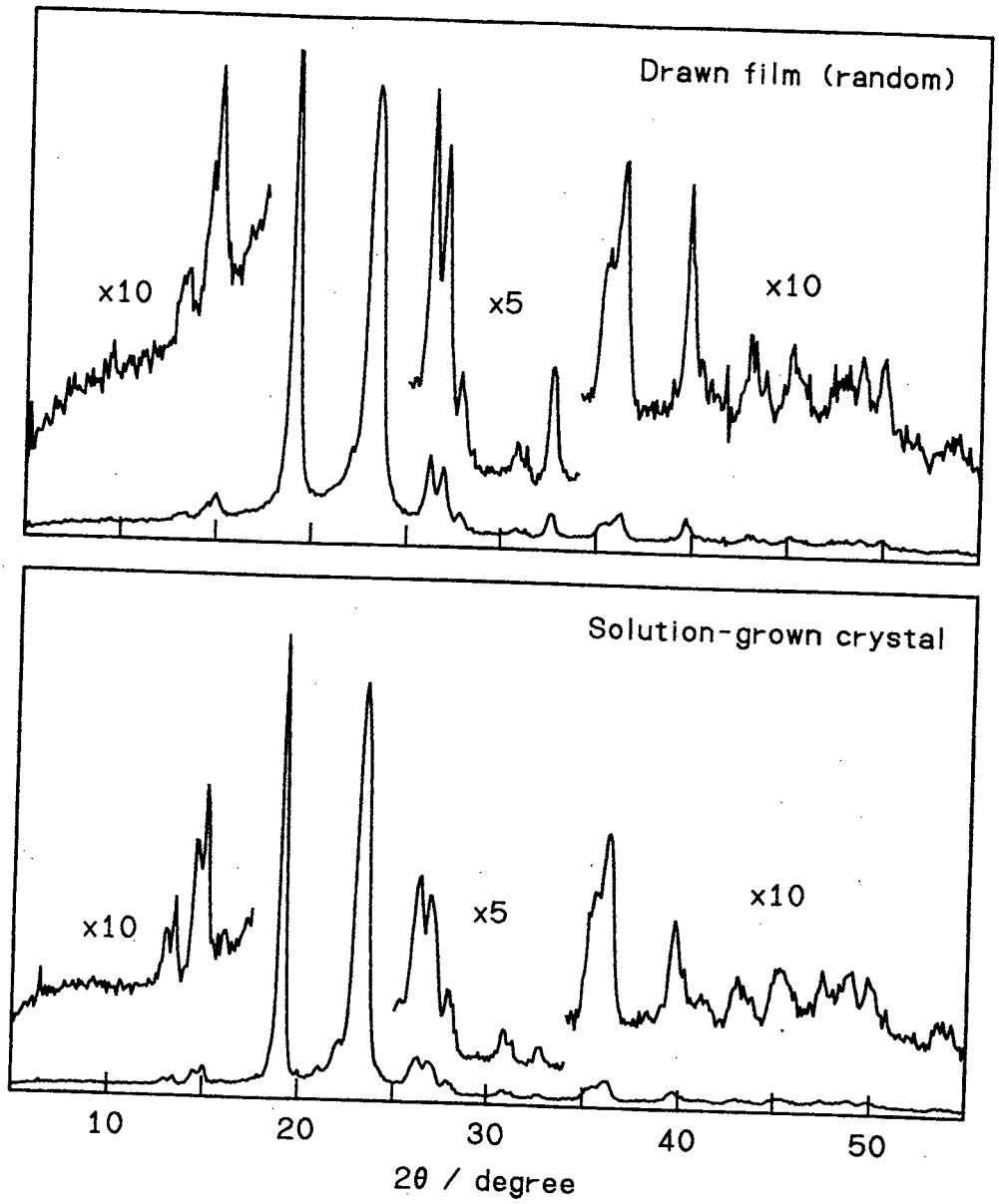

Figure 6–1 X–ray diffraction diagrams of poly(ethylene oxide) crystals.

polarization measurements were made on both samples. On the drawn film, spectra were measured with parallel- and perpendicular-polarized light. The result was in good accordance with the literature[35,36] and the symmetry species, infra-red-active A_2 and E_1, could be determined easily. The spectrum of the A_2 bands and that of the E_1 bands were separated by the spectral subtraction technique. For the solution-grown crystals, random and semi-plane-oriented samples were prepared. When the sample powder, mixed with a small amount of liquid paraffin, was sandwiched between two KBr windows without a spacer, the lamellar crystals were partly oriented with their *c*-axis directed normal to the window surface. On measuring the transmission spectrum of this sample, with the infra-red incidence nearly perpendicular to the window surface, the *c*-polarized A_2 bands should diminish in intensity compared with a spectrum measured on a randomly oriented sample.[23] By insertion of a spacer of sufficient thickness, randomly oriented solution-grown crystals could be prepared. The subtraction between the spectra of the random and the plane-oriented samples was performed after elimination of the background due to the liquid paraffin. Well-separated infra-red spectrum of the A_2 bands and that of the E_1 bands were obtained.

The E_1 bands of the drawn film and those of the solution-grown crystals are compared in *Figure 6-2* (upper), which showed no significant difference. Every bands appear at the same position within the error of the measurement. On the contrary, in the spectra of the A_2 bands (*Figure 6-2* lower), shifts were clearly found, *i.e.* bands of the drawn film at 1341.6, 1241.4, 1099.4 and 961.8 cm^{-1} shifted to 1344.8, 1242.8, 1118.4 and 966.0 cm^{-1}, respectively, in the spectrum of the solution-grown crystals.

The observed frequencies of the infra-red bands of PEO specimens are listed in *Table 6-1* along with their symmetry species and the frequency gaps

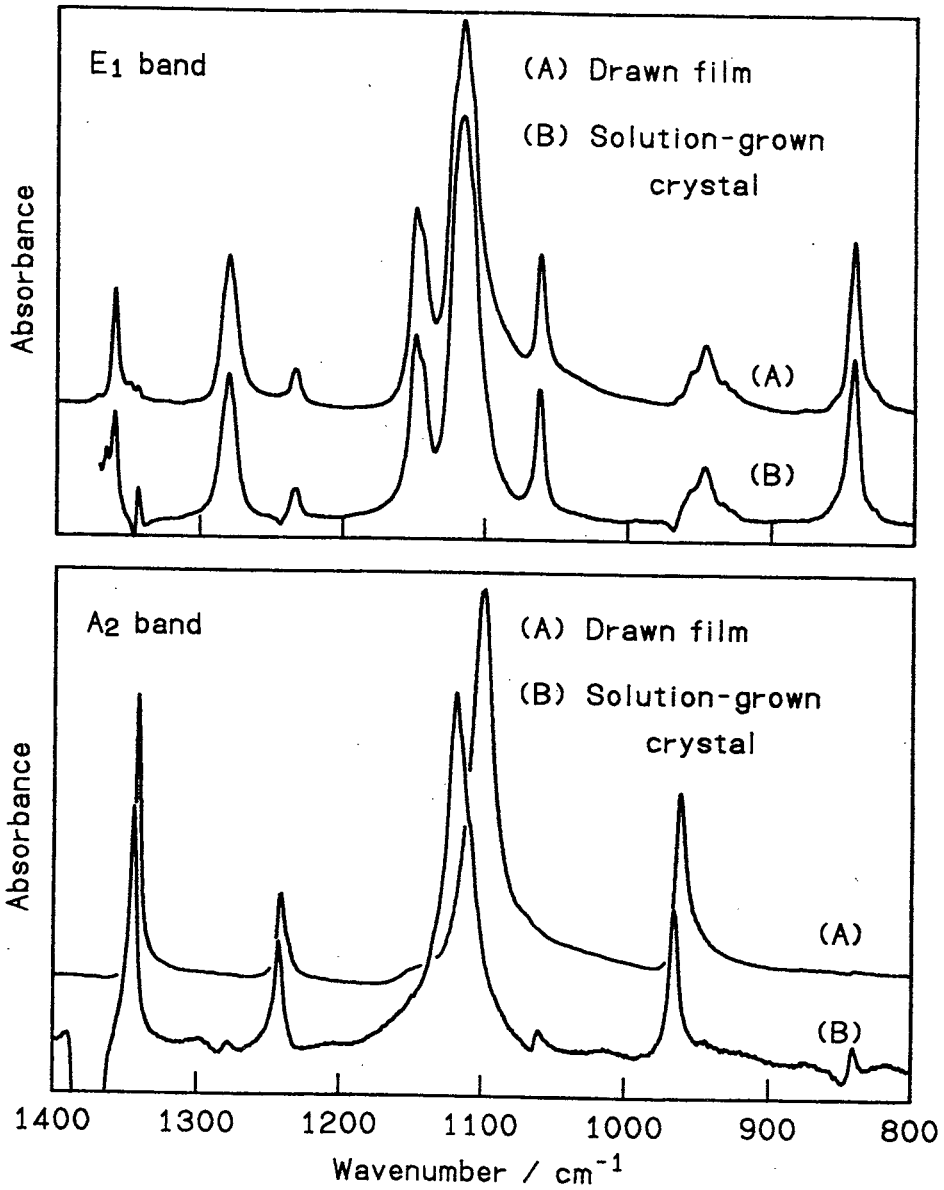

Figure 6–2 E_1 and A_2 bands in infra–red spectra of various poly(ethylene oxide) crystals obtained by a subtraction method.

Table 6–1 Infra–red bands of poly(ethylene oxide)

Species	Wavenumber (cm^{-1})		
	Solution–grown, ν_A	Drawn film, ν_B	$\nu_A-\nu_B$
E_1	1359.6	1359.6	0.0
A_2	1344.8	1341.6	3.2
E_1	1280.2	1280.2	0.0
A_2	1242.8	1241.4	1.4
E_1	1234.2	1234.2	0.0
E_1	1149.2	1149.4	–0.2
E_1	1116.0	1115.6	–0.4
A_2	1118.4	1099.4	19.0
E_1	1061.0	1061.0	0.0
A_2	966.0	961.8	4.2
E_1	946.6	946.6	0.0
E_1	842.4	842.6	–0.2

between two specimens. It was clear that no meaningful shift was found in the bands assigned to the E_1 species. It was also clear that the A_2 bands of the solution-grown crystals shifted to the high-frequency side compared with those of the drawn film, though the magnitudes of the shifts were not so large as were observed in the case of the *t*-POM crystals. It has also been noticed that the magnitudes of the bandshifts have some relation with the band intensity, *i.e.*, the stronger is band intensity the larger is bandshift.

Figure 6-3 shows Raman scattering spectra of the PEO samples, in which the bands assigned to Raman-active A_1 and E_1 species are observed. In the Raman spectra, no significant difference in frequency was observed, *i.e.*, the A_1 bands and E_1 bands appeared at the same positions.

These observations could be summed up as follows. The wide angel X-ray diffraction patterns of the PEO drawn film and the PEO solution-grown crystals were identical, *i.e.*, both samples had the same unit cell structure. The bands assigned to the A_2 symmetry species, whose transition dipoles were parallel to the *c*-axis, shifted towards the high-frequency side in solution-grown crystals, while the other bands, assigned to the A_1 or E_1 species, were unshifted. The results mentioned above are just the same as those found in *t*-POM, *t*-POM-d_2 and *o*-POM crystals.[23] Thus, frequency shifts of the parallel bands induced by change in morphology were also found for PEO.

6.3.2 *Spectral Change of Poly(ethylene oxide) by Mechanical Deformation and Heat Treatment*

The folded-chain structure constructed in as-solution-grown crystals of *t*-POM is destroyed more or less by the application of mechanical stress.

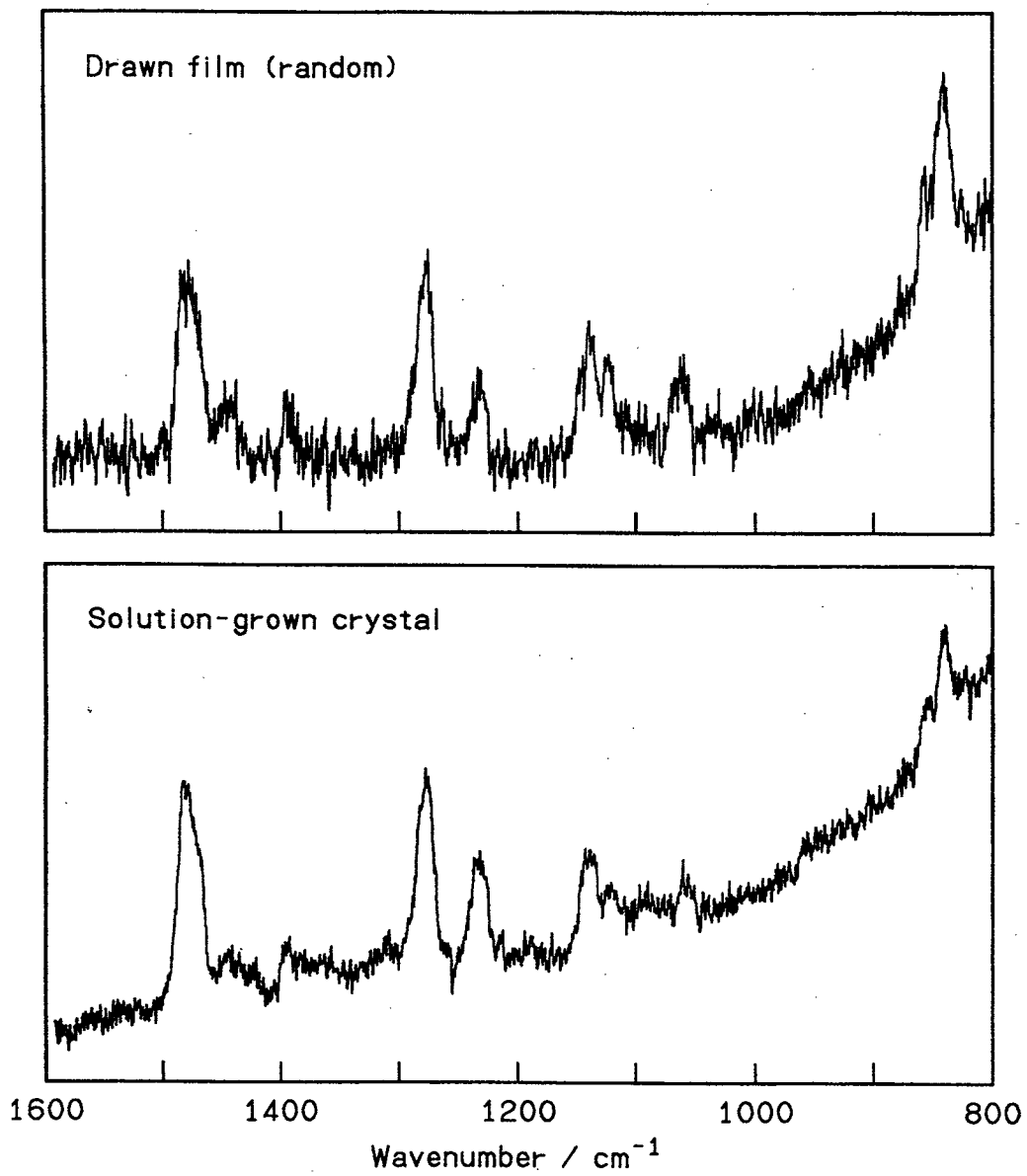

Figure 6–3 Raman spectra of poly(ethylene oxide) crystals.

The infra-red spectrum of the *t*-POM solution-grown crystals measured by the KBr pellet method changes to that of the extended-chain needle-like crystals.[24] Similar spectral change occurs in PEO. *Figure 6-4* (B) shows the infra-red spectrum of the PEO solution-grown crystals measured by the KBr pellet method. The spectrum measured with the Nujol mull method and those of the drawn film are also reproduced (*Figure 6-4* (A), (C)) for comparison. It is clear that the spectrum of the solution-grown crystals changes with the mechanical deformation, induced by shear stress applied during the milling with KBr powder. Though the polarization data could not be obtained by the KBr pellet method, it is reasonable to conclude that the A_2 bands measured with the KBr method appear at the same frequency as those of the drawn film.

Figure 6-5 shows the infra-red spectra of a KBr pellet of the PEO solution-grown crystals before (A) and after (B) the melt crystallization. The recrystallized sample gave rise to the spectrum situated in-between those of the starting and the ground samples.

These spectral behaviours of the PEO solution-grown crystals have also been observed for the *t*-POM solution-grown crystals[24] as was described in Chapter 4. These facts might be interpreted as follows. The folded-chain (solution-grown) crystals were destroyed and molecular chains were stretched by the shear stress during pelletization. The stretched chains form crystallites with larger dimension along *c*-axis, and give the infra-red spectrum of the extended-chain crystal type.

By the subsequent melt crystallization, the stretched chains folded again, however, the other chains cannot have enough mobility to form folded-chain crystallites. Thus, both crystallites of large and small size along *c*-axis exist, and the infra-red spectrum of the sample became the superposition of the spectra of the folded-chain type and the extended-chain type, as the

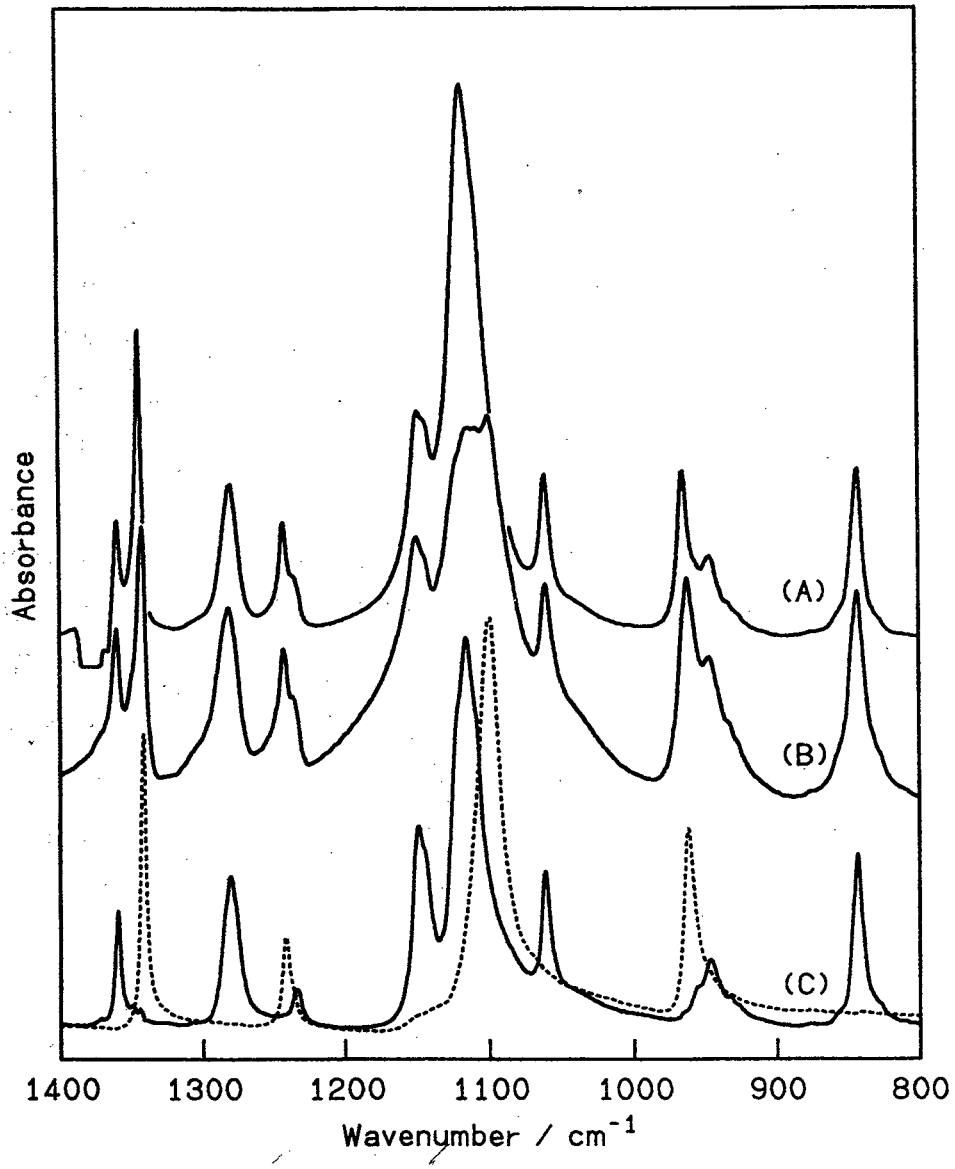

Figure 6–4 Infra–red spectra of poly(ethylene oxide) crystals. (A):solution–grown crystals (Nujol); (B):solution–grown crystals (KBr pellet); (C):drawn film, E_1 bands (——) and A_2 bands (·····)

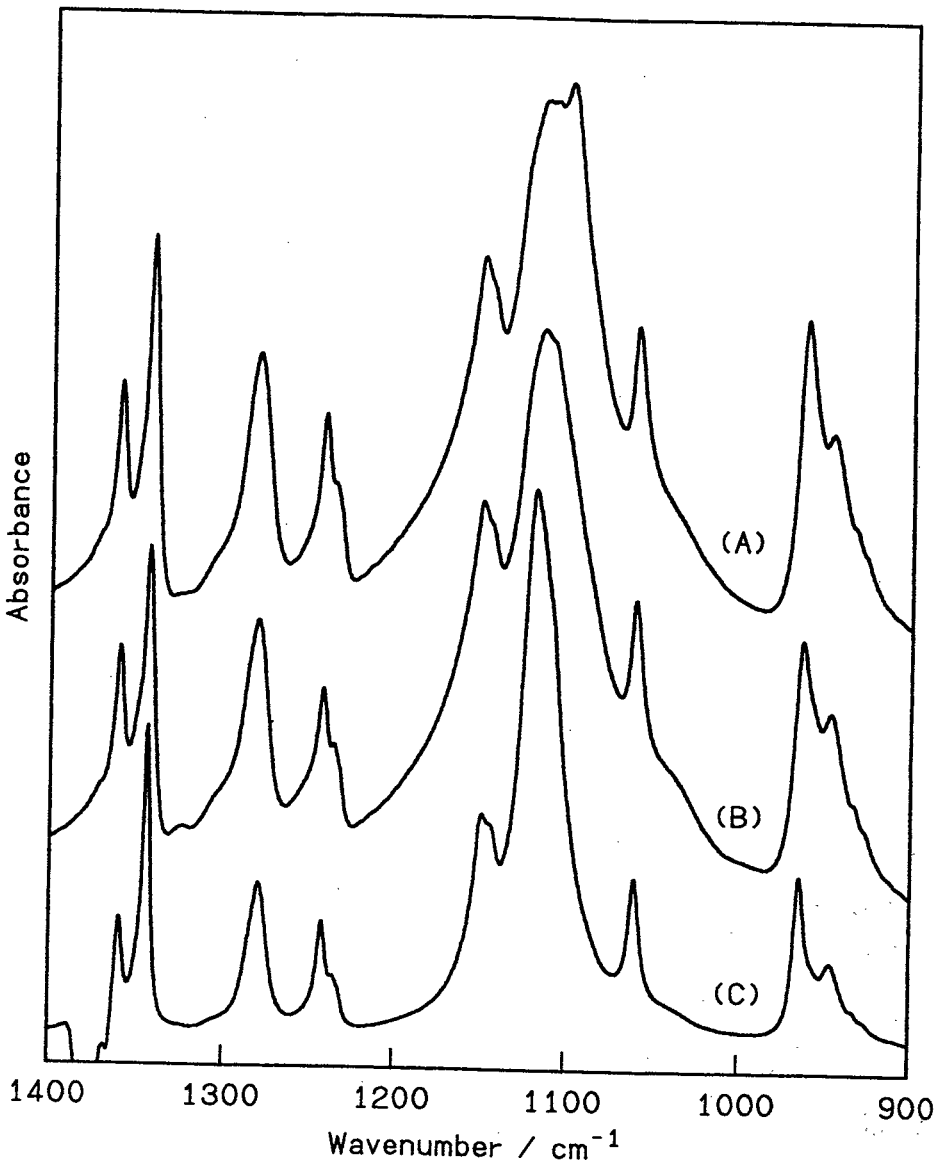

Figure 6–5 Infra–red spectra of poly(ethylene oxide) solution–grown crystals. (A):KBr, before melt crystallization; (B):KBr, after melt crystallization; (C):Nujol mull method.

result.

6.4 Conclusion

The drawn film and the solution-grown crystals of PEO, which give the same wide angel X-ray diffraction patterns, showed different infra-red spectra. The spectral subtraction method was very useful to clarify the spectral difference. The spectral change is related to the difference in morphology. In the vibrational spectra of the solution-grown crystals, only the A_2 parallel bands shifted towards the high-frequency side. The other bands, which are assigned to A_1 or E_1, remained at the same frequency. The infra-red spectrum of the solution-grown crystals changed to the drawn film type (extended-chain type) spectrum by application of mechanical deformation. By subsequent melt crystallization, the spectrum again changed and the solution-grown crystal type components appeared. This behaviour of the infra-red and Raman spectra of the PEO crystals was just the same as that of *t*-POM, and was considered to be caused by the same origin.

Though the mechanism is not completely understood, this morphology-dependent spectral change is common in *t*-POM, *t*-POM-d_2, *o*-POM and PEO crystals, *i.e.*, only the bands with the transition dipole parallel to the chain axis shift towards high-frequency side for the crystals with small crystallite size along the chain axis.

References

1 H. Tadokoro, S. Yasumoto, S. Murahashi and I. Nitta, *J. Polym. Sci.*, **44**, 266 (1960)

2 G. Carazzolo, *J. Polym. Sci. (A)*, **1**, 1573 (1963)

3 T. Uchida and H. Tadokoro, *J. Polym. Sci. (A-2)*, **5**, 63 (1967)

4 G. Carazzolo and M. Mammi, *J. Polym. Sci. (A)*, **1**, 965 (1963)

5 L. Mortillario, G. Galliazzo and S. Bessi, *Chem. Ind. (Milan)*, **46**, 139 (1964), *ibid* **46**, 144 (1964)

6 H. Tadokoro, M. Kobayashi, Y. Kawaguchi, A. Kobayashi and S. Murahashi, *J. Chem. Phys.*, **38**, 703 (1963)

7 V. Zamboni and G. Zerbi, *J. Polym. Sci. (C)*, **7**, 153 (1964)

8 L. Piseri and G. Zerbi, *J. Chem. Phys.*, **48**, 3561 (1968)

9 E. F. Oleinik and N. S. Enikolopyan, *J. Polym. Sci. (C)*, **16**, 3677 (1968)

10 L. Terlemezyan, M. Mihailov, P. Schmidt and B. Schneider, *Makromol. Chem.*, **179**, 807 (1978)

11 L. Terlemezyan, M. Mihailov, P. Schmidt and B. Schneider, *Makromol. Chem.*, **179**, 2315 (1978)

12 L. Terlemezyan and M. Mihailov, *Eur. Polym. J.*, **17**, 1115 (1981)

13 M. Shimomura and M. Iguchi, *Polymer*, **23**, 509 (1982)

14 A. H. Fawcett, *Polym. Commun.*, **23**, 1865 (1982)

15 L. Terlemezyan and M. Mihailov, *Polym. Commun.*, **25**, 80 (1984)

16 M. Iguchi, *Br. Polym. J.*, **5**, 195 (1973)

17 M. Iguchi and I. Murase, *J. Crystal Growth*, **24/25**, 596 (1974)

18 M. Iguchi, I. Murase and K. Watanabe, *Br. Polym. J.*, **6**, 61 (1974)

19 M. Iguchi, *Makromol. Chem.*, **177**, 549 (1976)

20 T. Mashimoto, T. Sakai and M. Iguchi, *J. Phys. (D)*, **12**, 1567 (1979)

21 D. C. Bassett, F. R. Dammont and R. Salovey, *Polymer*, **5**, 579 (1964)

22 D. R. Carter and E. J. Baer, *Appl. Phys.*, **37**, 4060 (1966)

23 M. Shimomura, M. Iguchi and M. Kobayashi, *Polymer*, **29**, 351 (1988)

24 M. Shimomura, M. Iguchi and M. Kobayashi, *Polymer*, **31**, 1406 (1990)

25 M.Iguchi, *Polymer*, **24**, 915 (1983)

26 M. Kobayashi, Y. Itoh, H. Tadokoro, M. Shimomura and M. Iguchi, *Polym. Commun.*, **24**, 38 (1983)

27 M. Kobayashi, H. Morishita, T. Ishioka, M. Iguchi and M. Shimomura, *J. Mol. Struct.*, **146**, 155 (1986)

28 M. Kobayashi, H. Morishita, M. Shimomura and M. Iguchi, *Macromolecules*, **20**, 2453 (1987)

29 M. Kobayashi, H. Morishita and M. Shimomura, *Rep. Prog. Polym. Phys. Jpn.*, **31**, 473 (1988)

30 M. Kobayashi, H. Morishita and M. Shimomura, *Macromolecules*, **22**, 3726 (1989)

31 Y. Takahashi and H. Tadokoro, *Macromolecules*, **6**, 672 (1973)

32 Y. Takahashi, I. Sumita and H. Tadokoro, *J. Polym. Sci., Polym. Phys. Ed.*, **11**, 363 (1973)

33 W. J. Barnes and F. P. Price, *Polymer* **5**, 283 (1964)

34 B. Lotz, D. C. Bassett and A. Keller, *Kolloid Z. Z. Polym.*, **209**, 115 (1966)

35 T. Yoshihara, H. Tadokoro and S. Murahashi, *J. Chem. Phys.*, **41**, 2902 (1964)

36 Y. Matsui, T. Kubota, H. Tadokoro and T. Yoshihara, *J. Polym. Sci. (A)*, **3**, 2275 (1965)

Chapter 7

Theoretical Explanation of the Shift of A_2 Mode in Infra-red Spectra of Polyoxymethylene

7.1 Introduction

Polyoxymethylene (POM) is usually crystallized in a trigonal modification consisting of 9/5 helical polymer chains. The two typical crystals of trigonal POM (*t*-POM) are known as needle-like crystals and solution-grown crystals. The needle-like crystal is a trigonal single crystal with fully extended chains and the solution-grown crystal is a well-known lamellar crystal with folded chains.

As described in Chapter 3, the vibrational spectrum of *t*-POM shows very specific changes depending on the state and/or the processing method of the samples.[1-6] The morphology dependence of the infra-red spectrum is the most characteristic feature. *Figure 7-1* shows the infra-red spectra of *t*-POM for two crystals with different morphologies. Symmetry species of the bands are also shown in the figure. Some bands assigned to the A_2 symmetry species exhibit anomalously large shifts between the needle-like crystals and the solution-grown crystals. The A_2 mode is characterized to have transition dipole moment parallel to the chain axis. The other infra-red-active mode E_1 (the transition dipole moment is perpendicular to the chain axis) and the Raman-active modes (A_1, E_1 and E_2) remain at nearly the same frequencies in both crystals. It should be noted that the powdered samples of these two crystals yield substantially identical wide angle X-ray diffraction patterns. Highly drawn POM film shows essentially the same spectra as the needle-like

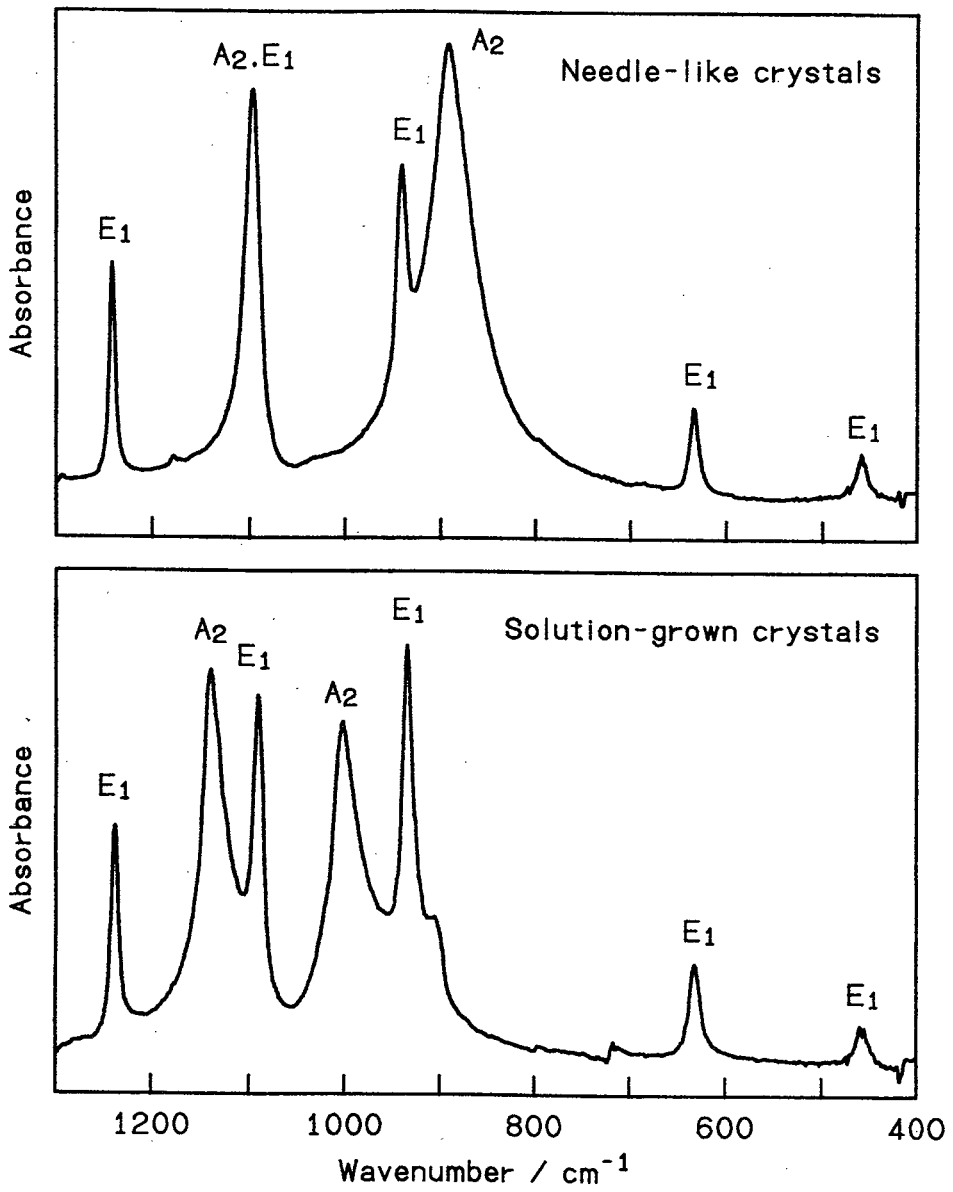

Figure 7–1 Infra–red spectra of polyoxymethylene crystals.
Assigned symmetry species are shown for each crystals.

crystals.

This large frequency shift for the specific infra-red spectral mode is actually related to the morphological change, although it has been thought that vibrational spectra in the infra-red region do not depend on the higher order structure such as the morphology. Since *t*-POM oligomers show nearly the same spectra as the solution-grown crystals, the frequency shift is related to the stem-length in the crystal,[1,7] as is discussed in Chapter 4.

Poly(ethylene oxide) (PEO) is the other polar polymer consisting of chains in 7/2 helical conformation. As shown in Chapter 6, PEO exhibits the similar spectral shift between the drawn film and the solution-grown crystals,[8,9] *i.e.* only bands of A_2 species show the shifts. Another modification of POM crystal, orthorhombic POM crystal consisting of 2/1 helical chains exhibited the same phenomenon. In this case, only B_1 bands appear at the different frequencies between the two orthorhombic modifications generated by pressure-induced phase transition from the trigonal extended-chain and folded-chain crystals.[10] It should be noted that only B_1 modes have transition moments parallel to the chain axis. (See Chapter 5)

The morphology-dependent frequency shifts of the parallel infra-red bands are not limited to *t*-POM to which the phenomenon has been mentioned for the first time, but are generally observed for some polymer crystals. The characteristic features of these specific shifts are summarized as follows. (1) As the crystal morphology goes from extended-chain crystal (ECC) to folded-chain crystal (FCC), only the infra-red bands with parallel polarization (the A_2 for *t*-POM and PEO, and the B_1 for *o*-POM) are shifted toward the high-frequency side. (2) The infra-red bands with perpendicular polarization (E_1 : *t*-POM and PEO, B_2 and B_3 : *o*-POM) are unshifted. (3)

Infra-red-inactive and Raman-active A_1 (for *t*-POM and PEO) and A (for *o*-POM) bands are unshifted. (4) The FCC-type spectrum is also obtained for the crystals of linear oligomers of POM containing no folded chain structure. Therefore, the FCC-type infra-red spectrum originates not from the folded-chain structure but from the lamellar-type crystal morphology. (5) The morphology-dependent frequency shifts of the parallel bands are closely related to the absorption intensity; the stronger is the band the larger is the bandshift.

The change is thought to be related to the crystallite size along the molecular axis. It was suggested that strong interactions among transition dipoles are important for this anomalous shift of the specific infra-red band.[10,11)]

In this chapter, a "dynamic ferroelectric" theory will be presented whereby the morphology-dependent shifts of the parallel bands are interpreted, because the dipolar interactions are important to the shift, large interactions are assumed for a crystal of sufficiently large stem-length, and the bandshifts will be derived.

7.2 **Model**

It is assumed that the bandshifts of the A_2 modes in *t*-POM are attributed to nonlinear terms caused by interactions among transition dipoles. As known well, ferroelectric state is one of the systems where dipole moments interactions cause nonlinear effect. In the ferroelectric state, dipoles are align in sufficiently large domains and the polarizability of such domains has polarization dependence due to the dipolar interactions. That nonlinear effect is essential for the ferroelectric phenomena. Here, the nonlinear effect in *t*-

POM crystal will be treated on the basis of ferroelectric theory. POM crystals have no permanent dipole moment, however, transition dipole moments align to the same direction along molecular chain (A_2 mode) for each instant of vibration. Here we assume that the transition dipolar interactions become significant when crystals have sufficiently large stem-length, and the "ferroelectric"-like state is achieved through in-phase oscillation of the transition dipoles. This stage changes with the time variation of each transition dipole moments, and can be called the "dynamic ferroelectric" state. In order to realize "dynamic ferroelectric" state, each dipole moments should align long enough along the same direction. For crystals with short stem-length, the interactions among transition dipole moments, especially long range interactions, are too small to realize the "ferroelectric"-like state even for an instant.

As written in textbooks[12], the local field E_{loc} in a dielectric medium is decomposed as follows:

$$\begin{aligned} E_{loc} &= E_0 + E_1 + E_2 + E_3 \\ &= E + (1/3\ \varepsilon_0) P + E_3 \end{aligned} \qquad (1)$$

where E_0 is the applied external field, $E_1 = -(L / \varepsilon_0) P$ is the depolarization field which depends on the shape of the medium (L is the geometrical depolarization factor, ε_0 is the vacuum permittivity, and P is the polarization), E is the macroscopic field in the medium and is described by $E = E_0 + E_1$, E_2 is the Lorentz cavity field given by $E_2 = (1/3\ \varepsilon_0) P$, and E_3 is the field caused by the interactions with surrounding dipoles and multipoles in the neighbourhood of the dipole at the origin. When multipolar interactions become large, the approximation $E_3 = c P + d P^3$ must be used. Thus

$$E_{loc} = E + \gamma P + \eta P^3 \qquad (2)$$

where γ and η include the effect of dipole–dipole interactions and other multipolar interactions, respectively. The parameters γ and η are positive.

Here, one–dimensional model is adopted where the dipole moments induced by an A_2 mode vibration are arranged linearly in the chain direction (see *Figure 7–2*). As known well, the infra–red absorption is due to the ionic polarization of vibrating molecules. The displacement at the n–th repeating unit in the i–th normal vibration of A_2 mode is denoted by $Q_i^{(n)}$, where a repeating unit consists of 9 monomers in the 9/5 helical POM chain. The polarization $p_i^{(n)}$ induced at the n–th repeating unit by $Q_i^{(n)}$ is given by $p_i^{(n)} = q_i^{(n)} Q_i^{(n)}$ where $q_i^{(n)}$ is an effective charge.

Infra–red absorption is observed only for the vibration with no phase difference between vibrating repeating units, so the polarization due to the i–th normal vibration is expressed by $P_i = (1 / N) \Sigma_{n=1}^{N} p_i^{(n)} = p_i^{(n)}$, and $P_i = q_i Q_i$, where $q_i = q_i^{(n)}$ and $Q_i = Q_i^{(n)}$. Although all vibrations contribute to total polarization P, only P_i needs to be considered instead of P hereafter, because each normal vibration occurs independently and has different frequency. Using local field, the polarization P_i is expressed by

$$P_i = \alpha_i(P_i)\, E_{loc}(P_i) \qquad (3)$$

where α_i is a polarizability. Here the P_i and E_{loc} dependence of α_i is very important to consider the "ferroelectric"–like state. Since the even powers of P_i for the polarizability are effective, $\alpha_i(P_i)$ can be expanded as follows:

$$\alpha_i (P_i) = \alpha_i^{(0)} + \alpha_i^{(2)} P_i^2 + \alpha_i^{(4)} P_i^4 + \ldots \quad . \qquad (4)$$

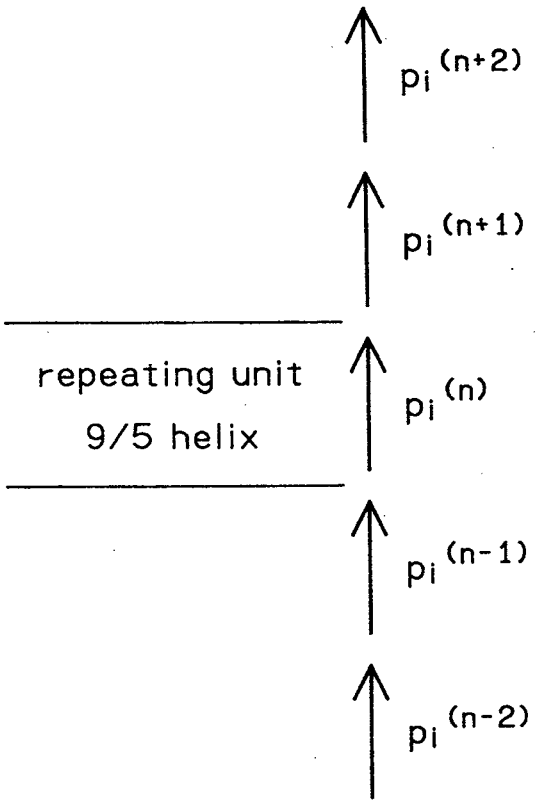

Figure 7–2 Linearly aligned induced polarizations for the *i*th A_2 mode vibration.

Eq. 2 can be written as

$$E_{loc}(P_i) = E + \gamma_i P_i + \eta_i P_i^3 \,. \tag{5}$$

P_i can be expanded as

$$P_i = b_1 E + b_3 E^3 + \ldots \,, \tag{6}$$

because only odd powers of E should be considered. Coefficients b_1 and b_3 can be derived as follows. Substitute eq. 3 using eqs. 4 and 5, and substitution of P_i with $(b_1 E + b_3 E^3 + \ldots)$ resulted

$$\begin{aligned} P_i &= b_1 E + b_3 E^3 + \ldots \\ &= \alpha_i^{(0)} E + \alpha_i^{(0)} \gamma_i (b_1 E + b_3 E^3 + \ldots) \\ &+ \alpha_i^{(2)} E (b_1 E + b_3 E^3 + \ldots)^2 \\ &+ \alpha_i^{(0)} \eta_i (b_1 E + b_3 E^3 + \ldots)^3 \\ &+ \alpha_i^{(2)} \gamma_i (b_1 E + b_3 E^3 + \ldots)^3 + \ldots \,. \end{aligned} \tag{7}$$

Then

$$\begin{aligned} &E (\alpha_i^{(0)} + b_1(\alpha_i^{(0)} \gamma_i - 1)) \\ &+ E^3 (b_3 (\alpha_i^{(0)} \gamma_i - 1) + b_1^2 \alpha_i^{(2)} + b_1^3 (\alpha_i^{(0)} \eta_i + \alpha_i^{(2)} \gamma_i)) \\ &+ (\text{higher terms of } E) = 0 \end{aligned} \tag{8}$$

as coefficients of E and E^3 terms are equal to zero, b_1 and b_3 can be written as

$$b_1 = \alpha_i^{(0)} / (1 - \alpha_i^{(0)} \gamma_i) \tag{9a}$$

$$b_3 = \alpha_i^{(2)} \alpha_i^{(0)2} / (1 - \alpha_i^{(0)} \gamma_i)^3 + (\alpha_i^{(2)} \gamma_i + \alpha_i^{(0)} \eta_i) \alpha_i^{(0)3} / (1 - \alpha_i^{(0)} \gamma_i)^4 . \quad (9b)$$

The coefficient $\alpha_i^{(2)}$ is important for the appearance of ferroelectric–like state.

Now, internal energy of the i–th vibration of the A_2 species, $U(P_i) = \int E \, dP_i$, will be derived, using $E = (1 / b_1) P_i - (b_3 / b_1^4) P_i^3 + \ldots$

$$U(P_i) = U(0) + (1 / 2b_1) P_i^2 - (b_3 / 4b_1^4) P_i^4 + \ldots . \quad (10)$$

The forth–order term of P_i in eq. 10 comes from the P_i dependence of the polarizability $\alpha_i(P_i)$, especially $\alpha_i^{(2)}$, and from the higher order term $\eta_i P^3$ in the local field (eq. 5). When the displacement x_i is induced by the polarization P_i, which is the variation of the minimum point of potential energy like thermal expansion and is different from the displacement of lattice vibration Q_i, the Helmholtz free energy $F(x_i, P_i)$ is given by

$$F(x_i, P_i) = F(0,0) + (k_i / 2) x_i^2 + (1 / 2b_1) P_i^2 - (b_3 / 4b_1^4) P_i^4 - h_i x_i P_i^2 \quad (11)$$

where k_i and h_i are the elastic constant for the displacement x_i and the coupling constant between x_i and P_i, respectively. Only the smallest order term of coupling between x_i and P_i is remained. The higher order terms such as P_i^6 are necessary to consider the stability of the system but not important to discuss the vibrational spectrum.

Let the external force be X_i, where $X_i = (\partial F_i / \partial x_i)_{Pi} = k_i x_i - h_i P_i^2$. ($X_i$ is constant from experimental condition.) Free energy, $G(X_i, P_i) = F(x_i, P_i) - x_i X_i$, is represented as

$$G(X_i, P_i) = G(0,0) + a_i^{(2)} P_i^2 - a_i^{(4)} P_i^4 \qquad (12)$$

where $a_i^{(2)} = (1 / 2b_1) - (h_i / k_i) X_i$ and $a_i^{(4)} = (b_3 / 4b_1^4) + (h_i^2 / 2k_i)$. Here must be noted that $a_i^{(4)}$ must be positive to realize static ferroelectric state. This corresponds to that $h_i^2 / 2k_i$ term is sufficiently large.

Accordingly the i–th vibration of A_2 species occurs in the usual harmonic field and the additional potential field, *i.e.*, the second and third terms in eq. 12, which come from the "dynamic ferroelectric" state. The Hamiltonian H_i for the i–th band of A_2 mode is given by

$$H_i = (1/2) (\dot{Q}_i^2 + \omega_i^{(0)2} Q_i^2) + a_i^{(2)} P_i^2 - a_i^{(4)} P_i^4 . \qquad (13)$$

The dot over Q_i denotes the time derivative and $\omega_i^{(0)}$ is a normal frequency determined by the force constant and the effective mass for the i–th vibration. Using $P_i = q_i Q_i$, and $\omega_i^2 = \omega_i^{(0)2} + 2a_i^{(2)} q_i^2$,

$$H_i = (1/2) (\dot{Q}_i^2 + \omega_i^2 Q_i^2) - a_i^{(4)} q_i^4 Q_i^4 \qquad (14)$$

where ω_i is a characteristic frequency for the i–th band including the $a_i^{(2)}$ term due to transition dipole moment interaction. The term $a_i^{(2)}$ would exist in other mode vibrations (for example, E_1 species). The effect of $a_i^{(2)}$ can be included in the estimation of force constants. The size effect of A_2 mode vibration of infra–red spectra is not related to $a_i^{(2)}$ term but related to $a_i^{(4)}$ term. In the ferroelectric state, where P^2 and higher terms in polarizability cannot be ignored, a sufficiently large domain in which dipole moments align to the same direction is necessary. Like ferroelectric state, the coefficient of $a_i^{(4)}$ would increase stepwise from zero to some value as the chain–stem–

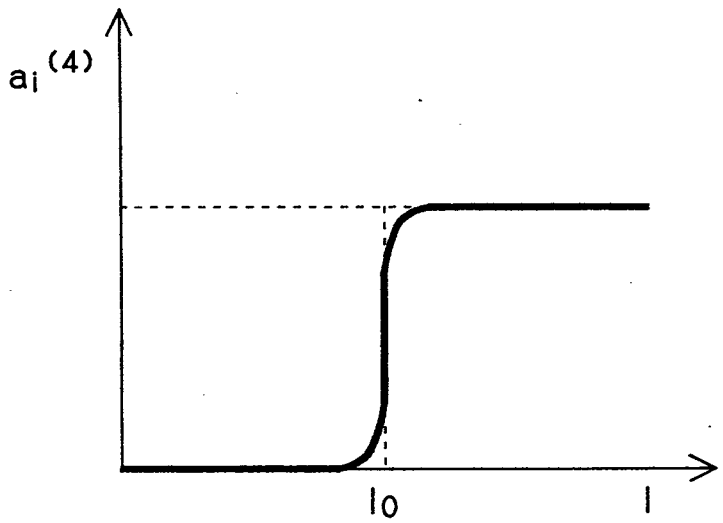

Figure 7–3 Schematic figure which shows the dependence of the coefficient $a_i^{(4)}$ on the chain stem length l in crystals.

length l in crystals becomes large beyond a critical value l_0, which is shown schematically in *Figure 7–3*.

The first–order perturbation theory of semiclassical quantum mechanics (electric field described classically) for a harmonic vibration gives the energy level W_{ni} for the i–th vibration.

$$W_{ni} = \hbar\omega_i (n_i + {}^1/_2) - a_i^{(4)} q_i^4 (\hbar^2 / \omega_i^2) [({}^3/_4) (2n_i^2 + 2n_i + 1)] \quad (15)$$

where n_i is the quantum number and $\hbar$ is Planck's constant divided by 2π.

The fundamental transition from $n_i = 0$ to $n_i = 1$, ω, is as follows:

$$\omega = \omega_i - 3a_i^{(4)} q_i^4 \hbar / \omega_i^2 . \quad (16)$$

The coefficient $a_i^{(4)}$ is not large for very small crystals such as the solution–grown single crystals because the length along the chain axis direction is too small (usually below 10 nm for POM) to yield the dynamic ferroelectric state. In this case, the frequency of infra–red absorption is given by ω_i. On the contrary, the needle–like crystals of t–POM have sufficiently large crystal length along the chain axis (~10 μm), and the ferroelectric–like state with a large nonlinear coefficient $a_i^{(4)}$ is realized and reveals the frequency ω. As mentioned above, the nonlinear coefficient $a_i^{(4)}$ is positive and ω is smaller than ω_i as seen from eq. 16. This result qualitatively coincides with the experimental result.

The effect of the dynamic ferroelectric state is very small on the absorption intensity because of the quasi–harmonic vibration. The absorption intensity can be approximated by the harmonic vibration.

7.3 Discussion

The model can qualitatively explain the experimental results, in particular the frequency shift due to the stem length difference. However, quantitative comparison with experiments is very difficult because $a_i^{(4)}$ cannot be directly estimated and amounts of the frequency shifts cannot be calculated. Instead of direct estimation, relative values of $a_i^{(4)}$ will be estimated from the observed amounts of the frequency shifts using eq. 16, and the estimated values will be discussed. From eq. 16 the relative frequency difference, $\Delta\omega / \omega_i = (\omega_i - \omega) / \omega_i$, for the i–th vibration is given by

$$\Delta\omega / \omega_i = 3\hbar\, a_i^{(4)}\, q_i^4 / \omega_i^3 \qquad (17)$$

The fourth power of q_i is estimated from the integrated absorbance area for the i–th band, Y_i, because the vibration is considered to be quasi–harmonic, and $Y_i \propto f_i\, q_i^2$, where f_i is the oscillator strength. The effect of f_i is neglected or included in the estimation of q_i. In *Table 7–1*, the observed values of ω_i and ω are cited from *Table 3–1*, and Y_i is calculated from the data of ref. 13, where Y_i is the relative value to that of the 1385 cm^{-1} absorption band. The values of $a_i^{(4)}$ are estimated using eq. 17 and are shown in *Table 7–1*.

The estimated coefficient $a_i^{(4)}$ of the COC antisymmetric vibration is the largest (for 1138 and 1000 cm^{-1}), and the internal rotation around the main–chain bonds also gives rise to a large value of $a_i^{(4)}$ (for 236 cm^{-1}). Rocking and wagging modes of CH_2 do not show any large nonlinear coefficient. This result is reasonable because a large nonlinear coefficient $a_i^{(4)}$ would arise from the complex interactions among atoms and electrons within the main chain. The atomic and electronic structure in the main chain would

Table 7–1 Estimation of relative values of nonlinear coefficient $a_i^{(4)}$ for each band of A_2 mode in polyoxymethylene

ω_i[a], cm^{-1} Solution–grown crystal	ω_i[a], cm^{-1} Needle–like crystal	Y_i[b], (relative value) Integrated absorbance area for needle–like crystal	$\Delta\omega / \omega_i$	$a_i^{(4)}$ (relative value)	Vibrational mode[c]
2983	2985		0		$\nu_a(CH_2)$
1385	1385	1	0	0	$w(CH_2)$
1138	1093	25	0.04	8	$\nu_a(COC)(77) + r(CH_2)(19)$
1000	895	70	0.11	2	$r(CH_2)(75) - \nu_a(COC)(21)$
236	220	4	0.07	5	$\tau_a(96) + r(CH_2)(3)$

[a] Cited from *Table 3–1* [b] Cited from ref 13. [c] Cited from ref 13.

change sensitively through the ferroelectric–like interaction of the transition dipole moments. On the other hand, rocking and wagging mode of CH_2 are not so sensitively influenced by the atomic and electronic structure of the main chain. To develop the detailed molecular theory of the anomalous shift of the infra–red bands, one must mainly take into account the change in the atomic and electronic structure of main chain.

In conclusion, the anomalous shift of the A_2 infra–red bands in *t*–POM is arises from the transition dipole moment interactions. Nonlinear vibrations appear in the A_2 modes of large stem–length samples (the needle–like crystals and highly drawn films) under the assumption of a dynamic ferroelectric state. This rather small (quasi–harmonic oscillation) but prominent nonlinear effect is large in the COC antisymmetric vibration and the internal rotation around the main–chain bonds.

References

1 E. F. Oleinik and N. S. Enikolopyan, *J. Polym. Sci. (C)*, **16**, 3677 (1968)

2 L. Terlemezyan, M. Mihailov, P. Schmidt and B. Schneider, *Makromol. Chem.*, **179**, 807 (1978)

3 L. Terlemezyan, M. Mihailov, P. Schmidt and B. Schneider, *Makromol. Chem.*, **179**, 2315 (1978)

4 L. Terlemezyan and M. Mihailov, *Makromol. Chem.*, **179**, 2807 (1978)

5 M. Shimomura and M. Iguchi, *Polymer*, **23**, 509 (1982)

6 M. Shimomura, M. Iguchi and M. Kobayashi, *Polymer*, **29**, 351 (1988)

7 M. Shimomura, M. Iguchi and M. Kobayashi, *Polymer*, **31**, 1406 (1990)

8 M. Shimomura, Y. Tanabe, Y. Watanabe and M. Kobayashi, *Polymer*, **31**, 1411 (1990)

9 M. Shimomura, Y. Tanabe, M. Iguchi, Y. Watanabe and M. Kobayashi, *J. Appl. Polym. Sci., Appl. Polym. Symp.*, **43**, 241 (1989)

10 M. Kobayashi, H. Morishita and M. Shimomura, *Macromolecules*, **22**, 3726 (1989)

11 P. Schmidt, B. Schneider, J. Baldrian, L. Terlemezyan, M. Mihailov and B. Ivanova, *Polymer*, **28** 217 (1987)

12 For example, H. Hrölich, "Theory of Dielectrics", Clarendon Press, Oxford (1958), M. Tokunaga, "Dielectrics", Baifukan (1991)

13 H. Tadokoro, M. Kobayashi, Y. Kawaguchi, A. Kobayashi and S. Murahashi, *J. Chem. Phys.*, **38**, 703 (1963)

Chapter 8

Summary and Conclusion

This thesis has dealt with the anomalously large infra-red spectral changes induced by change in crystal morphology of crystalline polymers. This phenomenon has been discovered for the first time in cases of the trigonal and orthorhombic modifications of polyoxymethylene (POM) and poly(ethylene oxide) (PEO). General features of this phenomenon, which is thereafter observed commonly in many systems, were investigated and interpreted in terms of the "dynamic ferroelectric" theory. The summary of Chapter 2 – Chapter 7 is as follows.

* * *

Chapter 2

Contrary to the general notion that vibrational spectroscopy in the mid infra-red region is hardly reflected to the difference in large-size or higher-order structure like crystal morphology, infra-red spectra of various POM samples were found to exhibit very large and systematic changes with difference in origin of samples and/or in history of sample processing, although all the samples investigated were in the highly crystalline trigonal phase (the stable modification). The absorption bands were classified into two categories; one changed sensitively in both frequency and intensity from sample to sample, and the other appeared commonly in all samples. Some of the former bands (at 1000 and 1138 cm^{-1}) were not assigned to the infra-red-active fundamentals of the 9/5 helix of trigonal POM, even though they got

strong intensities in solution-grown crystals. By detailed quantitative analysis of the absorption profile, the sample-sensitive bands, at 1000 and 1138 cm^{-1} were interpreted as resulted by high-frequency shifts of the 895 and 1093 cm^{-1} bands, respectively. The latter two bands appear with strong intensities in drawn film samples and are assigned to the A_2 fundamentals of the 9/5 helical POM molecule. The results indicated that some of the normal modes associated with the crystalline phase exhibited frequency shifts by as large as 100 cm^{-1} or more accompanied by change in state of the crystallite. Such a large spectral change has never been seen so far in both polymeric and non-polymeric compounds. Discovery of this extraordinary spectral phenomenon was the starting point of the present work on "morphology-dependent infra-red spectra".

Chapter 3

In order to clarify the origin of the large spectral changes, infra-red spectra of the following two trigonal POM samples, both are of extremely high crystallinity but different in crystal morphology, were investigated; (1) the typical extended-chain crystals (ECC) prepared by a cationic polymerization of trioxane, and (2) the typical folded-chain or lamellar crystals grown from a dilute bromobenzene solution. These two samples gave rise to essentially the same X-ray diffraction pattern characteristic of the trigonal modification. Nevertheless, the infra-red spectra of the two samples were quite different from each other. Moreover, the difference was very specific; only the A_2 bands having the transition dipole parallel to the chain axis (the parallel bands) were blue-shifted in the lamellar crystals compared with the ECC sample, whereas the E_1 bands having the transition moment perpendicular to the chain axis (the perpendicular bands), as well as the infra-

red-inactive Raman bands (the A_1 bands), were observed at the same positions in the two samples. This indicated that the sample-dependent infra-red spectral changes mentioned in Chapter 2 were concluded to be caused by the difference in "morphology of crystallites" rather than by that in crystallinity or amount and kind of crystal defects. The same morphology-dependent spectral changes were observed for the ECC and lamellar crystals of deuterated POM (POM-d_2). In both normal and deuterated POMs, infra-red spectra of highly drawn and high crystalline film samples were very close to that of idealized ECC.

Chapter 4

As for the molecular mechanism of the morphology-dependent infra-red spectral changes, the role of the "folded-chain" structure should be examined. To this end, infra-red spectra of a series of linear oligomers of POM having acetoxy terminal groups were investigated. Solution-grown solids of these oligomers form trigonal lamellar crystals with the extended short chains packed together directing the chain axis normal to the lamella face. No chain-folding structures are included in these samples. Nevertheless, these samples gave rise to the infra-red spectra typical of the folded-chain crystals (FCC) of high molecular weight POM. The result told us that the infra-red spectrum of FCC sample should be ascribed not to the folded-chain structure but to the lamellar type crystal morphology. The spectral changes induced by mechanical deformation and subsequent melt crystallization were also investigated for solution-grown samples of both the oligomers and high molecular weight POM.

Chapter 5

In order to know whether the very characteristic spectral changes are limited to trigonal POM or they are observed commonly in polymer crystals, infra-red spectra of orthorhombic modification of POM were investigated on two samples of typical ECC and FCC type morphology, which were derived, respectively, from the ECC and FCC crystals of trigonal POM through a pressure-induced solid-state phase transition. The results showed that the infra-red parallel bands belonging to the B_1 species exhibited similar significant blue-shifts in the FCC sample compared with those of the ECC one, whereas the B_2 and B_3 bands with the perpendicular polarization appeared at the same positions in the two samples. Thus, the specificity of the parallel bands in the morphology-dependent frequency shifts was confirmed for *o*-POM crystals.

Chapter 6

For the same purpose in Chapter 5, the morphology-dependent infra-red spectra were investigated for PEO using the solution-grown lamellar crystals and highly-drawn film samples (instead of idealized ECC samples). The A_2 bands of the solution-grown crystals shifted towards high-frequency side, though amounts of the shifts were smaller than those of POM, while the other bands, A_1 and E_1, remained at the same positions as those of the drawn film. It was concluded that the spectral change is due to the same mechanism as in POM. The results in Chapters 5 and 6 suggest that the morphology-dependent infra-red spectral change should be recognized as a common phenomenon of polymer crystals. The magnitude of the bandshift becomes detectable only when the strength of the band is large enough as will be discussed in Chapter 7.

Chapter 7

A phenomenological theory was proposed to explain the anomalous shift of infra-red parallel bands between ECC and FCC crystals of trigonal and orthorhombic POM and PEO. For crystals with sufficiently large stem-length, the strong interaction among transition dipole moments yields "dynamic ferroelectric" state, resulting in the large nonlinear vibration for the A_2 (or B_1 for orthorhombic POM) modes. This causes bandshift toward the low-frequency side. For small crystals, the interactions among transition dipole moments are too small to cause the nonlinear vibration, and the ordinary harmonic approximation can be applied. Thus, the magnitudes of the bandshifts have some relation to the strengths of the bands as has been seen experimentally.

* * *

As described in this thesis, the morphology-dependent infra-red spectral changes are found and the general characteristics of the phenomenon are clarified. Since this phenomenon is observed commonly in polymer crystals, the author hopes that the infra-red spectroscopy will be used as a new sensitive method for the investigation of the morphological changes occurring in various polymer crystals on crystallization process, the thermal and mechanical processing, and phase transition.

List of Publications

The contents of this thesis have been published in the following papers.

1) Infra-red study on the conformational regularity in needle-like and other polyoxymethylene crystals.
   M. Shimomura and M. Iguchi, *Polymer* **23**, 509 (1982)
2) Identification of orthorhombic polyoxymethylene generated in a cationic polymerization system of trioxane.
   M. Kobayashi, Y. Itoh, H. Tadokoro, M. Shimomura and M. Iguchi, *Polym. Commun.* **24**, 38 (1983)
3) Vibrational spectroscopic study on trigonal polyoxymethylene and polyoxymethylene-d_2 crystals.
   M. Shimomura, M. Iguchi and M. Kobayashi, *Polymer* **29**, 351 (1988)
4) Morphology dependence of vibrational spectra of polyoxymethylene and poly(ethylene oxide) crystals.
   M. Shimomura, Y. Tanabe, M. Iguchi, Y. Watanabe and M. Kobayashi, *J. Appl. Polym. Sci., Appl. Polym. Symp.* **43**, 241 (1989)
5) A_2 mode vibration in infrared spectrum of trigonal polyoxymethylene.
   Y. Tanabe and M. Shimomura, *Rep. Prog. Polym. Phys. Jpn.* **32**, 395 (1989)
6) Vibrational spectroscopic study on low molecular weight polyoxymethylene diacetate.
   M. Shimomura, M. Iguchi and M. Kobayashi, *Polymer* **31**, 1406 (1990)

7) Vibrational spectroscopic study on poly(ethylene oxide) crystals.
M. Shimomura, Y. Tanabe, Y. Watanabe and M. Kobayashi, *Polymer* **31**, 1411 (1990)

8) A_2 mode vibration in infrared spectrum of trigonal polyoxymethylene.
Y. Tanabe and M. Shimomura, *Macromolecules* **23**, 5031 (1990)

The related papers

1) Quantitative analysis of organic compounds on metal surface by Fourier transform infrared reflection spectrometry.
M. Shimomura, T. Matsui and S. Tanaka, *Bunseki Kagaku* **29**, 565 (1980) (in Japanese)

2) Analytical study on thin organic coatings on rough surfaces of aluminum plates by Fourier transform infrared reflection absorption spectrometry.
T. Matsui, M. Shimomura, T. Yamamoto, T. Kitamura and S. Tanaka, *J. Chem. Soc. Jpn.* 150 (1981) (in Japanese)

3) Analysis of photopolymers on electrochemically roughened and anodized aluminum plates by Fourier transform infrared reflection absorption spectrometry.
T. Yamamoto, T. Kitamura, M. Shimomura, T. Matsui and S. Tanaka, *J. Chem. Soc. Jpn.* 727 (1982) (in Japanese)

4) Infrared study on the conformational regularity in needle–like and other polyoxymethylene crystals.
M. Shimomura and M. Iguchi, *Bull. Res. Inst. Polym. Textiles* **147**, 7 (1985) (in Japanese)

5) Vibrational spectroscopic study on polymorphism and molecular aggregation states in polyoxymethylene.
M. Kobayashi, H. Morishita, T. Ishioka, M. Iguchi, M. Shimomura and T. Ikeda, *J. Mol. Struc.* **146**, 155 (1986)

6) Strain behavior of the crystal lattice of super-drawn films of ultra high molecular weight polyethylene under hydrostatic high pressure by WAXS.
K. Ito, H. Kyotani, M. Shimomura, Y. Maeda and Y. Tanabe, *Rep. Prog. Polym. Phys. Jpn.* **30**, 105 (1987)

7) Vibrational spectroscopic study on the solid-state phase transition of poly(oxymethylene) single crystals from the orthorhombic to the trigonal phase.
M. Kobayashi, H. Morishita, M. Shimomura and M. Iguchi, *Macromolecules* **20**, 245 (1987)

8) Vibrational spectroscopic study of orthorhombic polyoxymethylene.
H. Morishita, M. Kobayashi, M. Shimomura and M. Iguchi, *Sci. Bull. Fac. Educ., Nagasaki Univ.* **39**, 47 (1988) (in Japanese)

9) Mechanical properties and morphology of highly stretchable polyacetylene.
H. Kyotani, M. Shimomura, Y. Tanabe, Y. Watanabe, M. Suezaki, T. Kasai, K. Akagi and H. Shirakawa, *Rep. Prog. Polym. Phys. Jpn.* **31**, 265 (1988)

10) Pressure-induced phase transition of poly(oxymethylene) from the trigonal to the orthorhombic phase:effect of morphological structure.
M. Kobayashi, H. Morishita and M. Shimomura, *Rep. Prog. Polym. Phys. Jpn.* **31**, 473 (1988)

11) Synthesis of polyacetylene films with high density and high mechanical strength.

K. Akagi, Y. Suezaki, H. Shirakawa, H. Kyotani, M. Shimomura and Y. Tanabe, *Synthetic Metals* **28**, D1 (1989)

12) Mechanical properties of polyoxymethylene whiskers/ polyoxymethylene resin composite films.

M. Shimomura, Y. Maeda and Y. Tanabe, *J. Mater. Sci.* **24**, 2245 (1989)

13) Pressure-induced phase transition of poly(oxymethylene) from the trigonal to the orthorhombic phase : effect of morphological structure.

M. Kobayashi, H. Morishita and M. Shimomura, *Macromolecules* **22**, 3726 (1989)

14) Vibrational spectroscopic study on the solid-state phase transition of polyoxymethylene. I. On the phase transition from the orthorhombic to the trigonal system.

H. Morishita, M. Kobayashi, M. Shimomura, M. Iguchi and H. Kuwahara, *Sci. Bull. Fac. Educ., Nagasaki Univ.* **41**, 1 (1989) (in Japanese)

15) On the morphology of rod-like trigonal polyoxymethylene single crystals.

H. Morishita, M. Kobayashi, H. Kuwahara, M. Shimomura and M. Iguchi, *Sci. Bull. Fac. Educ., Nagasaki Univ.* **41**, 13 (1989)

16) Photochromism of vacuum-deposited triphenylformazan film.

K. Itoh, M. Shimomura, H. Kyotani and Y. Tanabe, *Rep. Prog. Polym. Phys. Jpn.* **32**, 391 (1989)

17) Cis–trans thermal isomerization of polyacetylene.
Y. Tanabe, H. Kyotani, M. Shimomura, K. Akagi, M. Suezaki, T. Kasai and H. Shirakawa, *Rep. Prog. Polym. Phys. Jpn.* **32**, 169 (1989)

18) Effect of higher order structure of thermal isomerization of polyacetylene.
H. Kyotani, M. Shimomura, Y. Tanabe, K. Akagi, T. Kasai, Y.–X. Zhang and H. Shirakawa, *Rep. Prog. Polym. Phys. Jpn.* **33**, 205 (1990)

19) Kinetic analysis of cis–trans thermal isomerization of polyacetylene.
Y. Tanabe, H. Kyotani, M. Shimomura, K. Akagi, M. Suezaki, T. Kasai and H. Shirakawa, *J. Polym. Sci. B, Polym. Phys.* **29(4)**, 501 (1991)

20) Morphology dependence of DSC curves for cis–trans isomerization of polyacetylene films.
H. Kyotani, M. Shimomura, Y. Tanabe, K. Akagi, T. Kasai, Y.–X. Zhang and H. Shirakawa, *Synthetic Metals* **41–43**, 151 (1991)

21) Analysis of thermal isomerization of polyacetylene films prepared by various methods.
H. Kyotani, M. Shimomura, K. Ito, Y. Tanabe, Y.–X. Zhang, K. Akagi and H. Shirakawa, *Rep. Prog. Polym. Phys. Jpn.* **34**, 141 (1991)

22) Mechanical properties of polyoxymethylene whiskers/ polyoxymethylene resin composite.
M. Shimomura, Y. Maeda and Y. Tanabe, *Bull. Res. Inst. Polym. Textiles* **168**, 33 (1992) (in Japanese)

23) Photochromic property of triphenylformazan films prepared by vacuum evaporation.

K. Ito, M. Shimomura, H. Kyotani and Y. Tanabe, *Jpn. J. Appl. Phys., Part 2* **31(2A)**, L106 (1992)

24) Spectroscopic determination of diffusion in Langmuir–Blodgett films – 1. Interlayer diffusion of cadmium arachidate and its deuterated analogue through a polymer interface.

M. Shimomura, K. Song and J. F. Rabolt, *Langmuir*, **8**, 887 (1992)

25) Vibrational spectroscopic study on trigonal polyoxymethylene and its deuterated analogue crystals.

M. Shimomura, M. Iguchi and M. Kobayashi, *Bull. Res. Inst. Polym. Textiles*, **172**, 73 (1992) (in Japanese)

26) Vibrational spectroscopic study on low–molecular–weight polyoxymethylene crystals.

M. Shimomura, M. Iguchi and M. Kobayashi, *Bull. Res. Inst. Polym. Textiles*, **172**, 81 (1992) (in Japanese)

27) Vibrational spectroscopic study on poly(ethylene oxide).

M. Shimomura, Y. Tanabe, Y. Watanabe and M. Kobayashi, *Bull. Res. Inst. Polym. Textiles*, **172**, 89 (1992) (in Japanese)

28) Development of highly conducting polyacetylene films with high tensile strength and high stretchability.

K. Akagi, K. Sakamaki, T. Kasai, H. Shirakawa, H. Kyotani, M. Shimomura and Y. Tanabe, *Proc. 36th Jpn. Cong. Mater. Res.* 260 (1993)